LEVEL II

(12)

DEPARTMENT OF EARTH AND PLANETARY SCIENCES
MASSACHUSETTS INSTITUTE OF TECHNOLOGY
CAMBRIDGE, MASSACHUSETTS 02139

RESEARCH IN SEISMOLOGY (ATTENUATION AND SOURCE MECHANISMS)

FINAL TECHNICAL REPORT

ARPA ORDER NO. - 3291

PROGRAM CODE NO. - 0D60

NAME OF CONTRACTOR - M.I.T.

EFFECTIVE DATE OF CONTRACT - 1 JUNE 1975

CONTRACT EXPIRATION DATE - 30 SEPTEMBER 1980

AMOUNT OF CONTRACT - $690,000

CONTRACT NO. - F44620-75-C-0064

PRINCIPAL INVESTIGATORS - M. NAFI TOKSÖZ, 617/253-6382
KEIITI AKI, 617/253-6397
SEAN C. SOLOMON, 617/253-3786

PROGRAM MANAGER - WILLIAM J. BEST, 202/767-4908

SHORT TITLE OF WORK - RESEARCH IN SEISMOLOGY

SPONSORED BY
ADVANCED RESEARCH PROJECTS AGENCY
ARPA ORDER NO. 3291

UNCLASSIFIED

SECURITY CLASSIFICATION OF THIS PAGE (When Data Entered)

REPORT DOCUMENTATION PAGE

READ INSTRUCTIONS BEFORE COMPLETING FORM

1. REPORT NUMBER: AFOSR-TR-81-0465	2. GOVT ACCESSION NO.: AD-A099160
3. RECIPIENT'S CATALOG NUMBER	
4. TITLE (and Subtitle): RESEARCH IN SEISMOLOGY (ATTENUATION AND SOURCE MECHANISMS)	5. TYPE OF REPORT & PERIOD COVERED: FINAL 6/1/75-9/30/80
	6. PERFORMING ORG. REPORT NUMBER
7. AUTHOR(s): M. Nafi Toksoz, Keiiti Aki, Sean C. Solomon	8. CONTRACT OR GRANT NUMBER(s): F44620-75-C-0064, ARPA Order-3291
9. PERFORMING ORGANIZATION NAME AND ADDRESS: Dept. of Earth and Planetary Sciences, Massachusetts Institute of Technology, Cambridge, Massachusetts 02139	10. PROGRAM ELEMENT, PROJECT, TASK AREA & WORK UNIT NUMBERS: 62701E, AO 3291
11. CONTROLLING OFFICE NAME AND ADDRESS: Advanced Research Projects Agency/NMR, 1400 Wilson Blvd., Arlington, Virginia 22209	12. REPORT DATE: Sep 80
	13. NUMBER OF PAGES: 201
14. MONITORING AGENCY NAME & ADDRESS (if different from Controlling Office): AFOSR/NP, Bolling AFB, Bldg. 410, Washington DC, 20332	15. SECURITY CLASS. (of this report): UNCLASSIFIED
	15a. DECLASSIFICATION/DOWNGRADING SCHEDULE

16. DISTRIBUTION STATEMENT (of this Report)

Approved for public release; distribution unlimited.

17. DISTRIBUTION STATEMENT (of the abstract entered in Block 20, if different from Report)

18. SUPPLEMENTARY NOTES

19. KEY WORDS (Continue on reverse side if necessary and identify by block number)

Crust-upper mantle structure, wave propagation, attenuation, source properties

20. ABSTRACT (Continue on reverse side if necessary and identify by block number)

(OVER)

DD FORM 1 JAN 73 1473 EDITION OF 1 NOV 65 IS OBSOLETE

UNCLASSIFIED

SECURITY CLASSIFICATION OF THIS PAGE (When Data Entered)

404784

20 ABSTRACT (Continue on reverse side if necessary and identify by block number)

Research activities described in this report include detailed studies of crust-upper mantle structures and their lateral variations, surface wave propagation and attenuation over regional distances, and the determination of source properties of "anomalous" earthquakes by combined studies of body and surface waves.

At regional distances, the lateral variations of the shallow structure have strong effects on the propagation of body and surface waves. The lateral heterogeneities are present not only in "tectonic" regions but also in the old geologic provinces. The horizontally layered models are becoming less representative of the structures in continental areas. Continental growth processes that include collisions, suturing, heating and melting, leave major heterogeneities that affect wave propagation, scattering and attenuation.

Similarly, complexities of the earthquake source, even for small events, are being found with more detailed studies. Body waves from such sources are being affected by source finiteness, asperities, rupture propagation and by the geologic structure. It is difficult to separate all these effects, especially for very shallow sources, where surface reflection further complicates the problem. Detailed analysis of body and surface waves is necessary to determine the source properties. An example of how this approach was utilized to study some anomalous events is shown in this report.

DD FORM 1 JAN 73 1473

Department of Earth and Planetary Sciences
Massachusetts Institute of Technology
Cambridge, Massachusetts 02139

RESEARCH IN SEISMOLOGY (ATTENUATION AND SOURCE MECHANISMS)

Final Technical Report

ARPA Order No. - 3291

Program Code No. - 0D60

Name of Contractor - M.I.T.

Effective Date of Contract - 1 June 1975

Contract Expiration Date - 30 September 1980

Amount of Contract - $690,000

Contract No. - F44620-75-C-0064

Principal Investigators - M. Nafi Toksöz, 617/253-6382
Keiiti Aki, 617/253-6397
Sean C. Solomon, 617/253-3786

Program Manager - William J. Best, 202/767-4908

Short Title of Work - Research in Seismology

Sponsored by
Advanced Research Projects Agency
ARPA Order No. 3291

ABSTRACT

The work during the final year of contract no. F44620-75-C-0064, "Research in Seismology (Attenuation and Source Mechanisms)" is described. This is separated into four areas:

1. Velocities and attenuation of surface waves in the earth;
2. Summary of crustal structure in the Middle East;
3. Source properties of shallow earthquakes; and
4. Three-dimensional crust-upper mantle models.

In addition, a cumulative list of publications is included.

TABLE OF CONTENTS

I. INTRODUCTION

This final report for contract no. F44620-75-C-0064, "Research in Seismology (Attenuation and Source Mechanisms)", covers the final year of the project. The work done in this period includes detailed studies of crust-upper mantle structures and their lateral variations, surface wave propagation and attenuation over regional distances, and the determination of source properties of "anomalous" earthquakes by combined studies of body and surface waves.

At regional distances, the lateral variations of the shallow structure have strong effects on the propagation of body and surface waves. The lateral heterogeneities are present not only in "tectonic" regions but also in the old geologic provinces. The horizontally layered models are becoming less representative of the structures in continental areas. Continental growth processes, that include collisions, suturing, heating and melting, leave major heterogeneities that affect wave propagation, scattering and attenuation.

Similarly, complexities of the earthquake source, even for small events, are being found with more detailed studies. Body waves from such sources are being affected by source finiteness, asperities, rupture propagation and by the geologic structure. It is difficult to separate all these effects, especially for very shallow sources, where surface reflection further complicates the problem. Detailed analysis of body and surface

waves is necessary to determine the source properties. An example of how this approach was utilized to study some anomalous events is shown in this report.

II. VELOCITIES AND ATTENUATION OF SURFACE WAVES IN THE EARTH

Measurement of Interstation Phase and Group Velocity and Q using Wiener Filtering, S.R. Taylor and M.N. Toksöz, Bull. Seism. Soc. Am., submitted, 1980.

Abstract

A method for calculating interstation phase and group velocities and relative attenuation coefficients using a Wiener (least squares) filtering technique is presented. The interstation transfer (or Green's) function is estimated from two stations laying along the same great circle path. The estimate is obtained from a Wiener filter constructed to predict the signal at the station further from the source from the signal recorded at the nearer station.

The interstation group velocity is obtained by applying the multiple filtering technique to the transfer function, and the interstation phase velocity from the phase of the transfer function. The amplitude spectrum of the transfer function is used to calculate relative attenuation between the two stations. The Q values calculated from the transfer function appear to be more stable than those obtained by taking spectral ratios.

The method is particularly useful for paths involving short station separations and is applied to a surface wave path crossing the Iranian Plateau.

INTRODUCTION

Analysis of surface wave dispersion and attenuation information is a useful means of determining crust and upper mantle structure, particularly in remote regions where additional geophysical data are sparse. A number of different schemes have been developed for the measurement and inversion of phase and group velocities and attenuation using various station-path configurations (cf. Kovach, 1978 for a review).

In setting up the surface wave inversion, it is necessary to parameterize the problem and define what phase and group velocities reveal about earth structure. Inversion of phase velocities alone presents a non-unique problem because of the trade-off between certain parameters such as velocity and layer thickness. However, inversion of group velocities alone results in a more non-unique problem (Pilant and Knopoff, 1970) resulting from the derivative relationship between phase and group velocity. Because of a constant of integration, two structures generating different phase velocity curves can produce identical group velocity curves. Although phase and group velocities are not completely independent variables, they do provide slightly differing sensitivities to a given structure and can be used simultaneously to increase resolution. Also, because anelasticity of the earth causes physical

dispersion of seismic waves, attenuation information can be used to correct phase and group velocity curves, or the different types of observations can be inverted simultaneously.

The two-station technique is commonly used for measurement of interstation phase velocities by calculating phase differences or attenuation by taking spectral ratios from two stations laying on the same azimuth from an earthquake. Interstation group velocities can be calculated by differentiating the phase velocity curve or by measuring group arrival times at each station either directly from the seismograms or by narrow bandpass filtering each seismogram and dividing the group delay into the station separation. Landisman et al., (1969) suggest measuring interstation phase velocities from the windowed cross-correlogram. Windowing where the correlation is high reduces the effect of random noise in the phase spectrum and stabilizes the phase velocities. Landisman et al., (1969) also note that the cross-correlation function approximates the interstation impulse response and application of the moving window technique or multiple filtering (Dziewonski et al., 1969) can be used to calculate interstation group velocities. Although this technique is useful for phase velocities, test cases shown below illustrate the measurements of interstation group velocities from the cross-correlogram can lead to errors of almost 10 percent for station separations of 500 km at periods of 20 seconds.

In this paper, we present a technique for measuring interstation phase and group velocities and attenuation from the interstation transfer function which is calculated using Wiener (or least squares) filtering, and apply the method to a surface wave path crossing the Iranian Plateau.

INTERSTATION TRANSFER FUNCTION USING WIENER FILTERING

Given two seismograms positioned along the same great circle path from a source, we want to estimate the interstation transfer function (also known as the medium impulse response or Green's function). The amplitude spectrum of the transfer function gives a measure of the spectral ratio between the two stations which can be used to determine Q, and the phase of the transfer function gives the phase delay of the system which will be used to calculate the interstation phase velocity. The shape of the transfer function in the time domain provides information on the dispersiveness of the system which will be used to estimate interstation group velocity.

Figure 1 illustrates the problem in the time and frequency domain where the input signal at station 1 drives the system and produces the output recorded at station 2. The convolution is given by the frequency domain representation

$$F_1(\omega)e^{i\phi_1(\omega)}\,F_m(\omega)e^{i\phi_m(\omega)} = F_2(\omega)e^{i\phi_2(\omega)} \qquad (1)$$

where the subscripts 1,2 and m refer to station 1, station 2, and the interstation medium, respectively. We wish to deconvolve the output by dividing (1) by the input and computing the transfer function

$$F_m(\omega)\,e^{i\phi_m(\omega)} = \frac{F_2(\omega)}{F_1(\omega)}\,e^{i(\phi_2-\phi_1)} \qquad (2)$$

This simple deconvolution can be very unstable, particularly in the presense of spectral holes for which frequencies the filter parameters (transfer function) will be indeterminant. Various deconvolution schemes can be used to find the filter coefficients and we have chosen a least squares or Wiener deconvolution (Wiener, 1949; Treitel and Robinson, 1966; Peacock and Treitel, 1969).

Let the vector $\underline{b}$ represent the input (signal at station 1) to the system $\underline{f}$, and $\underline{d}$ be the output (signal at station 2) where

$$\begin{aligned} \underline{b} &= (b0, b1, \ldots, bn) \\ \underline{d} &= (d0, d1, \ldots, dn+m) \qquad (3) \\ \underline{f} &= (f0, f1, \ldots, fm) \end{aligned}$$

We wish to construct a filter, $\underline{f}$, that will best estimate the

desired output, $\underline{d}$, when driven by an input $\underline{b}$. Letting the n+m length vector $\underline{c}$ represent the actual output, we design $\underline{f}$ such that the difference between the actual and desired output

$$e_t = c_t - d_t \qquad (4)$$

is minimized in a least squares sense (Figure 1c). This requires that the length E, of the error series, $\underline{e}$, is minimized

$$E = \underline{e}^T\underline{e} = \sum_\tau e_\tau^2 = \sum_\tau (c_\tau - d_\tau)^2 \qquad (5)$$

and we design $\underline{f}$ such that

$$\underline{b} * \underline{f} = \underline{c} \qquad (6)$$

or

$$c_\tau = \sum_{t=0}^{n+m+1} f_\tau \, b_{\tau-t}$$

where * denotes convolution. Using matrix notation, the convolution is given by

$$\begin{bmatrix} b0 & 0 & 0 & \dots & 0 \\ b1 & b0 & 0 & \dots & 0 \\ \vdots & \vdots & \vdots & & \vdots \\ bn & bn-1 & \dots & & b0 \\ \vdots & \vdots & & & \vdots \\ 0 & 0 & \dots & & bn \end{bmatrix} \begin{bmatrix} f0 \\ f1 \\ \vdots \\ fm \end{bmatrix} = \begin{bmatrix} c0 \\ c1 \\ \vdots \\ cm+n \end{bmatrix} \qquad (7)$$

Introduce the desired output $\underline{d}$, which is the signal at station 2, and solve for $\underline{f}$ such that the length squared of the difference vector $c_t - d_t$ is minimized

$$\begin{bmatrix} b0 & 0 & 0 & \dots & 0 \\ b1 & b0 & 0 & \dots & 0 \\ \vdots & \vdots & \vdots & & \vdots \\ bn & bn-1 & \dots & & b0 \\ \vdots & \vdots & & & \vdots \\ 0 & 0 & & \dots & bn \end{bmatrix} \begin{bmatrix} f0 \\ f1 \\ \vdots \\ fm \end{bmatrix} = \begin{bmatrix} d0 \\ d1 \\ \vdots \\ dm+n \end{bmatrix} + \begin{bmatrix} e0 \\ e1 \\ \vdots \\ em+n \end{bmatrix} \qquad (8)$$

In matrix shorthand

$$B\underline{f} = \underline{d} + \underline{e} \qquad (9)$$

We then solve for $\underline{f}$ using least squares

$$B^T B\underline{f} = B^T \underline{d} \qquad (10)$$

It turns out that the terms $B^T B$ give the autocorrelation of the input $\underline{b}$

$$a_\tau = \sum_{t=0}^{n} b_t d_{t+\tau} \qquad (11)$$

and $B^T \underline{d}$ is the cross-correlation vector of $\underline{b}$ and $\underline{d}$

$$cc_\tau = \sum_{t=0}^{n} b_t d_{t+\tau} \qquad (12)$$

Thus, the m-length Wiener filter results from the solution of the normal equations of the form

$$\begin{bmatrix} a0 & a1 & a2 & \dots & am \\ a1 & a0 & a1 & \dots & am-1 \\ \cdot & & & & \cdot \\ \cdot & & & & \cdot \\ \cdot & & & & \cdot \\ am & & \dots & & a0 \end{bmatrix} \begin{bmatrix} f0 \\ f1 \\ \cdot \\ \cdot \\ \cdot \\ fm \end{bmatrix} = \begin{bmatrix} cc0 \\ cc1 \\ \cdot \\ \cdot \\ \cdot \\ ccm \end{bmatrix} \qquad (13)$$

or from equation (1) we are solving

$$F_1^2 F_m e^{i\phi_m} = F_1 F_2 e^{i(\phi_2 - \phi_1)} \qquad (14)$$

The autocorrelation matrix in equation (13) is in a Toeplitz form with an interesting symmetry where all of the diagonals are the same and the main diagonal is the autocorrelation of the input at zero lag. Because of its symmetry, the system (13) can be solved efficiently and with a minimum of computer storage using Levinson recursion (Wiener, 1949; Treitel and Robinson, 1966). Although the system (13) is always nonsingular (assuming $a \neq 0$) (Ford and Herne, 1966), numerical instabilities may occur for large m. For this case the problem can be formulated using a stochastic framework where the input signal, $\underline{b}$, is contaminated by white noise, $\underline{n}$, with zero autocorrelation except at zero lag, where the autocorrelation equals the noise power. The actual input $\underline{x}$, is then given by

$$\underline{x} = \underline{b} + \underline{n} \qquad (15)$$

Assuming the noise is stationary, this method of solution is equivalent to the damped least squares technique. To do this we add

a small constant to the autocorrelation function at zero lag which stabilizes the solution.

Landisman et al., (1969) pointed out that application of multiple filtering to the windowed interstation cross-correlation function gives a good approximation to the interstation group velocity. However, for relatively short station separations where small phase errors are important, the method breads down. To illustrate this, we take identical signals for both stations and apply the cross-correlation and Wiener filtering operation to them. In this case, we assume that the impulse response of the interstation medium is a delta function where the output equals the input. Using the 12/9/72 seismic surface waves recorded at the WWSSN station WES shown in Figure 1, we compute the cross-correlation of the input with the output (Figure 2a, which is actually the autocorrelation of the input at station WES) and the interstation transfer function using the least squares deconvolution described above (Figure 2b). Both signals shown in Figure 2 are then windowed between lags of 0-400 seconds. Comparison of Figures 2a and b shows that the transfer function approximates a delta function much better than the "cross-correlogram". The phase and amplitude spectrum of the windowed transfer function gives a better approximation to that of a delta function than the cross-correlogram. Also shown in Figures 2 a and b is the envelope function fit to the narrow bandpassed

signals for two frequencies. As can be seen from Figure 2a, the time of maximum amplitude is at a lag of 10 seconds which can cause group velocity errors of about 8 percent over distances of 500 km. Between periods of 17 to 50 seconds, the lags of the maximum amplitude for the transfer function are all within two seconds or one digital point in this case where the sampling interval was 2 seconds. For periods below 17 seconds the error increased to 4 seconds (two digital points) which is the portion of the spectrum that was not flat.

Although the cross-correlogram gives an approximation of the impulse response of the interstation medium, test cases show that substantial errors of interstation group velocity determinations can occur for short station separations.

APPLICATION

The Wiener filtering technique is applied to a surface wave path from an event occuring in the Red Sea on March 13, 1967 (19:22:19.5; 19.673N, 38.742E; Mb = 5.7, depth = 31 km) crossing the Iranian Plateau between the WWSSN stations SHI and MSH (Δ = 15.98 and 24.70 degrees, respectively). Figure 3 shows the seismograms and corrected spectra and the interstation transfer function is shown in

Figure 4. Interstation phase and group velocities are shown in Figure 5. The interstation group velocities were calculated by applying the multiple filtering technique to the transfer function and the interstation phase velocities were calculated from a polynomial fit to the unwrapped phase of the transfer function using the formula

$$C(T) = \frac{\Delta x}{t_0 + (\phi_{tf}(T) \pm N)T} \qquad (16)$$

where Δx is the epicentral distance, t0 is the first time point of the transfer function, and ϕ_{tf} is the phase of the transfer function.

Q values along the travel path were calculated using

$$Q = \frac{\pi f}{u} \Delta x \Big/ \ln\left(A_{tf}(f)\sqrt{\frac{\sin\Delta_2}{\sin\Delta_1}}\right) \qquad (17)$$

where U is the group velocity and A_{tf} is the amplitude spectrum of the transfer function. Because of numerical instabilities involved in the Levinson recursion solution for the filter parameters, the absolute values of the transfer function may be shifted by an amount related to the damping used to solve the system (13). Thus, the spectrum of the transfer function is normalized to one, which gives a value of infinite Q at the frequency corresponding to the maximum

amplitude. The relative Q values for this path as calculated from the transfer function and by the method of spectral ratios are plotted in Figure 6.

Overall, the Q values calculated from the transfer function appear to be smoother than those from spectral ratios. For example, at periods around 18-19 seconds, the Q values from spectral ratios increase rapidly to about 450 which may be due to effects of multipathing. In contrast, because of the least squares technique used, the Q values from the transfer function at periods of 18-19 seconds are stabilized by those of neighboring periods. For periods greater than 25 seconds, the Q values from the transfer function are quite flat relative to those from spectral ratios.

CONCLUSIONS

In this paper, we have applied the Wiener filtering technique to seismograms lying on the same great circle path from an earthquake in order to calculate the interstation transfer function. Interstation phase and group velocities and relative attenuation coefficients can be calculated from the transfer function and inverted simultaneously for structure. The method is particularly useful across paths involving short station separations.

REFERENCES

Der, Z.A., and M. Landisman, Theory for errors, resolution, and separation of unknown variables in inverse problems, with application to the mantle and the crust in southern Africa and Scandinavia, Geophys. J.R. astr. soc., 27, 137-178, 1972.

Dziewonski, A., S. Bloch, and M. Landisman, A technique for the analysis of transient seismic signals, Bull. Seism. Soc. Am., 59, 427-444, 1969.

Ford, W.T. and J.H. Hearne, Least-squares inverse filtering, Geophys., 31, 917-926, 1966.

Kovach, R.L., Seismic surface waves and crustal and upper mantle structure, Rev. of Geophys. Space Phys., 16, 1-13, 1978.

Knopoff, L. and F.S. Chang, The inversion of surface wave dispersion data with random errors, J. Geophys., 43, 299-309, 1977.

Landisman, M., A. Dziewonski, and Y. Sato, Recent improvements in the analysis of surface wave observations, Geophys. J. R. astr. Soc., 17, 369-403, 1969.

Pilant, W.L. and L. Knopoff, Inversion of Phase and group slowness dispersion, J. Geophys. Res., 75, 2135-2136, 1970.

Peacock, K.L., and S. Treitel, Predictive deconvolution: theory and practice, Geophys., 34, 155-169, 1969.

Treitel, S. and E.A. Robinson, The design of high resolution digital filters, IEEE Trans. Geoscience Electronics, 4, 25-38, 1966.

Weiner, N., Time Series, M.I.T. Press, Cambridge, MA, 163pp., 1949.

Wiggins, R.A., Interpolation of digitized curves, Bull. Seism. Soc. Am., 66, 2077-2081, 1976.

FIGURE CAPTIONS

Figure 1 Schematic illustration of the interstation Green's function. (a) Seismogram b at the station nearest to the source is convolved with the interstation Green's function f to give the output d recorded at the station furthest from the source. (b) Frequency domain representation of Figure 1a and (c) elements of least-squares filtering.

Figure 2 Comparison of performance from cross-correlogram (a) versus interstation transfer function (b) for modeling the interstation medium response. In this case, the input equals the output and the medium response should be a delta function. (a) Cross-correlogram, spectrum, and narrow band-passed signal for frequencies of 0.05 and function calculation using Wiener filtering, and narrow band-passed signals and envelope functions for same two frequencies in (a).

Figure 3 Seismograms and spectra for 3/13/67 earthquake recorded at MSH and SHI.

Figure 4 Interstation Green's and Transfer function calculated between MSH and SHI for 3/13/67 earthquake.

Figure 5 Phase velocity and group velocity calculated from interstation transfer function between MSH and SHI using 3/13/67 earthquake. (a) Phase velocity. (b) Group velocity from application of multiple filtering technique to interstion Green's function. High numbers correspond to maximum power.

Figure 6 Q values between MSH and SHI measured from interstation transfer function for 3/13/67 earthquake. (a) Q from interstation transfer function using normalized spectrum (see text). (b) Normalized Q values calculated by taking spectral ratios.

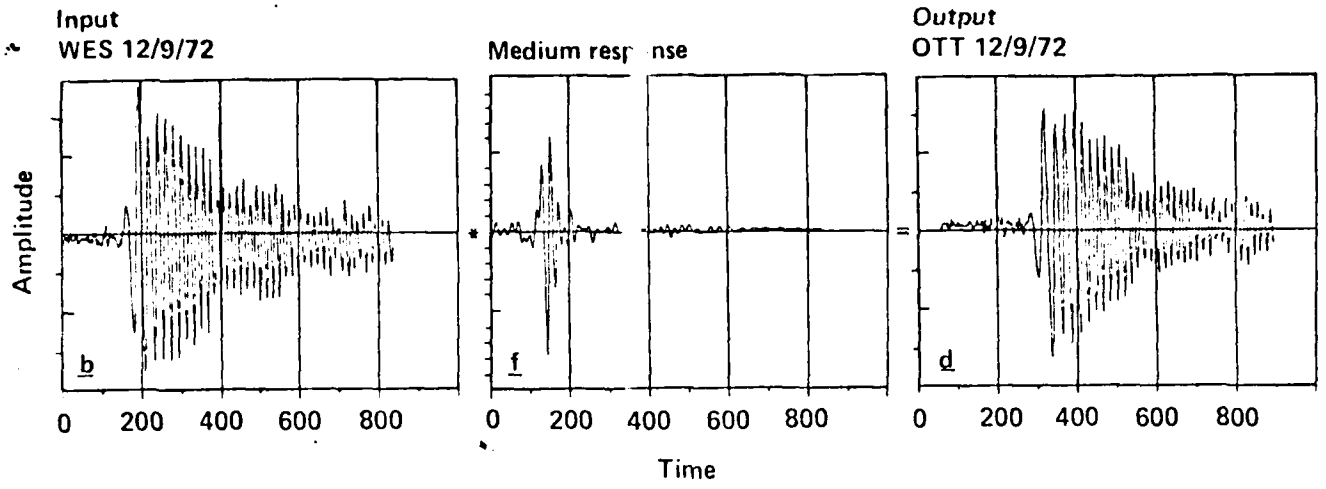
Input
WES 12/9/72
Medium response
Output
OTT 12/9/72
Amplitude
b
f
d
0
200
400
600
800
Time

(a)

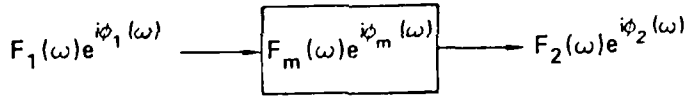
$F_1(\omega)e^{i\phi_1(\omega)}$
$F_m(\omega)e^{i\phi_m(\omega)}$
$F_2(\omega)e^{i\phi_2(\omega)}$

(b)

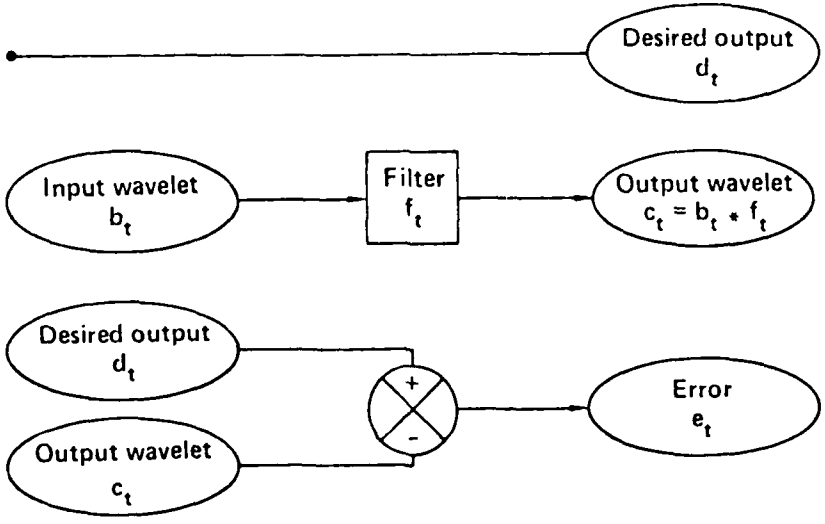
Desired output
d_t
Input wavelet
b_t
Filter
f_t
Output wavelet
$c_t = b_t * f_t$
Desired output
d_t
Output wavelet
c_t
+
-
Error
e_t

(c)

Figure 1

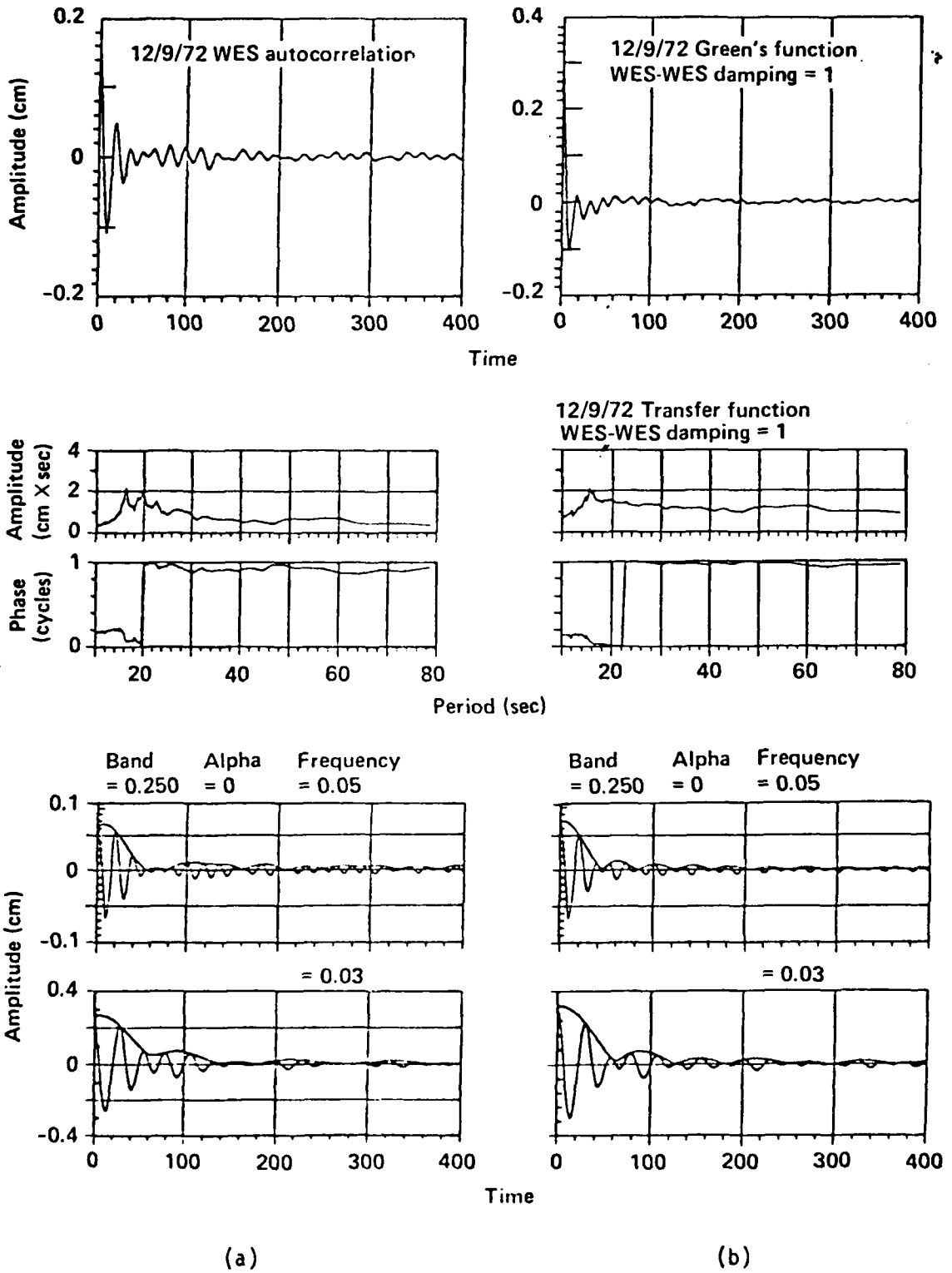
12/9/72 WES autocorrelation
12/9/72 Green's function
WES-WES damping = 1
Amplitude (cm)
Time
12/9/72 Transfer function
WES-WES damping = 1
Amplitude (cm X sec)
Phase (cycles)
Period (sec)
Band = 0.250
Alpha = 0
Frequency = 0.05
= 0.03
Amplitude (cm)
Time
(a)
(b)

Figure 2

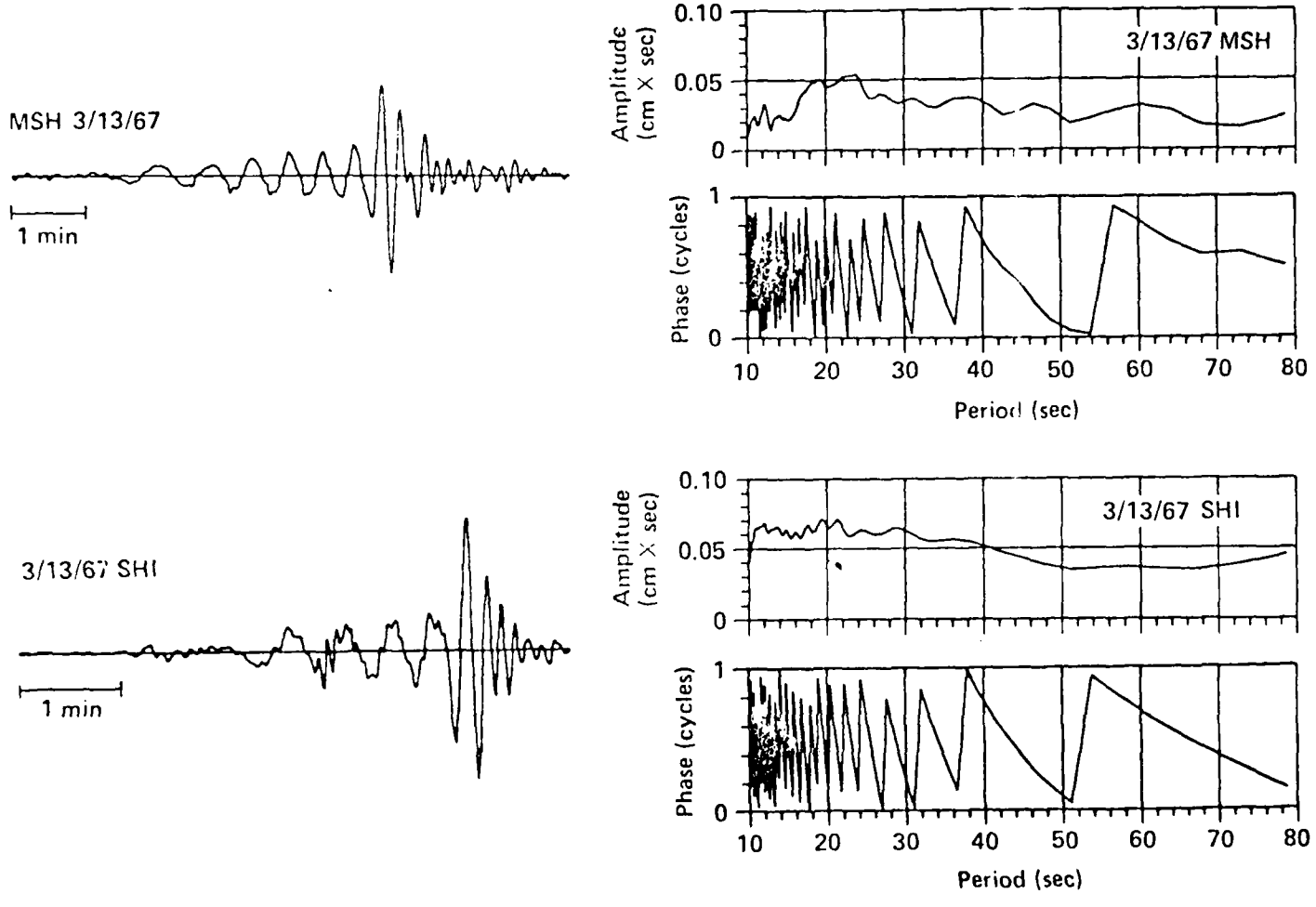
MSH 3/13/67
1 min
3/13/67 SHI
1 min
Amplitude (cm × sec)
0.10
0.05
0
3/13/67 MSH
Phase (cycles)
1
0
10
20
30
40
50
60
70
80
Period (sec)
Amplitude (cm × sec)
0.10
0.05
0
3/13/67 SHI
Phase (cycles)
1
0
10
20
30
40
50
60
70
80
Period (sec)

Figure 3

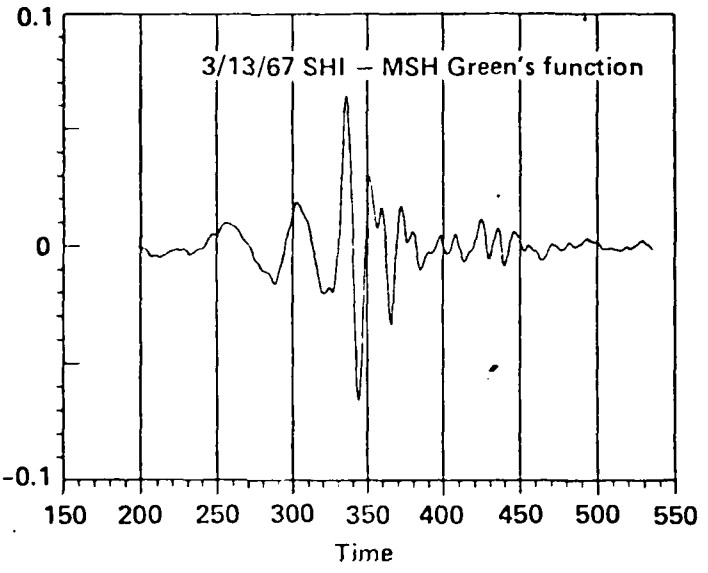
3/13/67 SHI – MSH Green's function
0.1
0
-0.1
150
200
250
300
350
400
450
500
550
Time

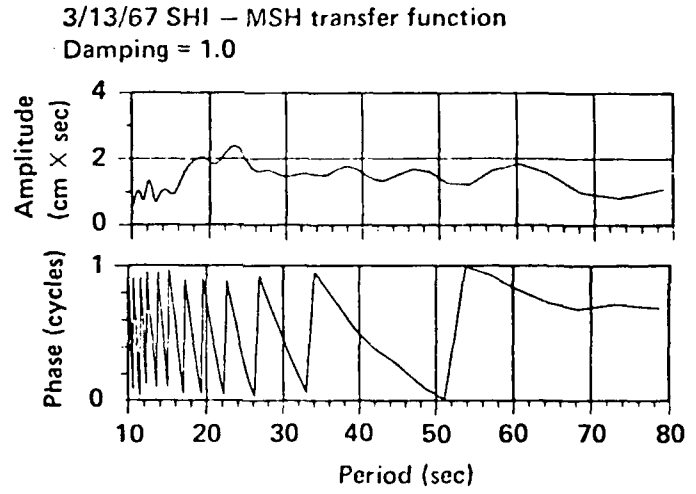
3/13/67 SHI – MSH transfer function
Damping = 1.0
Amplitude (cm × sec)
4
2
0
Phase (cycles)
1
0
10
20
30
40
50
60
70
80
Period (sec)

Figure 4

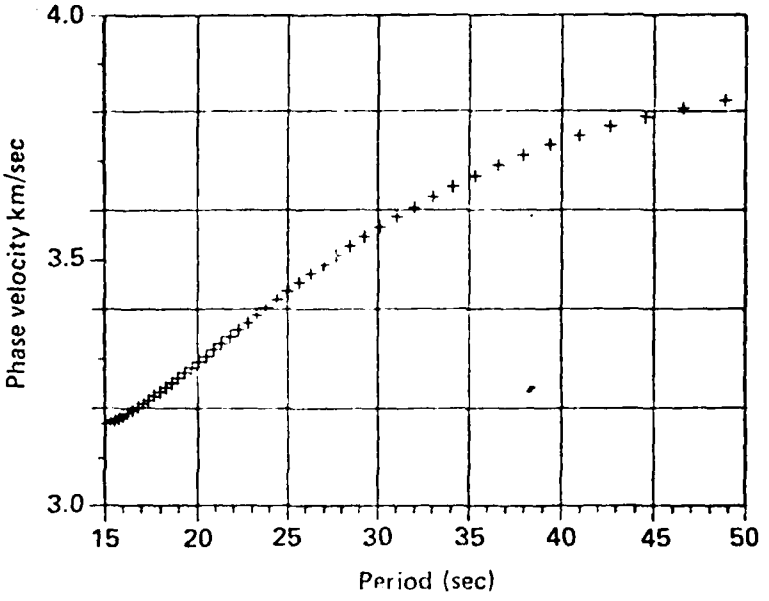
4.0
3.5
3.0
Phase velocity km/sec
15
20
25
30
35
40
45
50
Period (sec)

(a)

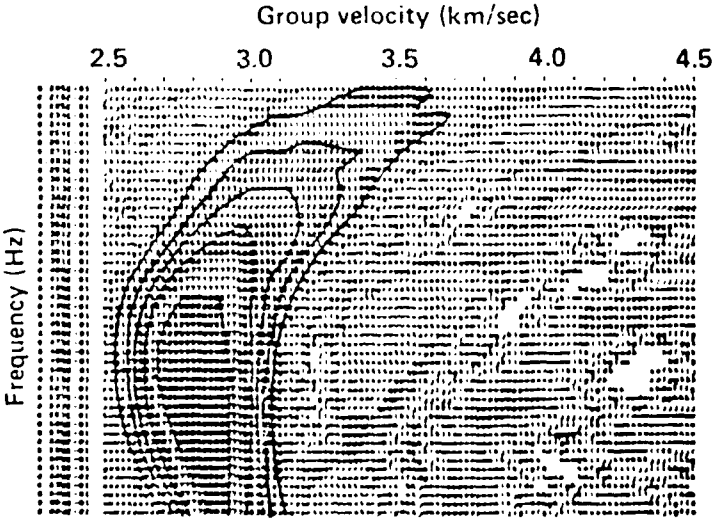
Group velocity (km/sec)
2.5
3.0
3.5
4.0
4.5
Frequency (Hz)

(b)

Figure 5

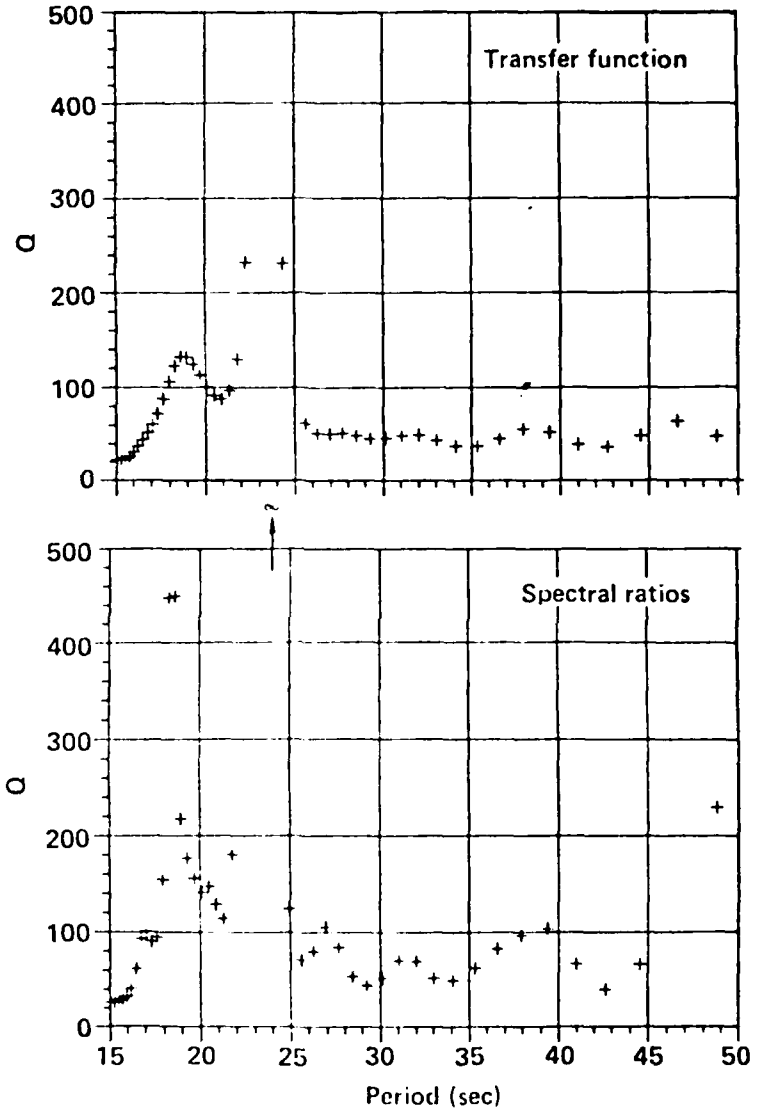
Transfer function
Spectral ratios
Q
Q
500
400
300
200
100
0
15
20
25
30
35
40
45
50
Period (sec)

(a)

(b)

Figure 6

III. SUMMARY OF CRUSTAL STRUCTURE IN THE MIDDLE EAST

Structure and Seismic Properties of the Alpine-Himalayan Zone, K.M. Tubman and M.N. Toksöz

Surface Wave Propagation: Velocities and Attenuation

We have made phase velocity, group velocity, and attenuation measurements for both Rayleigh and Love waves between the periods of 10 and 60 seconds in the Middle East and Southern Asia. Figure 1 shows some of the paths which have been used. These new data have been added to other available measurements (Niazi, 1968; Patton, 1978; Knopoff and Fouda, 1975; Bird, 1976; Bird and Toksöz, 1977). As can be seen from Figure 1, coverage of the Middle East and South Central Asia is very good.

When measuring velocities, an effort is made to choose stations and events so that all lie along the same great circle. Interstation velocities can then be calculated using a method developed by Taylor and Toksöz (1980). This method is a modification of that of Dziewonski et al. (1969). Wiener deconvolution is used to find the transfer function of the interstation medium. This transfer function represents the observed signal at the second station, given an impulse source at the first station. It contains information about the phase and group delay of waves travelling between stations. This method is particularly useful for closely spaced stations. In this situation the use of the cross-correlogram, as was done by Dziewonski et al. (1969), can lead to errors in the calculation of group velocities.

Figure 2 gives a comparison of group velocities for

different regions. These show wide variations. The velocities in Tibet are markedly different and much lower. Paths across the Arabian Peninsula have the highest velocities. However, these are somewhat lower than the Canadian Shield velocities. It is interesting to note that the velocities vary significantly within a given region such as Iran.

To determine structure for slightly different paths, we inverted both phase and group velocities. Phase and group velocity data in Iran are shown in Figure 3. The velocities across the Iranian plateau are noticeably different from those along the Zagros mountains. The airy phase is observed at longer periods under the Zagros, indicating a thicker crust than under the plateau. At longer periods (greater than 35 seconds) the velocities along the Zagros become higher than those across the plateau. This is most likely due as much to low velocities in the lower crust-upper mantle under the plateau as to high velocities in the Zagros.

These conclusions are supported by a study of P_n waves across the Iranian plateau which gives a low P_n velocity of 7.9 km/sec. Chen et al. (1980) also found low P_n velocities (8.0 km/sec) in Iran, with no evidence for S_n propagation across the Iranian plateau (Chen, 1979, personal communication). Canitez and Toksöz (1980) found P_n velocities of 7.9 km/sec under the eastern Turkish plateau. Under the Zagros belt, however, P_n velocities are high (8.1 km/sec) and the crust is thicker - about 50 km (Islami, 1972; Akascheh and Nasseri, 1972).

The surface wave velocities were inverted giving a crustal thickness of 45-50 km in Iran. Phase and group velocities were inverted simultaneously for shear velocity using a maximum likelihood technique. The inversion is weighted in both model and data space. Chen et al. (1980) suggest a crustal thickness of 34 km in northern Iran and 49 km in the south. The surface wave velocities inverted were for the path SHI-MSH. MSH is in northeastern Iran and SHI is to the southwest of the Zagros, so the derived structure gives a good average for Iran.

Phase and group velocity data for Tibet are shown in Figure 4 along with the theoretical models fitted. The crustal thickness in Tibet is 70 km. The velocity profiles are shown in Figure 5. These indicate a low velocity zone within the crust. The resolution of the surface wave data is not sufficient to determine the presence of the low velocity zone in the P velocity profile. However, the velocity models based on refraction studies also suggest a low velocity zone in the crust (Teng et al., 1980).

Phase and group velocities determined for the Arabian Peninsula are shown in Figure 6. Also shown are velocities from Knopoff and Fouda (1975) and Niazi (1968). Phase velocities for the Canadian Shield (Brune and Dorman, 1963) are given for comparison. The Arabian Peninsula is generally considered to be a simple stable shield area, but Figure 6 demonstrates systematic variations in velocities. Both phase and group

velocities display a trend towards higher velocities to the north and to the west. The north-south variation can be seen by comparing the curves for the paths AAE-SHI, Red Sea-SHI, SHI-HLW, and SHI-JER. The velocities steadily increase as the path moves northward. An increase in velocity is also seen from the east to the west, as shown by the curves for Arabian Sea-JER and Gulf of Aden-JER. The differences decrease at longer periods, indicating a more uniform structure at depth. An inversion of the velocities along the path from the Red Sea to SHI yields a crustal thickness of about 38 km. This path crosses the central region of the peninsula so it can be taken as an average structure for Arabia.

Attenuation values for the surface waves determined using the method of Tsai and Aki (1969) are shown in Figures 7-9. Values given in Figure 7 are for Rayleigh waves and the path SHI-MSH in Iran. Attenuation is least between periods of 20 and 25 seconds. Q decreases as period decreases from 20 seconds. This is probably due to the combination of scattering and lower pressures at upper layers. At pressures less than about 2 kb, Q increases significantly with pressure (Toksöz et al., 1979; Johnston et al., 1979; Johnston and Toksöz, 1980). There are peaks and low points in the Q^{-1} curve at longer periods. It is not yet clear whether these are due to change with depth of physical attenuation in layers or whether they are due to scattering or frequency dependence of Q. A similar pattern of peaks and

lows persists in Tibet (Figure 8) and in Turkey (Figure 9). These areas also have low velocities in the lower crust (Bird, 1976; Bird and Toksöz, 1977; Chen and Molnar, 1980; Canitez and Toksöz, 1980; Kenar and Toksöz, 1980).

To determine the causes of variation of measured attenuation with period, a systematic study needs to be undertaken. The attenuation peaks and minima, shown in Figure 10, are too sharp to be easily explainable by change of Q with depth. Selective scattering of certain wavelengths by structural heterogeneities can give strong amplitude variations and apparent peaks in Q^{-1}. At higher frequencies ($f > 1$ hz), Q^{-1} may be frequency dependent and may have some relaxation peaks (Aki, 1980; Spencer, 1981). It is not clear whether such peaks may play an important role in the period range of 10-100 sec. Comparison of short period Q^{-1} values obtained from body waves and higher modes (Lg, Rg) with those of fundamental mode Rayleigh and Love waves may shed light on the importance of frequency dependence of Q.

References

Akascheh, B. and S. Nasseri, Die machtigkeit der erdkruste in Iran, J. Earth Space Phys., 1, 1972.

Aki, K., Scattering and attenuation of shear waves in the lithosphere, J. Geophys. Res., 85, 6496-6504, 1980.

Bird, G.P., Thermal and mechanical evolution of continental convergence zones: Zagros and Himalayas, Ph.D. Thesis, M.I.T., Cambridge, MA, 1976.

Bird, G.P. and M.N. Toksöz, Strong attenuation of Rayleigh waves in Tibet, Nature, 266, 163-165, 1977.

Brune, J. and J. Dorman, Seismic waves and earth structure in the Canadian Shield, Bull. Seism. Soc. Am., 53, 167-210, 1963.

Canitez, N. and M.N. Toksöz, Crustal structure in Turkey, Tectonophysics, in press, 1980.

Chen, C.Y., W.P. Chen and P. Molnar, The uppermost mantle P wave velocities beneath Turkey and Iran, Geophys. Res. Lett., 7, 77-80, 1980.

Chen, W.P. and P. Molnar, Constraints on the seismic wave velocity structure beneath the Tibetan Plateau and their tectonic implications, J. Geophys. Res., in press, 1980.

Dziewonski, A., S. Block and M. Landisman, A technique for the analysis of transient seismic signals, Bull. Seism. Soc. Am., 59, 427-444, 1969.

Islami, A.A., A study of the depth of the Mohorovicic discontinuity in western Iran and the velocity of the P_n wave, J. Earth and Space Phys., 1, 1-12, 1972.

Johnston, D.H. and M.N. Toksöz, Ultrasonic P and S wave attenuation in dry and saturated rocks under pressure, J. Geophys. Res., 85, 925-936, 1980.

Johnston, D.H., M.N. Toksöz and A. Timur, Attenuation of seismic waves in dry and saturated rocks: II. Mechanisms, Geophysics, 44, 691-711, 1979.

Kenar, O. and M.N. Toksöz, Crustal structure and attenuation in Turkey from surface wave data, in preparation, 1980.

Knopoff, L. and A.A. Fouda, Upper mantle structure under the Arabian Peninsula, Tectonophys., 26, 121-134, 1975.

Niazi, M., Crustal thickness in the Central Saudi Arabian Peninsula, Geophys. J. R. Astr. Soc., 15, 545-547, 1968.

Patton, H.J., Source and propagation effects of Rayleigh waves from central Asian earthquakes, Ph.D. Thesis, M.I.T., Cambridge, MA, 1978.

Spencer, J.W.,Jr., Stress relaxations at low frequencies in fluid-saturated rocks: attenuation and modulus dispersion, J. Geophys. Res., in press, 1981.

Taylor, S.R. and M.N. Toksöz, Measurement of interstation phase and group velocities and Q using Wiener deconvolution, Bull. Seism. Soc. Am., submitted, 1980.

Teng, Ji-wen, Xiong Shao-po, Sun Ke-zhong, Yin Zhou-xun, Yao Hung, Chen Li-fang, Mu Teng, Lai Ming-hui, Wu Ming-chu, Su De-yuan, Wang Shao-zhou, Huang Wen-jian, Ou Ren-sheng, Hao We-cheng, Shao An-min, Gao En-yuan, Wang Meng-Lin, Lin Zhong-yang, Qu Ke-xin, Explosion seismic study for velocity distribution and structure of the crust and upper mantle from Damxung to Yadong of Xizang Plateau, Proc. Symp. on Qinghai-Xizang Plateau, 81-82, 1980.

Toksöz, M.N., D.H. Johnston and A. Timur, Attenuation of seismic waves in dry and saturated rocks: I. Laboratory measurements, Geophysics, 44, 631-690, 1979.

Tsai, Y.B. and K. Aki, Simultaneous determination of the seismic moment and attenuation of seismic surface waves, Bull. Seism. Soc. Am., 59, 275-287, 1969.

Figure Captions

Figure 1 - Map showing some of the paths crossing the Alpine-Himalayan convergence zone for which surface wave velocities have been measured.

Figure 2 - Rayleigh wave group velocities along various paths in South Central Asia.

Figure 3 - Rayleigh wave phase and group velocities in Iran.

Figure 4 - Rayleigh wave phase velocity (c) and group velocity (u) for the average of all paths crossing Tibet. Data from Bird (1979) and Chen and Molnar (1980).

Figure 5 - Crustal S-wave velocity model resulting from the inversion of Rayleigh wave data combined with the refraction P-wave profile (Teng et al., 1980) shown at right. Dotted area indicates the region of high attenuation.

Figure 6 - Rayleigh wave phase and group velocities across the Arabian Peninsula.

Figure 7 - Q^{-1} values for Rayleigh waves along the path SHI-MSH in Iran.

Figure 8 - Q^{-1} values for Rayleigh waves in Tibet.

Figure 9 - Q^{-1} values for Love waves in Turkey.

Figure 10 - Comparison of crustal structures in different regions. Heavy lines indicate the bottom of the crust (Moho discontinuity). The number in each layer is the shear velocity. "Iran" is the average model for the Iranian Plateau.

The Arabian Peninsula (a shield) model is included for comparison.

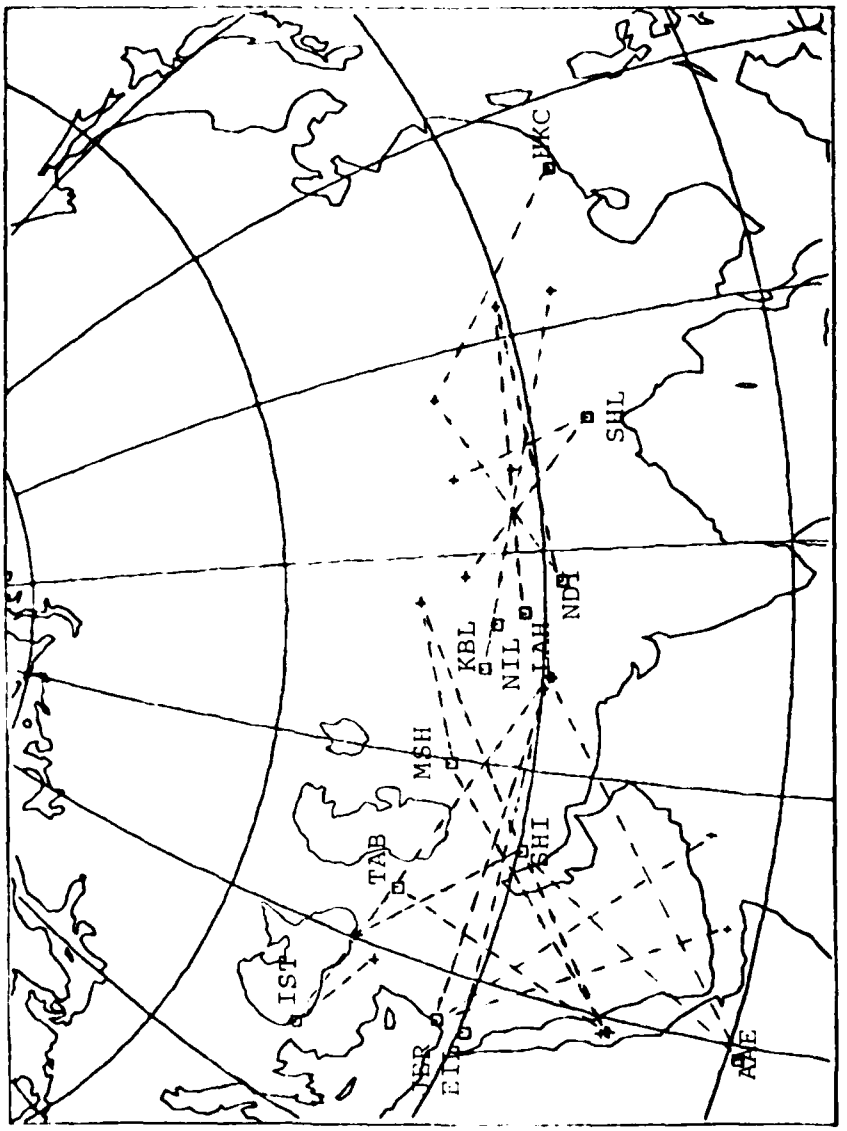

Figure 1

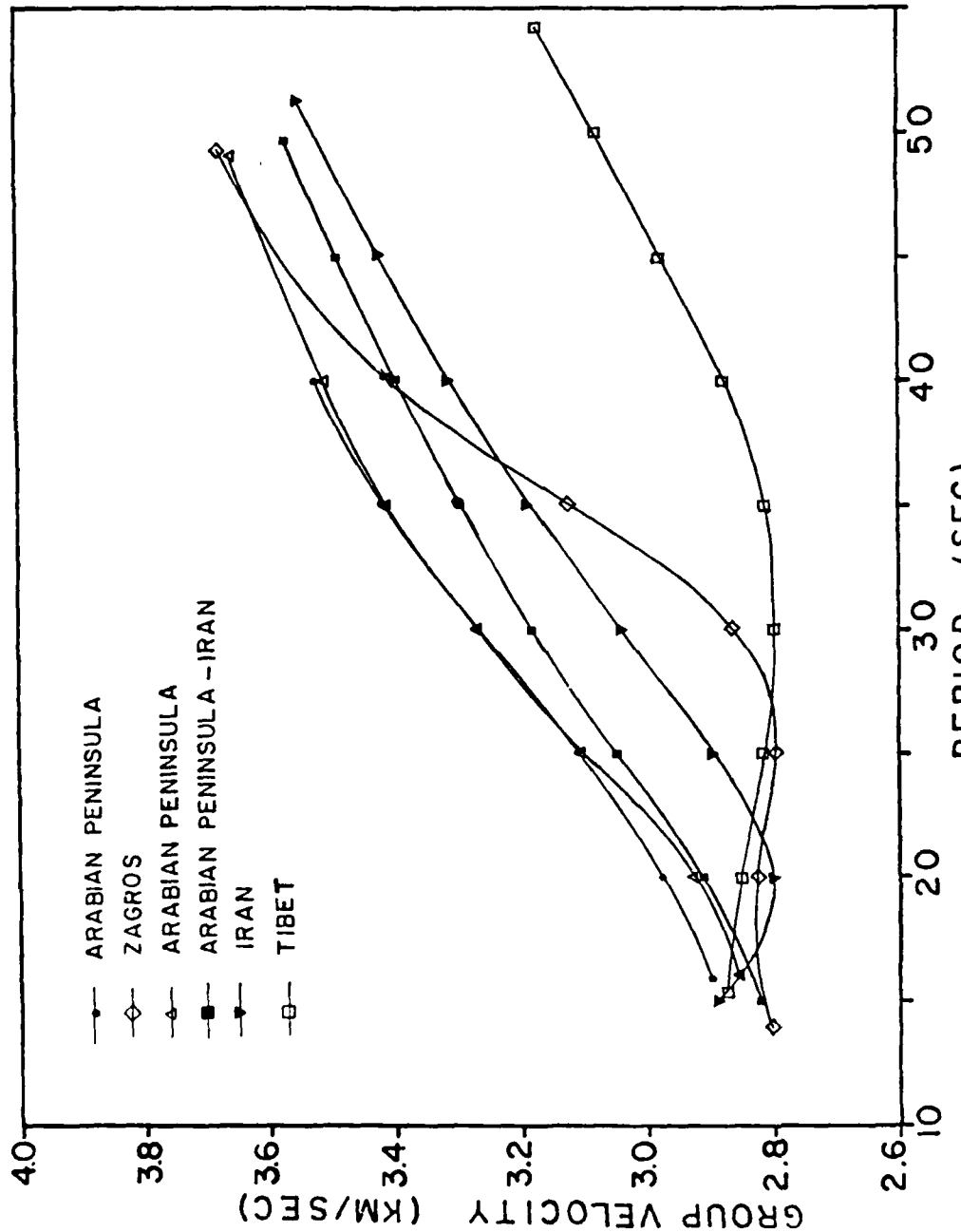
ARABIAN PENINSULA
ZAGROS
ARABIAN PENINSULA
ARABIAN PENINSULA-IRAN
IRAN
TIBET
GROUP VELOCITY (KM/SEC)
PERIOD (SEC)
4.0
3.8
3.6
3.4
3.2
3.0
2.8
2.6
10
20
30
40
50

Figure 2

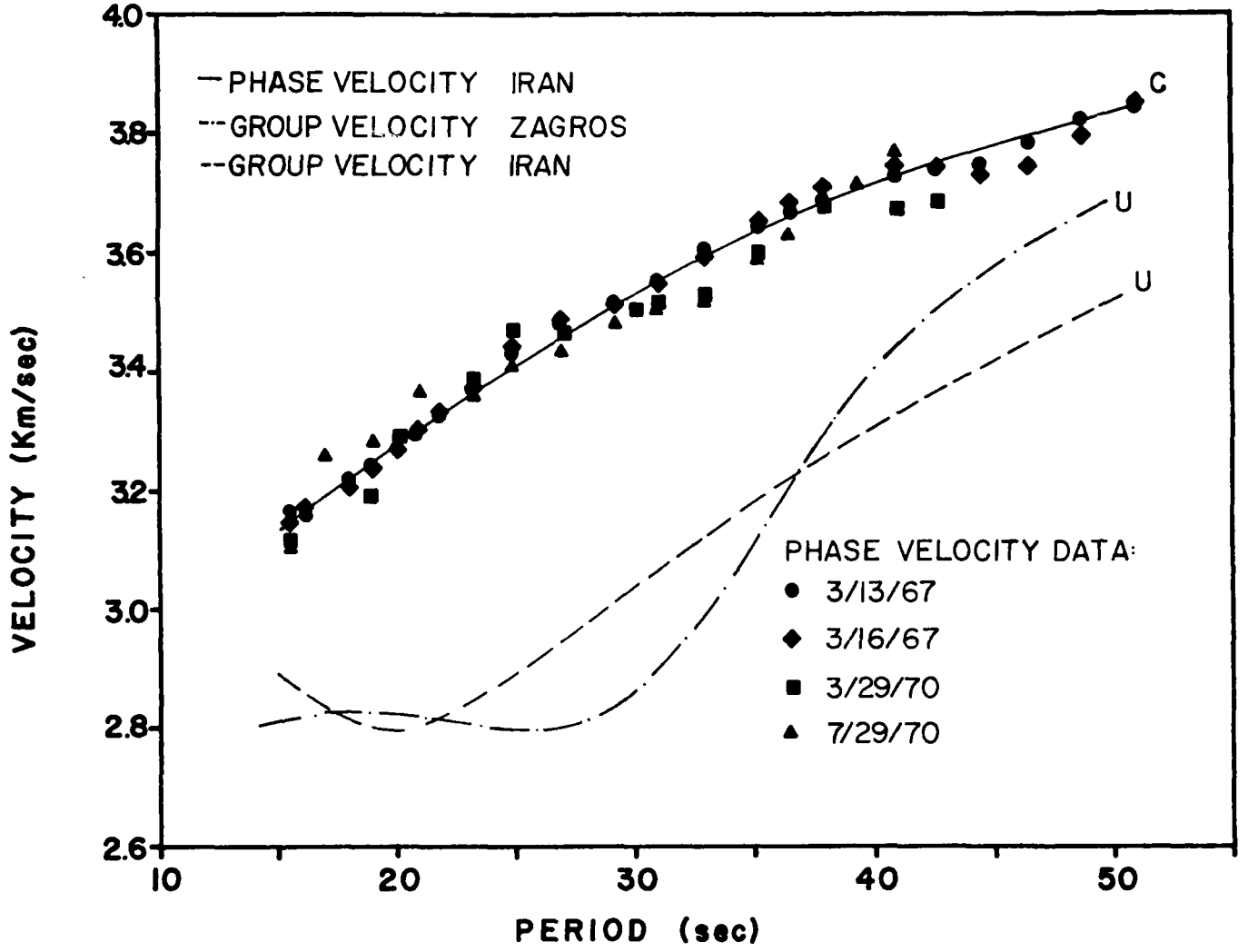
PHASE VELOCITY IRAN
GROUP VELOCITY ZAGROS
GROUP VELOCITY IRAN
C
U
U
PHASE VELOCITY DATA:
3/13/67
3/16/67
3/29/70
7/29/70
VELOCITY (Km/sec)
4.0
3.8
3.6
3.4
3.2
3.0
2.8
2.6
10
20
30
40
50
PERIOD (sec)

Figure 3

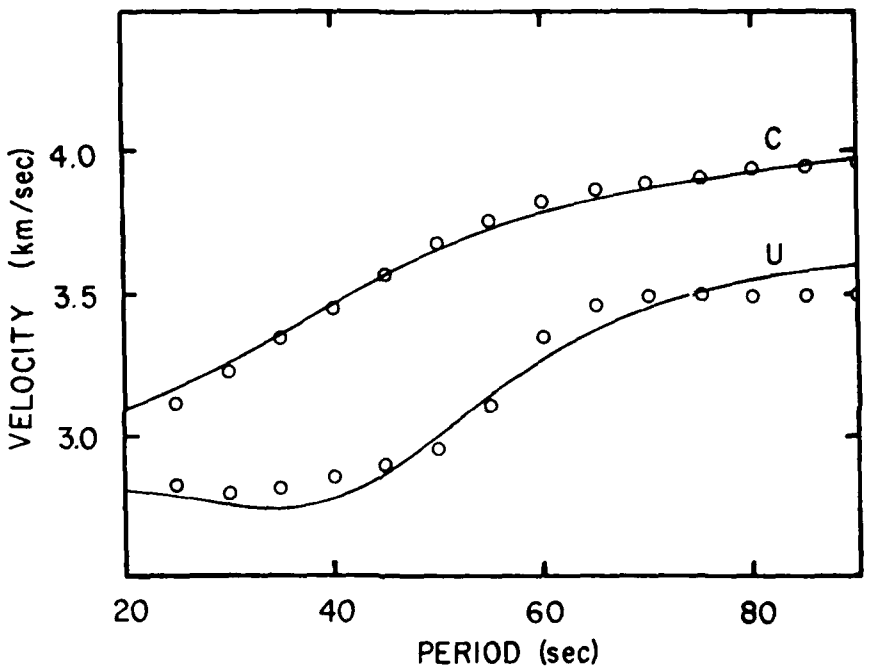

Figure 4

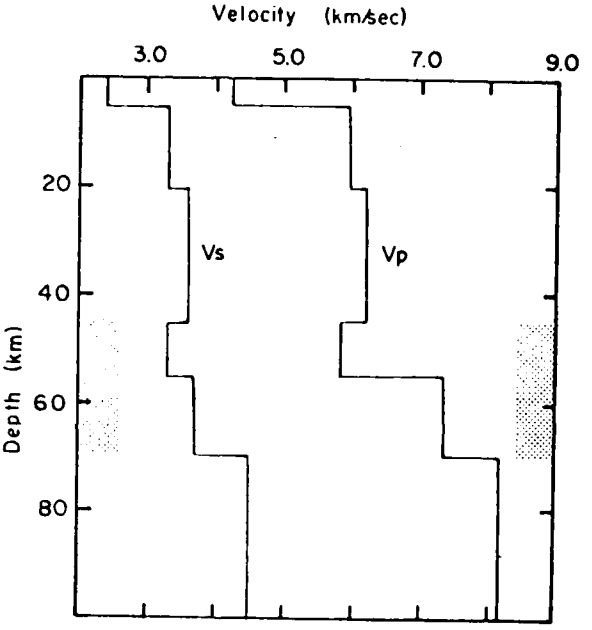

Figure 5

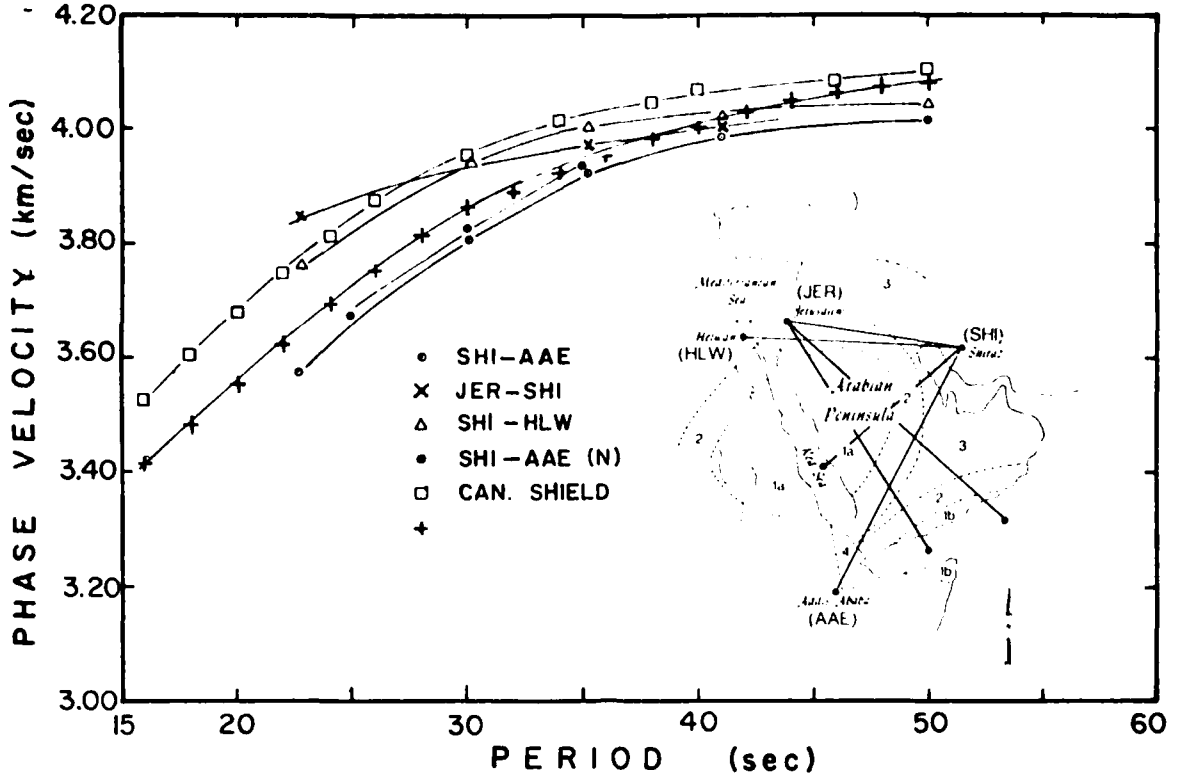
PHASE VELOCITY (km/sec)
4.20
4.00
3.80
3.60
3.40
3.20
3.00
15
20
30
40
50
60
PERIOD (sec)
SHI–AAE
JER–SHI
SHI – HLW
SHI – AAE (N)
CAN. SHIELD
(JER)
(SHI)
(HLW)
Arabian
Peninsula
(AAE)

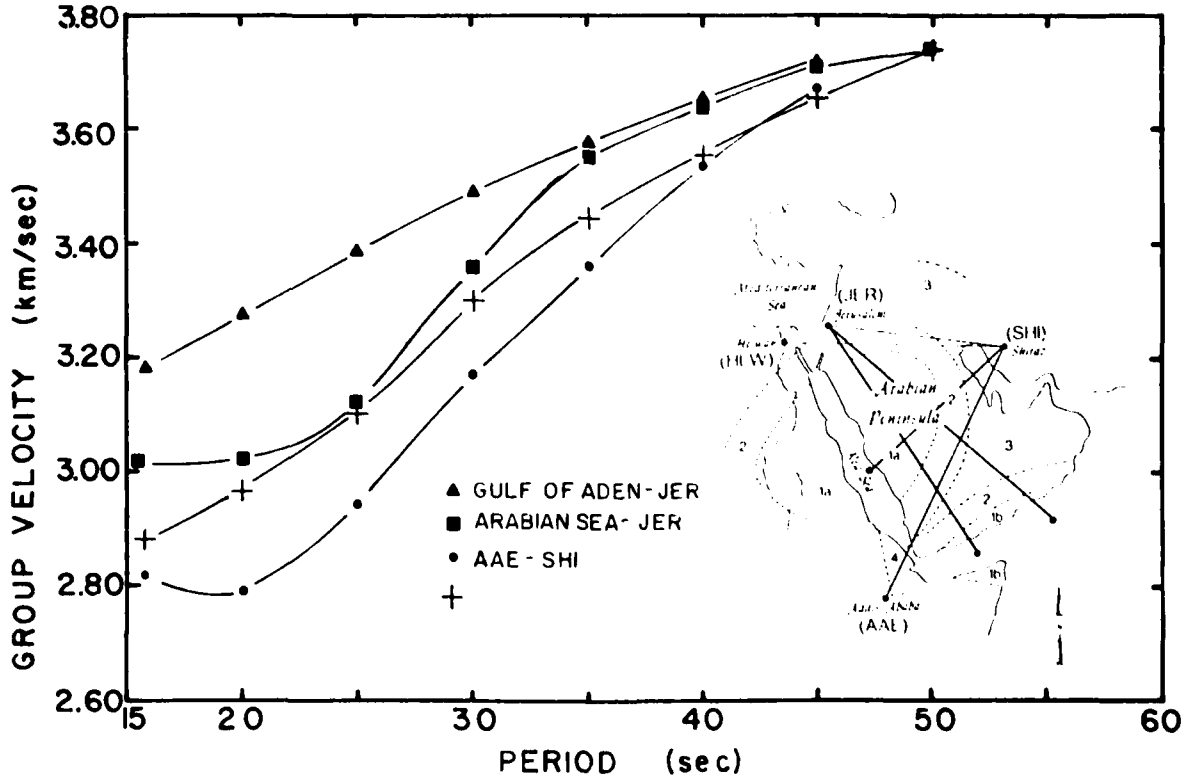
GROUP VELOCITY (km/sec)
3.80
3.60
3.40
3.20
3.00
2.80
2.60
15
20
30
40
50
60
PERIOD (sec)
GULF OF ADEN-JER
ARABIAN SEA- JER
AAE - SHI
(JER)
(SHI)
(HLW)
Arabian
Peninsula
(AAE)

Figure 6

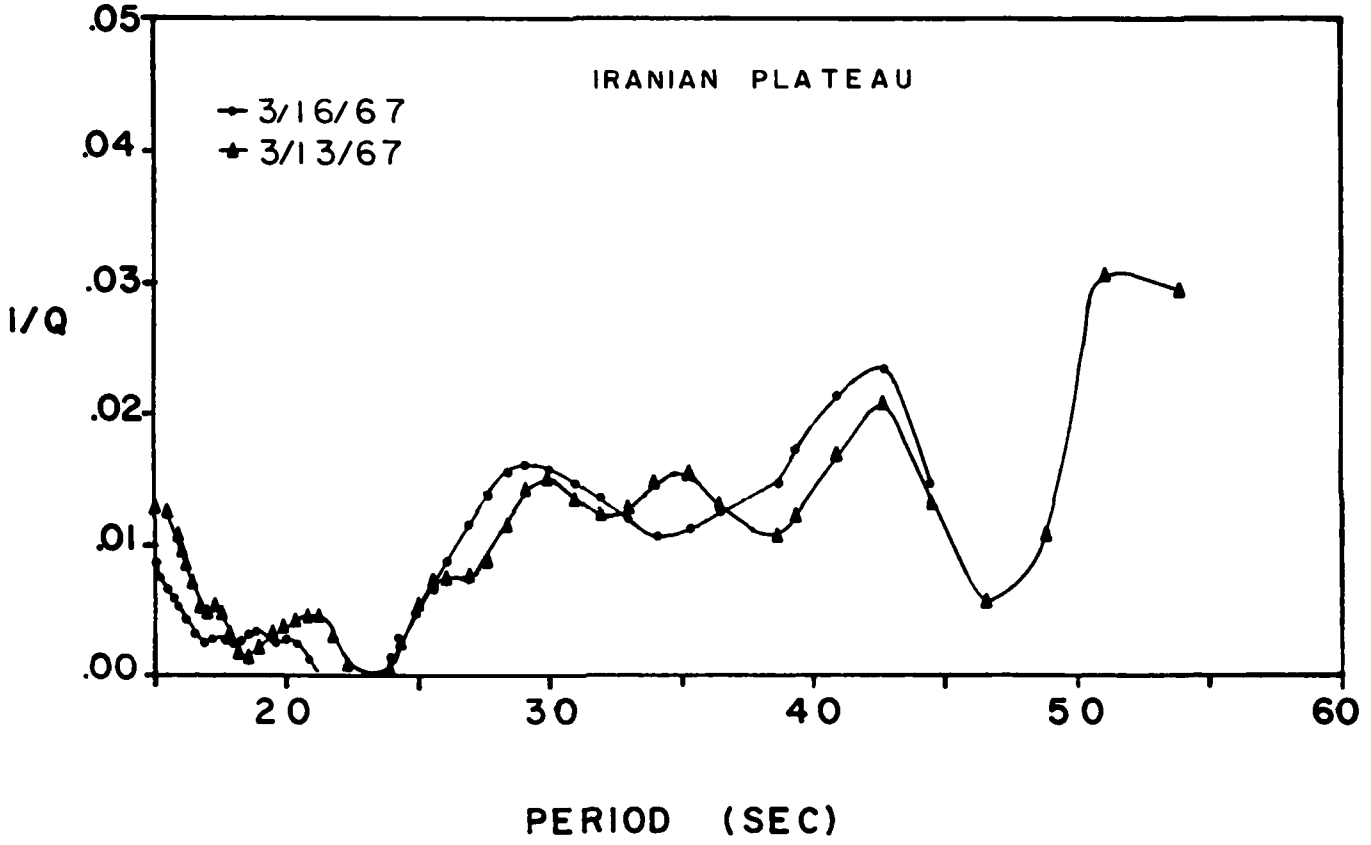
IRANIAN PLATEAU
3/16/67
3/13/67
1/Q
.05
.04
.03
.02
.01
.00
20
30
40
50
60
PERIOD (SEC)

Figure 7

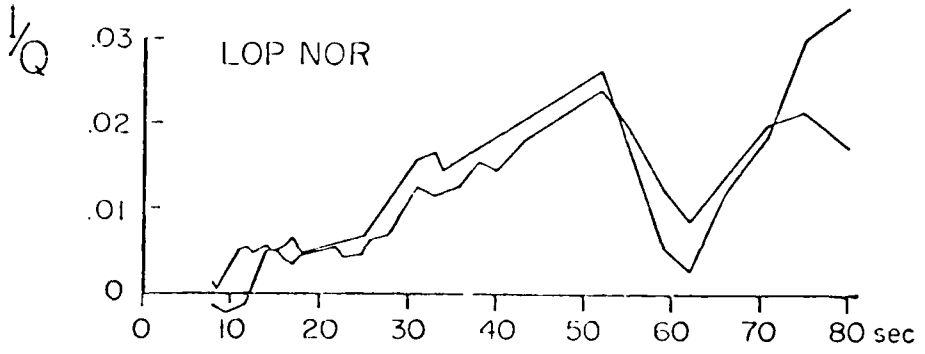

Figure 8

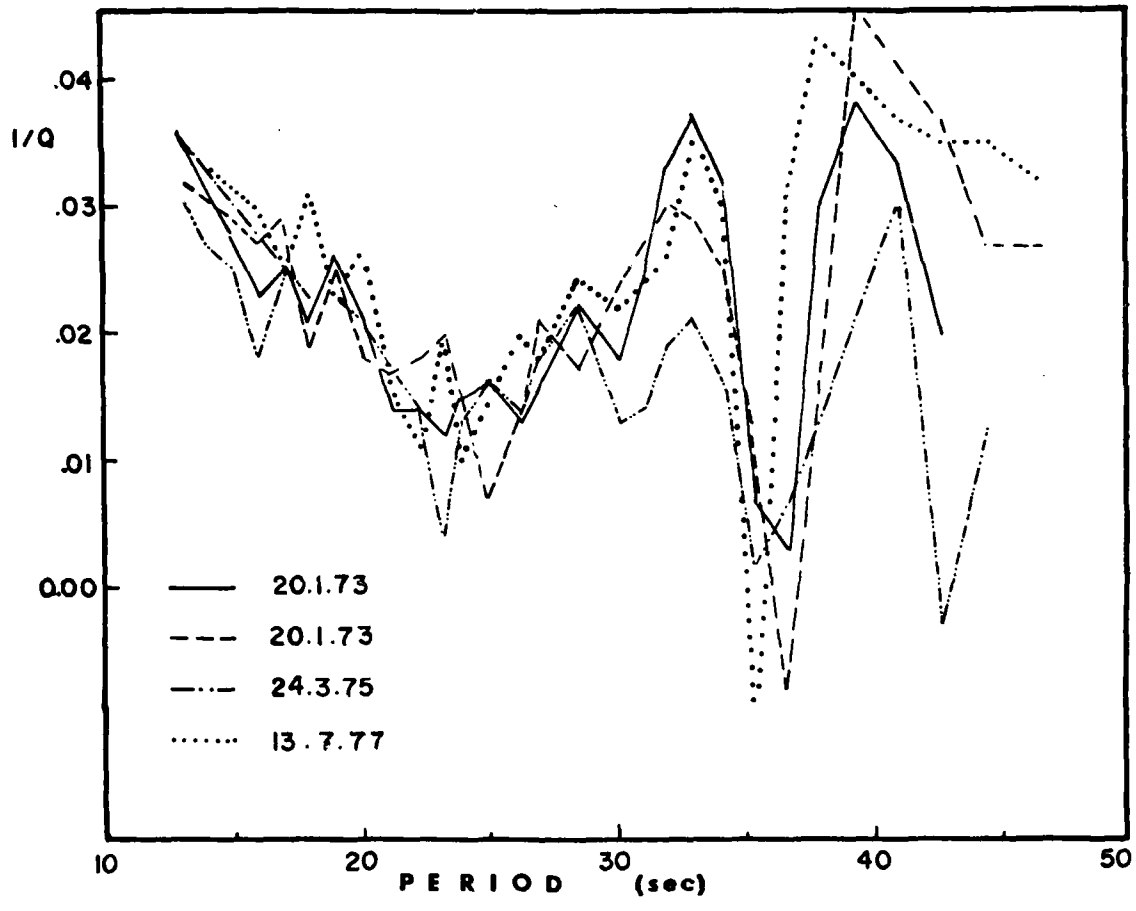
.04
1/Q
.03
.02
.01
0.00
20.1.73
20.1.73
24.3.75
13.7.77
10
20
30
40
50
PERIOD (sec)

Figure 9

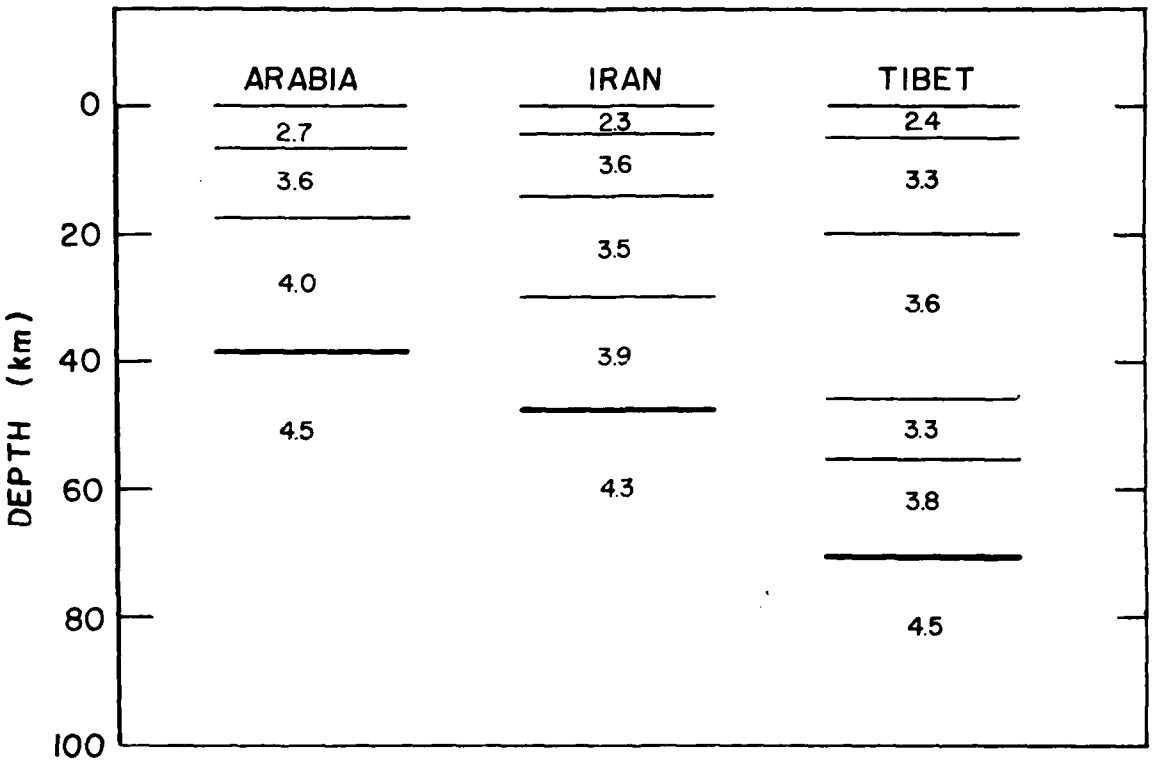
ARABIA
IRAN
TIBET
DEPTH (km)
0
20
40
60
80
100
2.7
3.6
4.0
4.5
2.3
3.6
3.5
3.9
4.3
2.4
3.3
3.6
3.3
3.8
4.5

Figure 10

IV. SOURCE PROPERTIES OF SHALLOW EARTHQUAKES

Source Characterization of Two Reykjanes Ridge Earthquakes: Surface Waves and Moment Tensors; P Waveforms and Non-Orthogonal Nodal Planes, A.M. Trehu, J.L. Nabelek and S.C. Solomon, J. Geophys. Res., in press, 1981.

Abstract

Well constrained fault plane solutions from P wave first motions for mid-ocean ridge normal faulting earthquakes usually require non-orthogonal nodal planes. Local structural effects and/or departures from a double couple source mechanism have been invoked to explain this phenomenon. In order to obtain an independent determination of the source mechanisms for the April 24, 1970 and April 3, 1972 events on the southern Reykjanes Ridge, we invert the Rayleigh wave radiation pattern to obtain the source moment tensor. The moment tensor formulation should be particularly well-suited to this problem because it is not restricted a priori to a double couple source mechanism. A potential drawback of the technique, however, is the requirement that phase velocities along the earthquake-station paths be known very accurately in order to obtain the source phase from the observed phase and an objective of this study was to determine whether a regionalized phase velocity model compiled from published dispersion curves is adequate. The results of the moment tensor inversion for both events indicate shallow normal faulting with the tension axis approximately horizontal and perpendicular to the local strike of the ridge. Apparent departures from a pure double couple source seem to result from errors in the data and the poor

resolution of the M_{xz} and M_{yz} components of the moment tensor for shallow sources. After performing the inversion under a series of increasingly more stringent constraints we conclude that the data for both events are compatible with pure double couple sources with moments of 4.8 and 7.5 x 10^{24} dyne-cm, respectively. We then show that interference between P, pP, and sP due to shallowness of the source can account for the observed non-orthogonality and match the observed P waveforms for the April 3, 1972 event with theoretical seismograms calculated for a shear fault whose orientation is consistent with the surface wave solution. The best fit to the data is obtained for a long, narrow fault (13 km by 3 km), with rupture initiating near the sea floor. The moment indicated by the P waves is 7.5 x 10^{24} dyne-cm. These source parameters give an average displacement of about 60 cm and a stress drop of 30-60 bars, taking into account various uncertainties. Although we might expect attenuation to be high in the mid-ocean ridge environment, the average attenuation required to fit the teleseismic data is not higher than normal ($t^* = 1$ sec). The P waves from the April 24, 1970 earthquake were too small to be suitable for quantitative modeling by synthetic seismograms but are qualitatively consistent with a shallow fault model similar to that for the larger event. We conclude that the faulting process described by these two earthquake mechanisms is directly related to the formation of rift valley topography.

INTRODUCTION

Fault plane solutions of ridge crest earthquakes regularly indicate non-orthogonal nodal planes for normal faulting events [Sykes, 1967, 1970, Solomon and Julian, 1974]. Because orthogonal nodal planes are implicitly required by the double couple faulting mechanism from which the fault plane solution is derived, either a process must be found whereby the true body wave radiation pattern is distorted to yield an apparent non-orthogonality or an alternative faulting mechanism must be found. Several explanations for this phenomenon have been proposed. Solomon and Julian [1974] demonstrated that a low velocity wedge below the ridge, the existence of which is predicted by thermal models and confirmed by surface wave and refraction studies, can focus rays from a source on the ridge, thus collapsing the apparent dilatational quadrant. Other explanations include: 1) an explosive volcanic component superimposed upon the double couple [Solomon and Julian, 1974]; 2) a mechanism of extensional failure in a porous, fluid saturated medium [Robson et al., 1968]; and 3) interference between P, pP and sP resulting from the shallowness of the source [Hart, 1978].

Focusing of rays below the source or interference at the surface are explanations invoking structural effects which would distort the apparent body wave radiation pattern of a double couple fault but which should not strongly affect the surface wave radiation pattern. A true source mechanism of an explosion or of tensional cracking, on the other hand, should be manifested in the surface waves as well as in the body waves. An independent source mechanism determination

obtained from the surface waves should therefore help to distinguish the cause of the non-orthogonality. The recently developed technique of inverting surface wave data to obtain the source moment tensor should be especially suited to this problem as the moment tensor is not restricted a priori to correspond to a double couple. The surface wave solution can then provide a base from which the body wave problem can be reexamined.

The frequency of teleseismically observable events combined with a fortuitous location with respect to azimuthal coverage by the World Wide Standard Seismograph Network makes the southern Reykjanes Ridge an excellent laboratory for studying the mechanism of faulting on a slowly spreading ridge and the phenomenon of non-orthogonal nodal planes. Although one could argue that the area might be anomalous due to proximity to the Iceland hotspot, topographically and geochemically the ridge south of about 59°N appears to be beyond the hotspot's direct influence [Vogt and Johnson, 1975]. Spreading direction is approximately perpendicular to the ridge and the axis is broken by an axial valley characteristic of its spreading rate. This contrasts with the obliquely spreading, smooth, shallow ridge to the north. The seismicity south of 59°N is also much more characteristic of that of the "average" Mid-Atlantic Ridge [Francis, 1973]. North of 59°N the Reykjanes Ridge is nearly aseismic, resembling in this respect a fast spreading rise. The southern Reykjanes Ridge, on the other hand, has experienced several earthquakes with body wave magnitude m_b up to 5.5 since the inception of the WWSSN. Detailed bathymetric

studies show that the transition between the two regimes is marked by a several-fold increase in offset across the fault scarps which border the axial constructional volcanic pile [Laughton et al., 1979].

Figure 1 is a topographic map of the area showing earthquakes with m_b greater than 5 which were recorded between 1962 and 1978. Most of the ridge earthquakes display the pronounced distortion of the body wave radiation pattern characteristic of mid-ocean ridge events. Note, however, that for the April 24, 1970 earthquake at 56°N compressional first arrivals appear nearly to cover the focal sphere. This mechanism, determined by Einarsson [1979], originally inspired our interest in the area. Einarsson suggested that this event might be an extreme manifestation of the non-orthogonality. An analysis of the surface wave radiation pattern was undertaken to determine whether this event might perhaps be an explosion.

In this paper, the Rayleigh wave displacement spectra from the April 24, 1970 Reykjanes Ridge earthquake are inverted to obtain the source moment tensor. A moment tensor solution was also obtained for the April 3, 1972 event (Figure 1), which yielded a well-constrained fault plane solution from P wave first motions requiring nodal planes separated by approximately 60°. The locations of these events are given in Table 1. The moment tensor solutions for both events indicate shallow normal faulting with the tension axis perpendicular to the strike of the spreading center.

We then show that the apparent non-orthogonality of the

body wave solution for the April 3, 1972 event may be attributed to interference effects between direct P, pP and sP and that the body waveforms can be reconciled with the source mechanism obtained from the surface waves. We conclude that the April 24, 1970 event was too small to yield a reliable fault plane solution if the amplitude of the back· ound noise and expected amplitude of the first arrival are considered. The observed body waves from the slightly larger April 3, 1972 event, however, are matched with synthetic seismograms calculated for a finite fault with an orientation corresponding to the moment tensor solution and suggest a narrow, long, shallow fault plane which reached the seafloor. This mechanism may correspond to faulting which breaks through the thin axial crust and contributes to the topography of rift valley and mountains.

SOURCE MECHANISM FROM SURFACE WAVES

Background

Surface waves are especially useful for studying oceanic earthquakes because such events are often too small to yield reliable fault plane solutions [Kafka and Weidner, 1979]; those fault plane solutions which have been obtained for spreading center events raise questions concerning the basic assumptions about the source mechanism. The radiation pattern of surface waves can be used to obtain an independent determination of the source mechanism. Moreover, because the surface waves used for this determination have a longer wavelength than the body waves used for the fault plane solution, they are less affected by structural anomalies immediately below the ridge axis.

The representation of the far field displacement in terms of the moment tensor was first presented by Gilbert [1970] and Gilbert and Dziewonski [1975] for free oscillations and was extended to surface waves by McCowan [1976] and Mendiguren [1977] and to body waves by Stump [1976] and McCowan [1977]. Seismic waves radiated from a source at a given depth can be expressed as a linear combination of the moment tensor components. For surface waves, the inversion to obtain the moment tensor is much more rapid than the traditional trial and error method of calculating theoretical spectra for all possible combinations of strike, dip, and slip of a double couple fault and matching the observed amplitude and phase spectra independently [e.g., Ben-Menahem and Toksöz, 1962, 1963; Mitchell, 1973; Patton, 1976]. Another advantage of the moment tensor representation is that it is not

restricted to a double couple source mechanism and should therefore provide insights into possible departures from this generally assumed faulting model. Other possible mechanisms contain isotropic and/or compensated linear vector dipole components [Knopoff and Randall, 1970]. For example, a tensional crack corresponds to the superposition of an explosion and a compensated linear vector dipole.

The formulation of the problem of retrieving the moment tensor from the vertical component of the Rayleigh wave is given in Appendix I. In summary, the moment tensor components can be retrieved from the real and imaginary parts of the observed source spectrum [Mendiguren, 1977; Patton and Aki, 1979]:

$$\text{Real} = A_{ij}\cos\phi_{ij} = M_{zz}G_2(h,f_i) + (M_{xx}+M_{yy})G_1(h,f_i) - (M_{yy}-M_{xx})G_1(h,f_i)\cos 2\theta_j + 2M_{xy}G_1(h,f_i)\sin 2\theta_j + E_{ij}^{R} \quad (1a)$$

$$\text{Imaginary} = A_{ij}\sin\phi_{ij} = M_{xz}G_3(h,f_i)\cos\theta_j + M_{yz}G_3(h,f_i)\sin\theta_j + E_{ij}^{I} \quad (1b)$$

In (1), A_{ij} and ϕ_{ij} are the amplitude and phase delay observed at station j and frequency f_i after having been corrected for the effects of propagation and the source time function, θ_j is the azimuth of station j with respect to the earthquake, and the E_{ij}^{R} and E_{ij}^{I} are error terms. The G_K are real functions of depth and frequency and are calculated for the appropriate source velocity and density structure using Saito's [1967] algorithm;

G_k calculated for an oceanic model (Table 2) are displayed in Figure 2. For a given depth, the moment tensor components can be obtained from a one step inversion of the real and imaginary parts of the spectrum. Depth can be determined by inverting for the moment tensor at a series of depths and choosing that depth which minimizes the residual $E^2 = \sum_{ij} \{(E_{ij}^R)^2 + (E_{ij}^I)^2\}$.

The resolving power of the inversion is determined by the behavior of the functions G_k over the period range of the data. We see from equation (1a) that, with data from only a single frequency, we cannot independently determine $(M_{xx}+M_{yy})$ and M_{zz}; even with data from a range of frequencies, G_1 and G_2 have too similar a frequency dependence over the frequency range of long period surface wave data to permit independent resolution of the diagonal components for most source depths [Mendiguren, 1977]. The constraint $\sum_{i=1}^{3} M_{ii}=0$, equivalent to no volume change, can be analytically imposed without destroying the linearity of the problem. Under this constraint, however, an explosive component in the source will masquerade as a vertically oriented compensated linear vector dipole. This effect will be examined further in the discussion of the surface wave results. We can also see that G_3 approaches 0 as depth decreases because it is proportional to one of the stress eigenfunctions (Appendix I). This results in poor resolution of the M_{xz} and M_{yz} copmonents for very shallow sources and we may be forced to impose an additional constraint. If we have evidence indicating that the principal stress axes are approximately horizontal and vertical, we can assume

that the imaginary part of the spectrum is due to noise in the data and solve for M_{xx}, M_{yy}, M_{zz}, and M_{xy} with M_{xz} and M_{yz} identically equal to 0. This constrains the corresponding double couple fault mechanism to be either dip-slip with a dip of 45° or vertical strike-slip. At a single frequency, depth cannot be determined from the imaginary part and, even with data from a range of frequencies, the depth resolving power is poor.

A drawback of the moment tensor inversion method is the requirement that the phase velocity along the earthquake-station path be known very accurately [Aki and Patton, 1977] in order to correct the observed phase back to the source. In the moment tensor formulation, amplitude and phase cannot be decoupled without destroying the linearity of the problem (for an example of a non-linear inversion using amplitude data alone,

see Kafka and Weidner, 1979).

The relationship between the observed phase and the ϕ_{ij} of equation (1), in units of cycles, is:

$$\phi_{ij} = \phi_{ij}^{observed} - \phi_{ij}^{instr} + [T_j - D_j/C_{ij}]f_i + 0.125 \pm n$$

where ϕ_{ij}^{instr} is the instrument phase response; T_j is the time between the origin time and the beginning of the digitized record; D_j is epicentral distance in km; C_{ij} is the phase velocity; the constant 0.125 includes the effects of the source time function (assumed to be a step) and the asymptotic expansion of the Hankel function for the notation of equations (A5) and (1); and n is a constant which arises from the periodicity of the phase and is determined by C_{ij}. If we assume that T_j and D_j are known exactly, the error in ϕ_{ij} due

to an error ΔC_{ij} in C_{ij} is $\Delta t_{ij} = (f_i D_j \Delta C_{ij})/C_{ij}$. Numerical experiments [Patton and Aki, 1979] indicate that random errors on the phase of up to $\pm$ 0.125 cycles lead to the introduction of an apparent non-double couple component of 0 to 10%; an error of up to 0.25 cycles can lead to 36% non-double couple. The orientation of the principal axes of the moment tensor, however, remains very stable. For values typical of our dataset, an epicentral distance of 2500 km and a velocity of 4 km/sec, the phase change for a 50 second wave resulting from .25% error in the phase velocity is .13 cycles. For a given error in C, the error increases with increasing epicentral distance and decreasing period.

In his application of the method to a family of earthquakes in central Asia, Patton [1980] began by calculating phase velocities for the station-source paths by the method of Weidner and Aki [1973] using two neighboring earthquakes with different known source mechanisms to separate the path and source effects. The moment tensors of other earthquakes in the region were then calculated using these path parameters. An iterative scheme was adopted whereby, once the mechanism of an earthquake had been determined, its "known" mechanism was used to refine the values of the path parameters. A motivation for conducting the moment tensor inversions for the Reykjanes Ridge earthquakes was to see if reasonable results could be obtained simply by using a regionalized velocity model to correct for propagation and thus obtain a source mechanism solution for a single isolated event. An excellent azimuthal distribution of stations with short,

structurally simple earthquake-station paths coupled with the availability of Rayleigh wave phase velocity studies in the North Atlantic Ocean and adjacent continental regions suggested that such an approach might be fruitful.

Data

For the April 24, 1970 event, vertical component Rayleigh waves from 23 stations of the WWSSN and Canadian network were digitized at an interval of 2 seconds. Each digitized time series was then Fourier analyzed and corrected for instrument response, geometrical spreading, and attenuation. The Q model of Tsai and Aki [1969] was used. Amplitude spectra were equalized to a common distance of 4000 km. To decrease the effect of amplitude fluctuations due to multipathing, the amplitude spectra were smoothed by averaging over a frequency window of 0.0025 Hz centered at each frequency.

The phase spectra were corrected for propagation effects using the regionalized phase velocity model of Figures 3 and 4. Regional boundaries were determined from geologic and bathymetric considerations. The oceanic domain was divided into young and old lithosphere roughly by the 20 m.y. isochron, and the continental margin was defined by the 4000 m isobath. For several necessary continental provinces, phase velocity dispersion curves were not available in the literature for the entire period range from 20 to 100 seconds and an appropriate curve was extrapolated from curves published for geologically similar regions. The estimated errors on the phase velocities given by the authors of the regional studies range from about 0.2% (oceanic regions and recent studies of continental regions) to 1.0% (older continental studies).

Table 3a shows the percentage of each earthquake-station path within a given region. These percentages were used to calculate an appropriate phase velocity for each period at each station.

The corrected source spectra were then sampled at 2 second intervals in period. Examples of seismograms and corrected source spectra are shown in Figure 5a. Only data for periods between 30 and 60 seconds were used in the inversion. The earthquake was too small to excite waves at periods much greater than 60 seconds and data at periods shorter than 30 seconds were considered unreliable because of the effects of structural heterogeneities along the path and of phase velocity errors on the phase correction. The source spectra were then examined visually to see if phases were coherent. A few stations were dropped from the calculations at this stage leaving 16 stations (256 data) for the final inversion. The rejected stations usually corresponded to long paths with sections parallel to structural discontinuities and the incoherency of the phase was probably due to the interference effects of multipathing. Spurious phases or amplitudes at certain periods for otherwise coherent spectra were also noted and assigned zero weight (e.g., 52 sec period at station VAL; see Figure 5a).

The vertical component of the Rayleigh wave for the April 3, 1972 event was treated similarly to that for the 1970 event except that amplitude spectra were not smoothed. The stations used for the analysis of this event are shown in Figure 3, the regionalization of the paths is given in Table 3b, and a sample of the data is shown in Figure 5b.

Periods from 32 to 78 seconds at 19 stations were used for a total of 456 data.

The data for the 1972 earthquake were filtered using the time variable filter technique of Landisman et al. [1969] to avoid potential interference from higher modes and multi-pathing. This time variable filtering did not significantly change the source spectrum at most stations. Erratic phase values were not eliminated by the filtering although they were sometimes shifted by up to $\pm$4 seconds in period (Figure 5b). For one station, BLA, the analysis did suggest interference from a mode clearly separated in time from the fundamental mode. In this case, the filtering smoothed the source spectra significantly (Figure 5b) suggesting that the technique will be useful for treating the data from events less auspiciously located with respect to the WWSSN than those along the southern Reykjanes Ridge. Using filtered data did not improve the resolution of the inversion and in the rest of this study only results obtained from the unfiltered data will be presented.

Results

The inversions were performed under a series of increasingly more stringent constraints. With all six moment tensor components unconstrained (constraint 1 in table 4) the diagonal components were poorly resolved. The no-volume-change constraint was therefore imposed (constraint 2). It then became apparent that the sources were very shallow and that large, poorly determined M_{xz} and M_{yz} components were dominating the solutions. As normal faulting with the

tension axis approximately horizontal was indicated, the constraint that the imaginary part of the spectrum be zero was then imposed, both without and with the no-volume-change constraint (constraints 3 and 4, respectively).

The residuals of the inversions, normalized to the number of data minus the degrees of freedom, are plotted against depth in Figure 6. The behavior of the residuals with depth is similar for the two events. For the inversion of the real part, we observe minima for both shallow (4-10 km, or 1-7 km below sea-floor) and deep (80-90 km) depths, regardless of the constraint imposed. This ambiguity is to be expected because, over the period range of the data, the behavior of G_1 and G_2 is similar for both shallow and deep events. The minima are more sharply defined when the constraint $\sum_{i=1}^{3} M_{ii} = 0$ is imposed. The inversion of the imaginary part provides no constraint on the depth. Imposing the constraint that the imaginary part of the spectrum is zero and that the observed amplitude reflects the real part decreases the residuals. Since one would expect to obtain larger residuals for the more highly constrained case, this behavior implies that by recasting the amplitude and phase spectra in terms of real and imaginary components, we are actually adding noise to the real part. This question will be discussed further when the results of the inversion under the various constraints are compared to the observations.

The results of the inversion for depths corresponding to minima in the residuals are given in Tables 4a and 4b. The errors for the eigenvalues and eigenvectors represent the first order perturbation resulting from errors in the moment tensor components [Mathews and Walker, 1964; Strelitz, 1980].

First, note that although the calculated errors on the diagonal components are so large as to render the solution meaningless when the trace is not constrained to be 0 (solutions for a depth of 4 km below sea floor, constraints 1 and 3) the orientation of the principal axes and the percentage of double couple mechanism in the solution are similar to those for the corresponding solutions with the trace constrained (constraints 2 and 4, respectively). By imposing the no-volume-change constraint we are not suppressing any information which could otherwise be extracted from the data.

Next, let us discuss the results of the inversion under constraint (2). For shallow depths the solutions indicate normal faulting with tension approximately perpendicular to the spreading center. They do, however, contain important strike-slip components and suggest significant departures from a pure double-couple source mechanism. We can also observe a marked rotation of the axes as depth increases from 1 to 7 km below the sea floor. Examination of the individual moment tensor components reveals that, as depth decreases, the solution becomes increasingly dominated by the M_{xz} and M_{yz} components. The reason for the instability of the inversion of the imaginary part for shallow sources has been discussed above.

In order to avoid problems due to the poor resolution of M_{xz} and M_{yz}, we tried performing the inversion under constraint (4), assuming a normal faulting mechanism (ϵ_{ij} = 0.5 cycles for all i and j). For both events, the solution for a depth of 1 to 7 km below sea floor is very stable: double-couple normal faulting along a strike parallel to that of the spreading center. The moments

increase regularly with depth; for a depth of 7 km (1 km below sea floor) the moments are 4.8 and 7.5 x 10^{24} dyne-cm for the 1970 and 1972 events, respectively.

The solutions at 80 km under constraints (2) and (4) indicate primarily non-double couple source mechanisms and do not bear any apparent relationship to the local geologic setting. The interchanging of the compression and tension axes relative to the shallow solutions (constraint 4) indicates that the ambiguity in determination of depth from the minimum in the residuals of the surface wave inversion is a direct result of the similar behavior, with opposite sign, of G_1 and G_2 for both shallow and deep sources. In the next section we will see that the body waves are not compatible with a deep source and the solutions at 80 km will not be considered further.

Discussion

The fault plane solutions corresponding to the moment tensors obtained under constraints (2) and (4) for a depth of 7 km are superimposed on the observed P-wave fault plane solutions in Figures 7a and 7b. We can see that the P-wave first motion pattern for the 1972 event displays the non-orthogonal nodal planes characteristic of mid-ocean ridge normal faulting events (Figure 7b). For the 1970 event, the data coverage is less complete and the observed nodal planes are poorly constrained but are consistent with a normal faulting solution requiring non-orthogonal nodal planes. The large strike slip component in both moment tensor solutions under constraint (2) implies a pronounced assymetry

in the P-wave radiation pattern which is not observed. Except for the observed non-orthogonality, the P-wave first motion patterns are consistent with the results of the surface wave inversion under constraint (4).

It has been noted that the residuals of the inversion are smaller under constraints (3) and (4) than under (1) and (2), implying that by separating the observed spectrum into its real and imaginary parts one is actually adding noise to the real part. An examination of the fit of the solution to the data, expressed both as real and imaginary part and as amplitude and phase provides insights into this behavior. For the 1970 event (Figure 8), the observed value of the imaginary part is generally greater than that of the model (Figure 8a) and the phase is about 0.1 cycle less (Figure 8b). From equation (2), an origin time error of 5 seconds can result in a 0.1 cycle underestimation of the initial phase delay for a 50 second wave. If the true initial phase delay is 0 or .5 cycles, the result of such an error in the real part is to underestimate the amplitude and consequently the moment. That this is indeed happening is clear in Figure 8b where the amplitude data is compared to the solutions calculated under constraints (2) and (4).

By comparing Figures 8a and 9a to Figures 8b and 9b, we see that the variation in the imaginary part of the spectrum with azimuth leading to large M_{xz} and M_{yz} components is primarily controlled by the variation in phase and that stations in the Caribbean (215° to 230° azimuth) are particularly important in defining this pattern. These stations have long earthquake-station paths relative to most

of the other data used in this study and therefore have a greater potential error due to phase velocity errors. Moreover, the phase velocity over the Caribbean portion of the path is poorly known. Weidner [1974] found anomalous phase velocities for paths to stations in the Caribbean from earthquakes along the Mid-Atlantic Ridge at 35°N and 15°N and attributed this to anomalously thick sediment cover. Inclusion of his model into the regionalization further decreases the initial phase at station CAR by about 0.23 cycles at 40 seconds where the effect is maximum and by .05 seconds at 80 seconds. Another possible source of error in the initial phase is epicentral mislocation; a mislocation of 12 km will impart a sinusoidal variation to the corrected initial phase with a maximum amplitude of about 0.1 cycles at 30 seconds and .04 cycles at 80 seconds.

If the true initial phase were close to 0.5 cycles at all azimuths, these errors would dominate the behavior of the imaginary part and induce additional noise on the real part. That the residuals decrease when the inversion is performed under constraints (3) and (4) suggests that this is indeed happening to some degree for the events studied in this paper. Although the sources for the two events studied may indeed contain minor M_{xz} and M_{yz} components, the values obtained from the inversion of the imaginary part seem to be over-estimated and we are unable to resolve their magnitude from our data.

Before proceeding to the body wave analysis, we should examine the effect on the inversion of the no-volume-change

constraint when the source actually contains a volume change component because this constraint must usually be imposed to resolve the diagonal components of the moment tensor. For a shallow explosive source with moment tensor $M_o \begin{bmatrix} 1 & 0 & 0 \\ 0 & 1 & 0 \\ 0 & 0 & 1 \end{bmatrix}$, the inversion should yield a solution of $b \cdot M_o \begin{bmatrix} \frac{1}{2} & 0 & 0 \\ 0 & \frac{1}{2} & 0 \\ 0 & 0 & -1 \end{bmatrix}$ which corresponds to a compensated linear vector dipole (CLVD) with compression along the z axis and tension along x and y. The factor b depends on depth and is close to 1 for a shallow source [Patton, 1978]. An explosion should be clearly distinguishable from a double-couple both with and without the no-volume-change constraint. A vertical tension crack in the y-z plane corresponds to the sum of a CLVD, with tension along x and compression along y and z, and an explosion. Under the $\sum_{i=1}^{3} M_{ii} = 0$ constraint, the explosive component will masquerade as a CLVD with compression along z; the sum of the two CLVD, assuming $b = 1$ and $\lambda = \mu$, is $M_o \begin{bmatrix} 13/6 & 0 & 0 \\ 0 & 1/6 & 0 \\ 0 & 0 & -14/6 \end{bmatrix}$ resembling a source with 86% double-couple mechanism. For the events studied in this paper, the double couple component of the source remains stable when the no-volume-change constraint is removed and the CLVD component distributes itself between the new CLVD and the explosive components; moreover, the double couple component increases as the residuals decrease. This suggests that the sources were primarily double-couple and that noise in the data is appearing as apparent non-double-couple components.

In summary, the inversion of the surface waves to obtain the source moment tensor for two events on the Reykjanes Ridge indicates double couple source mechanisms corresponding to normal faulting along planes with a dip of about 45° and strike parallel to the local strike of the spreading center. Both events appear to have been very shallow (1-7 km below sea floor). This study has demonstrated the difficulty in resolving M_{xz} and M_{yz} components of the moment tensor for very shallow events using data that is less than perfect. Because errors in the corrected initial phase due to mislocation and origin time errors alone are large enough to severely affect the determination of M_{xz} and M_{yz}, the corrected source phase obtained using a regionalized phase velocity model is not adequately accurate to resolve these two components of the moment tensor. We have not determined whether the regionalized model is adequate for slightly deeper events for which the inversion is not inherently plagued by this problem.

BODY WAVE ANALYSIS

Background

A striking feature discerned in the surface wave analysis of the two mid-ocean ridge events is the exceptionally shallow focal depth. This result suggests that interference between the direct and reflected body wave phases, as proposed by Hart [1978], might be responsible for the apparently non-orthogonal nodal planes. For a dip-slip fault, arrivals reflected from the surface at the epicenter can have much larger amplitudes than and opposite polarities to the direct arrivals. If the source is shallow, the temporal separation of the arrivals is less than the pulse width of the impulse response of the long period WWSSN seismometer convolved with the attenuation operator. The arrivals interfere destructively and the apparent nodal planes can be shifted well into the dilatational quadrant. Langston [1976] used such interference to constrain the depth of the 1967 Koyna, India, earthquake and cautioned that interference could lead to errors when determining fault plane solutions from first motion polarities for earthquakes with shallow focal depths.

We first present a simple hypothetical case of a shallow dip-slip fault in a homogeneous halfspace and show that the interaction of surface reflections with the direct arrivals can indeed cause an apparent reversal of the first motion polarity at certain take-off angles.

We then demonstrate that the surface wave and the body wave observations can be reconciled for the April 3, 1972 earthquake if the event originated near the ocean floor. Although the April 24, 1970 event was too small to be suitable for quantitative modelling by synthetic seismograms, a qualitative inspection of the observed P waves suggests that interference could be responsible for the apparent reversal of first motion polarity.

The method used to calculate the synthetic seismograms is an extension of the point-source formulation of Bouchon [1976] to a finite fault. Seismograms are calculated by numerical integration of point sources distributed on a rectangular grid approximating the fault area. Rupture propagation is simulated by progressively firing individual point sources in a circular pattern radiating from the rupture origin with an appropriate rupture velocity. In order to approximate a smooth rupture, the grid spacing must be such that the firing intervals are smaller than the shortest period important to the problem. As attenuation and the response of the long period WWSSN instrument effectively filter out periods shorter than 4 sec, a grid spacing of 1 km is appropriate for a rupture velocity between 2 and 3 km/sec. The method incorporates the propagator matrix formulation [Haskell, 1953] for computation of the crustal response at the source and receiver and is particularly well suited for crustal structures which cause extensive reverberation (e.g., structures with a water layer). A more detailed description of the method is presented in Appendix II.

The fault geometry and the medium parameters used in the example are shown in Figure 10. The fault is an 11 by 11 km rectangle which is located in a homogeneous half-space and whose top edge reaches the surface. The rupture velocity is 2.5 km/sec (0.8 times the shear velocity of the medium). Each point source has a rise time of 0.3 seconds. We have investigated three possible situations (Figure 10): rupture initiation 1) at the top,
2) in the center, and 3) at the bottom of the fault. Figure 11 shows synthetic P wave seismograms calculated for the three models depicted in Figure 10. Also shown are the theoretical nodal planes and the projections of the ray paths onto the focal sphere. The dip of the fault is 55°. In all figures the calculated seismograms begin at the time of the first expected arrival. No motion will be observed at that time if interference is cancelling the first motion. In the examples, the seismograms are equalized to a common radius on the focal sphere and the vertical/horizontal scale ratio is kept constant; the relative variations in amplitude for different ray paths are as shown.

Points B, C and D lie within the theoretical dilatational quadrant and we would therefore expect to observe downgoing first pulses. This is indeed what we observe when the rupture initiates at the center or at the bottom of the fault. An important aspect of the finite source model which influences the relative amplitude of the direct and reflected arrivals is vertical directivity; down-

ward rupture propagation increases the amplitudes and shortens the effective time functions of the direct arrivals and decreases the amplitudes and lengthens the effective time functions of the reflected arrivals whereas upward propagation has the opposite effect. Because of directivity, the first motion has a larger amplitude if the rupture initiates at the center than at the bottom. Although directivity enhances direct arrivals the most when rupture propagates from top to bottom, it plays a secondary role if the hypocenter is very shallow. In this case, destructive interference between the direct arrivals and surface reflections effectively masks the direct arrivals for certain take-off angles. First arrivals along ray paths B and C appear to be compressional although they lie well within the theoretical dilatational quadrant. The nodal plane appears to be shifted into the dilatational quadrant by approximately 15°. Figure 12 illustrates the distortion of the fault plane solution for a 45° dipping fault with rupture initiating near the free surface. If noise were superimposed on the signal, the observable dilatational quadrant would be further reduced.

The fault geometry and medium parameters affect the degree to which interference influences the wave form. For large faults, the finiteness and directivity strongly influence the radiation pattern. Because the vertical directivity for a rupture propagating from top to bottom increases the amplitude of the direct arrivals, decreasing the width of the fault will diminish this effect and increase the

amount of observed non-orthogonality. Effects which increase the effective rise time will also cause an emergent direct P arrival and may further contribute to the distortion of the apparent dilatational quadrant (e.g., higher attenuation, lower rupture velocity, and longer rise time).

To apply the results for a normal fault to thrust faulting, only the polarity of the seismograms must be changed. These results can also be generalized to include earthquakes originating beneath low velocity layers such as water or sediment, the base of which provides sufficient impedance contrast to produce large reflections. The predicted distortion of the apparent first motions, however, applies only to normal and thrust faults. For strike-slip faults, the direct P and sP have the same polarity and, while pP has opposite polarity, its amplitude is too small to entirely cancel the direct arrival.

Data

The P-wave fault plane solution based on long period observations from the earthquake of April 3, 1973 is shown in Figure 7b and exhibits characteristically non-orthogonal nodal planes. Examples of the P waveforms used in the body wave analysis (Table 5) are shown in Figure 13. Several seconds of background noise preceding each P arrival are shown in order to illustrate the signal-to-noise ratio. This event is among the largest recorded on the Mid-Atlantic ridge and provides the best possible data from this tectonic region. In order to avoid complications due either to

core or upper mantle structure, only stations at epicentral distances between 30° and 80° were used [Burdick and Helmberger, 1979]. Seismograms were equalized by correcting for differences in instrument magnification and for geometrical spreading. The correction for geometrical spreading was calculated using the formula of Carpenter [1966] and the P-wave travel times of Herrin [1968]. The similarity in shape and amplitude of seismograms from neighboring stations indicates that background noise and crustal structure below the receivers do not significantly affect the observations. One nodal plane appears to pass through stations OXF and FFC; first motions at stations TUC, DUG, and EDM begin to show a dilatational character whereas BKS, CAR and COL are clearly dilatational. The other apparent nodal plane passes between stations KBL and JER. The monochromatic oscillations in the later portion of the seismogram are due to reverberation within the water layer.

Results

The synthesized seismograms are compared to the observations in Figure 14. The best overall match was obtained with a source mechanism compatible with that obtained from the surface wave inversion under constraint 4. The model parameters used in the synthesis are shown in Figure 15. The data do not enable us to determine which of the two nodal planes corresponds to the actual fault plane and the westward dipping plane was arbitrarily chosen.

The match between the synthetic and observed waveforms

is quite good. The fact that the observations tend to show a larger amplitude for the water reverberations than the theoretical seismograms indicates that the fault broke the sea floor. In the calculation of theoretical seismograms, the fault stops just below the surface of the sea floor; a finite displacement of the sea floor would enhance the amplitude of water arrivals. The period of the water reverberations constrains the water depth to be 2.8 km, in good agreement with the bathymetric data (Figure 1). The best overall match was obtained for a fault length of 13 km and a width of 3 km with rupture initiating near the sea floor and propagating bilaterally. We assumed a rupture velocity of 2.6 km/sec (0.8 x shear wave velocity). If the rupture propagation were not perfectly bilateral the fault could be somewhat shorter. Unilateral rupture propagation, however, does not fit the observations as it would require a noticeable directivity effect for stations with northern and southern azimuths. The width of the fault is constrained by the observed non-orthogonality. Keeping the other parameters unchanged, the width can be increased to 4 km without significant deterioration of the overall match. Lowering the rupture velocity may further slightly increase the maximum acceptable width and decrease the length. For a 44° dip this bound on width implies that the fault is confined to the upper 3 km or less of the crust.

Figure 16a illustrates the sensitivity of the solution to the fault geometry. For the 13 x 3 km fault, the effect of vertical directivity is negligible and interference between the direct and reflected phases determines the apparent non-orthogonality. For a 6 km wide fault with rupture propagation from top to bottom, however, the downward directivity enhances the amplitude of the direct arrival so that it can be observed at take-off angles corresponding to the examples in Figure 16a. For bottom-to-top propagation, the direct and reflected arrivals from a 6 km wide fault are sufficiently separated in time for the direct arrival to be observed. (Although top-to-bottom rupture propagation matches the observed seismograms better than bottom-to-top propagation for a 3 km wide fault, we do not ascribe any tectonic signifance to this observation).

In Figure 16a we can also see that a model of a point source below the sea floor at a depth of 0.35 km matches the observed data as well as the 13 x 3 km finite fault model. This is not surprising since for such a narrow fault the effect of vertical directivity is negligible. Although one might argue that extension of the point source model to a finite fault is therefore not justified, for this event we are able to constrain the fault geometry by using a finite fault model and we feel that this added information is useful for understanding the tectonic processes involved.

The seismograms in Figure 16b were calculated for the moment tensor obtained from the surface wave inversion under constraint 2 for a depth of 4 km below sea floor (Table 4b). The overall match is worse than that for the solution under constraint 4 supporting the conclusion that the magnitude of the M_{xz} and M_{yz} components of the moment tensor is indeed an artifact of their poor resolution for shallow sources.

The average moment from the body wave analysis is 7.5×10^{24} dyne-cm, the same as that obtained from the surface waves. This moment corresponds to about 60 cm of average displacement on the fault. The body wave moment was calculated by normalizing the amplitude of the synthetic seismograms to the first upgoing pulse of the observed P waves. The variation in the moment obtained from individual stations (Figure 14) indicates that the average value may be in error by as much as 50 percent.

For a dip-slip fault the stress drop can be expressed as

$$\Delta\sigma = \frac{4(\lambda+\mu)M_o}{\pi(\lambda+2\mu)LW^2} \qquad (3)$$

where λ and μ are the Lame's constants, M_o is the scalar seismic moment of the double couple, and L and W are the length and width of the fault [Knopoff, 1958]. Allowing for the uncertainties discussed above, the stress drop is between 30 and 60 bars. This stress drop is similar to that found for other interplate events [Kanamori and Anderson, 1975].

The attenuation correction was applied by keeping a constant value of $t^* = T/Q$, where T is the travel time and Q is the average quality factor along the path. A t^* of 1 second yielded a satisfactory match to the observed data, whereas a value larger than this produced overly smooth synthetic waveforms.

We have also examined the short period seismograms. At most stations, a low energy first arrival followed about 1.5 sec later by a much stronger arrival was observed (Figure 17). The short period first motion arrival time corresponds well to the expected first motion time indicated by the synthetic long period records (Figure 14). In order to determine whether the larger arrival could be a depth phase, we calculated seismograms using the instrument response of the WWSSN short period seismometer but were not able to match the observations by either a simple point source or a smoothly rupturing fault. A match could be obtained only if we assumed a discontinuous rupture process. Because of the large degree of non-uniqueness involved in modelling short period seismograms, we did not pursue this analysis further.

A poor signal-to-noise ratio for the P waves from the April 24, 1970 earthquake made them unusable for quanititative waveform modelling. However, because of the similarity of the source mechanisms deduced from the source moment tensor inversions, we used the synthetic waveforms calculated for the April 3, 1972 event for a qualitative comparison. Examples of seismograms corresponding in distance and

azimuth to those used to model the April 3, 1972 event are shown in Figure 18. If the amplitude of the background noise and expected amplitude of the first arrival are considered, it is not surprising that all the first motions were originally picked to be compressional. First motion polarity determinations at several stations were later revised to be "possible" dilatations (e.g., KBL, TAB; Figure 18). The observed waveforms can qualitatively be explained by a shallow fault, similar to that deduced for the April 3, 1972 event.

Discussion

In summary, the body waveforms for the April 3, 1972 Mid-Atlantic ridge earthquake can be matched without invoking anomalous ray propagation if the source is confined to the upper 3 km or less of the crust. The non-orthogonality of the P-wave fault plane solution can be entirely explained in terms of interference between the direct and reflected phases. Because of the trial-and-error technique used in the P-wave analysis we must, however, admit the possibility of non-uniqueness in the solution.

The moment tensor inversion from the surface waves show that the source was consistent with a pure double-couple mechanism. Because of the long periods used in the surface wave inversion, however, one might argue that a small precursor with an explosive or tensile mechanism could cause the non-orthogonality of the P-wave nodal planes and not be observable by the surface waves. Although

this is a valid argument, it is not easy to prove because precursors of any mechanism would cause an emergent P wave which, especially for a shallow source, would be very difficult to pick. Although the short period seismograms indicate discontinuous rupture, the agreement between the arrival time measured on the short period records and that predicted by the synthetic seismograms argues against this explanation.

Thermal models of mid-ocean ridges and observed attenuation of teleseismic S waves passing under the southern Reykjanes Ridge [Solomon, 1973] suggest that we might also expect high attenuation of teleseismic P waves. The P-wave attenuation ($t^* = 1$ sec), however, does not appear to be larger than average. The results for P and S waves are not necessarily contradictory. If the low Q zone in the vicinity of the ridge crest is caused by partial melting, the compressional waves should be less affected than shear waves.

Our results do not exclude the possibility of a small amount of focusing contributing to the non-orthogonality. This would allow a slightly wider fault than that indicated by our analysis. We prefer that shallowness of the source be the explanation for the anomalous P-wave fault plane solutions because of the simplicity of such a mechanism and because of the agreement between the results of the body wave synthesis and surface wave inversion.

CONCLUSIONS

The major conclusions of this study are:

(1) The source moment tensor can be retrieved from the Rayleigh wave radiation pattern for a single isolated event. This method of obtaining the source mechanism is useful for small events for which the body wave fault plane solutions may be inconslusive and/or perplexing. For very shallow sources, however, the M_{xz} and M_{yz} components become poorly resolved and very sensitive to errors in the data; moreover, the three diagonal components cannot be independently determined. By comparing the results of the inversion performed under a series of increasingly more stringent constraints, we are able to qualitatively evaluate the validity of imposing constraints which lead to a stable solution.

(2) The final moment tensor solutions for two events along the southern Reykjanes Ridge indicate double couple, normal faulting mechanisms with the tension axis approximately horizontal and oriented perpendicular to the spreading center. For both events, the surface waves indicate a focal depth of 1-7 km below the sea floor.

(3) The non-orthogonality of the nodal planes frequently observed in the body wave fault plane solutions for mid-ocean ridge normal faulting events can be attributed to extreme shallowness of the source which results in interference between the direct and reflected phases and effectively masks the first motion recorded on long period seismograms.

(4) Comparison of observed P-waveforms from the April 3, 1972 Reykjanes Ridge event to those calculated for a fault with an orientation obtained from the surface wave analysis

indicates that the source was a long, narrow fault which broke the sea floor.

The faulting process implied by these results provides additional constraints on models of spreading center tectonics and thermal structure. The double couple nature of the solutions relates these earthquakes to tectonic rather than volcanic processes and supports the evidence from seismicity and topography which associates teleseismically observable ridge-crest activity with rift valley formation. An important question about mid-ocean ridges concerns the depth of hydrothermal circulation and its effect on the thermal structure of the crust. The close agreement between observed ridge crest topography and that calculated for the simple model of a conductively cooling slab suggests that extensive hydrothermal circulation is restricted to the top few kilometers of the crust [Fehn and Cathles, 1979]. On the other hand, deep (5-8 km) hydrothermal circulation has been invoked in order to depress the isotherms enough to produce a cold brittle layer of sufficient thickness to support faults with the dimensions implied by the moments of the largest spreading center events if it is assumed that length-width ratios and stress drops are similar to those observed for other plate boundary earthquakes [Solomon, 1979]. The long, narrow fault plane suggested by an analysis of the body waves from the earthquake on the Reykjanes Ridge, however, can be entirely accommodated within the brittle crust determined from the purely conductive model of Sleep [1975] if it is assumed that the earthquake occurred 10 km from the axis, along the rift valley walls (Figure 19). An as yet unanswered question

is whether the length-width ratio will increase with increasing moment; the largest earthquake studied from this region had a moment of 2×10^{25} dyne-cm [Hart, 1978], approximately twice that of the larger event studied here. Further studies of fault dimensions, stress drops, and recurrence intervals for ridge earthquakes in regions spanning a range of spreading rates should permit the incorporation of time dependent faulting and stress release in models which simulate the spreading process and are used to explain the relationship between spreading rate, topography, and magma supply [e.g., Sleep and Rosendahl, 1979].

Acknowledgements

We thank Paal Einarsson for first drawing our attention to the unusual earthquake of April 24, 1970, and for an early preprint of his paper. We also thank Kei Aki, Doug McCowan, Howard Patton and Gerardo Suarez for assistance with the moment tensor analysis, and Michel Bouchon for advice on body wave synthesis. This research was supported by the Division of Earth Sciences, National Science Foundation, under NSF Grant EAR77-09965; by the Advanced Research Projects Agency under Contract F44620-75-C-0064 administered by the Air Force Office of Scientific Research; and by fellowships from the National Science Foundation (A.M.T.) and the Alfred P. Sloan Foundation (S.C.S.).

APPENDIX I. Moment Tensor Source Representation and Surface Wave Radiation

The displacement at $\underset{\sim}{y}$ at time ζ in the direction $\hat{k}$ due to a seismic source at time t can be represented as:

$$u_k(\underset{\sim}{y},\zeta) = \int_{-\infty}^{\infty} dt \{ \int_V dV_x G_{kj}(\underset{\sim}{y},\zeta;\underset{\sim}{x},t) \gamma_j^V(\underset{\sim}{x},t) + \int_S dS_x G_{kj}(\underset{\sim}{y},\zeta;\underset{\sim}{x},t) \gamma_j^S(\underset{\sim}{x},t) \} \tag{A1}$$

where V is the source volume, S is the surface of the source volume, γ_j^V and γ_j^S are the equivalent volume and surface forces corresponding to a physical mechanism, $G_{kj}(\underset{\sim}{y},\zeta;\underset{\sim}{x},t)$ is the impulse response or Green's function of the medium, and repeated indices imply summation [Aki and Richards, 1980]. If the "moment density tensor" $\underset{\sim}{m}$ is defined to be a symmetric tensor such that $m_{ij,i} = -\gamma_j^V$ in V and $n_i m_{ij} = \gamma_j^S$ on S ($\underset{\sim}{n}$ being the unit normal to the surface), we can regroup the expression for displacement into one term using Gauss's theorem [Backus and Mulcahy, 1976]:

$$\begin{aligned} u_k(\underset{\sim}{y},\zeta) &= \int_{-\infty}^{\infty} \{ - \int_V dV_x G_{kj} m_{ij,i} + \int_S dS_x G_{kj} n_i m_{ij} \} dt \\ &= \int_{-\infty}^{\infty} - \{ \int_V dV_x G_{kj} m_{ij,i} + \int_V dV_x (G_{nj} m_{ij})_{,i} \} dt \\ &= \int_{-\infty}^{\infty} dt \int_V dV_x m_{ij} G_{kj,i} = \int_{-\infty}^{\infty} dt \; M_{ij} G_{kj,i} \end{aligned} \tag{A2}$$

For an effective point source, the "moment tensor" $\underset{\sim}{M}$ can be defined as the integral of the moment density tensor over the source volume and surface and can be retrieved from the far-field displacement radiation pattern [for free oscillations see: Gilbert, 1970; Gilbert and Dziewonski, 1975; for surface waves: McCowan, 1976; Mendiguren, 1977; for body waves: McCowan, 1977; Strelitz, 1978]. The advantage of this representation is that the inversion of far-field displacements to obtain the moment tensor is linear and is not dependent on a presupposed source mechanism.

We can then relate observed moment tensors derived from data to phenomenological source models through the equivalent body forces. Although the total equivalent force is uniquely determined from the resulting motion, the interpretation in terms of a phenomenological source model, however, is not unique as a given moment tensor can result from several different linear combinations of moment tensors. This ambiguity is inherent in any determination of source mechanism from the displacement field [Aki and Richards, 1980].

If we assume that the principal stress axes of the various components are coincident, the diagonalized moment tensor can be uniquely decomposed into isotropic, double couple, and compensated linear vector dipole components. We first remove the isotropic part:

$$\underset{\sim}{M}' = \underset{\sim}{M} - 1/3\ (\text{trace}\ \underset{\sim}{M})\ \underset{\sim}{I} = M_o \begin{bmatrix} 1 & 0 & 0 \\ 0 & f-1 & 0 \\ 0 & 0 & -f \end{bmatrix},\ 0 \leq f \leq 1/2 \qquad \text{(A3)}$$

where $\underset{\sim}{I}$ is the identity matrix. We may then separate the double couple and compensated linear vector dipole components [Knopoff and Randall, 1970]:

$$M' = M_o \left\{ (1 - 2f) \begin{bmatrix} 1 & 0 & 0 \\ 0 & -1 & 0 \\ 0 & 0 & 0 \end{bmatrix} + 2f \begin{bmatrix} 1 & 0 & 0 \\ 0 & -1/2 & 0 \\ 0 & 0 & -1/2 \end{bmatrix} \right\} \qquad \text{(A4)}$$

The double couple scalar moment, M_{DC}, is $(1 - 2f)M_o$ and the corresponding fault plane solution can be obtained from the principal axes of the moment tensor. M_{DC} can be related to the dimensions of a shear fault: $M_{DC} = \mu\bar{u}A$ where μ is the shear modulus, $\bar{u}$ is average displacement, and A is fault area [Aki, 1966].

In this study, the moment tensor is derived from the surface wave radiation pattern. For a vertically heterogeneous earth, the Fourier spectrum of the vertical component of the fundamental Rayleigh wave due to a point source with a step function source time function is:

$$u(r,\theta,\omega) = Ae^{i\phi} = \frac{Y_1(0,\omega)}{4CUI_1} \sqrt{2/(\pi kr)}\ \exp[-i(\omega r/c - \pi/4)]$$

$$\{ (M_{xx} + M_{yy}) \frac{kY_3(h,\omega)}{2} + M_{zz} \frac{-Y_2(h,\omega) - \lambda(h)kY_3(h,\omega)}{\lambda(h) + 2\mu(h)} \qquad \text{(A5)}$$

$$- (M_{yy} - M_{xx}) \frac{kY_3(h,\omega)\cos 2\theta}{2} + M_{xy}kY_3(h,\omega)\sin 2\theta$$

$$-i(M_{xz} \frac{Y_4(h,\omega)\cos\theta}{\mu(h)} + M_{yz} \frac{Y_4(h,\omega)\sin\theta}{\mu(h)}) \}$$

where A and Φ are the observed amplitude and phase at the angular frequency ω and the M_{ij} are the moment tensor components in cartesian coordinates with the x, y, and z axes pointed East, North, and Up [Mendiguren, 1977]. The position of the receiver is expressed in polar coordinates where r is distance and θ is azimuth measured counterclockwise from East. The $Y_i(h,\omega)$ are the eigenfunctions derived by Saito [1967] for the surface wave excitation problem and are functions of angular frequency and depth h; $\lambda(h)$ and $\mu(h)$ are the Lame coefficients; $\omega^2 I$, k, C, and U are the kinetic energy, wave number, phase velocity, and group velocity. The moment tensor components can be retrieved through a linear inversion of the real and imaginary parts of the observed radiation pattern if a good azimuthal distribution of stations is available.

APPENDIX II. Method of P-wave Synthesis for Finite Sources

A fundamental assumption in calculations of teleseismic body waves from shallow sources is that only the free surface and the crustal and uppermost mantle structure at the source and receiver have a significant effect on the shape of the seismograms. Gradients within the mantle are considered to be too small to cause converted or reflected phases and travel time caustics, and the effect of the mantle portion of the propagation path is restricted to geometrical spreading and attenuation. For epicentral distances between 30° and 80° these assumptions are well justified [Burdick and Helmberger, 1978]. The synthetic seismogram is obtained by convolution of the response of the source U(t) with the responses of the receiver I(t), the crust below the receiver R(t), attenuation A(t) and geometrical spreading G.

Our technique for calculating source response is an extension of the formulation of Bouchon [1976] for a double-couple point source to a finite fault with circular rupture propagation. Contributions from point sources distributed along the fault surface on an equally spaced grid are numerically integrated. Rupture propagation is simulated by progressively firing individual point sources in a circular pattern radiating from the origin with a constant rupture velocity. In order to approximate a smooth rupture, the grid spacing must be such that the firing intervals are smaller than the shortest period important to the problem. The integration is performed in the frequency domain and then transformed back into the time domain. This enables

efficient use of the propagator matrix algorithm of Haskell [1953] to obtain the response of the medium. This approach is particularly useful for the case examined in this paper because of the prolonged ringing of the P-wave in the water layer. The ray-theoretical approach [e.g. Langston and Helmberger, 1974] is less efficient for such a large number of rays. Although we integrate in the frequency domain, we can separate individual phases by setting appropriate potentials to zero.

The problem configuration is the same as in the work of Bouchon [1976]. We assume that the dislocation has the same time dependence at any point on the fault surface and can be written in the form

$$D(\underset{\sim}{\xi},t) = F(\underset{\sim}{\xi})E(t-|\underset{\sim}{\xi}-\underset{\sim}{\xi}_o|/c) \qquad (A6)$$

Its Fourier transform is

$$\hat{D}(\underset{\sim}{\xi},\omega) = F(\underset{\sim}{\xi})\hat{E}(\omega)\exp(-i\omega|\underset{\sim}{\xi}-\underset{\sim}{\xi}_o|/c) \qquad (A7)$$

where $\underset{\sim}{\xi} = (\xi_1,\xi_2)$ is a point on the fault surface, $\underset{\sim}{\xi}_o$ is the point of origin of the rupture, c is the rupture velocity, and ω is the angular frequency. The fault is a rectangle of length $L = N\Delta\xi$, parallel to the surface, and of width $W = M\Delta\xi$, dipping at an arbitrary angle; $\Delta\xi$ is the grid spacing; and N and M are integers. The far-field P wave displacement spectrum due to this source can be expressed as

$$\hat{U}(\omega) = \Delta\xi^2 \sum_{n=1}^{N} \sum_{m=1}^{M} \mu_j \hat{D}(\xi,\omega) \exp[ik(\xi_1 \cos\phi - \xi_2 \cos d \cdot \sin\phi)]$$

$$\cdot \sum_{\ell=1}^{4} g_{\ell j}(\omega) \exp[i\Delta_{\ell j}(z_o + \xi_1 \sin d)] \qquad \text{(A8)}$$

with

$$\xi_1 = (n - \tfrac{1}{2})\Delta\xi, \quad \xi_2 = (m - \tfrac{1}{2})\Delta\xi$$

where z_o is the depth to the top of the fault; k is the horizontal wave number which is determined by the take-off angle; ϕ and d are azimuth and dip of the fault; and μ_j is the shear modulus. The subscript j refers to the layer within the crustal model in which the point source is located. The terms $g_{\ell j}$ and $\Delta_{\ell j}$ are as defined by Bouchon [1976] and are related to the up and downgoing P and S waves excited by a source located within the layer j.

Following the same notation, the response of the crustal layers below the receiver to an incident P wave can be written in the form

$$\hat{R}(\omega) = [(A_{21} - A_{11})\nu_1 - (B_{11} + B_{21})k]\alpha_n/\omega \qquad \text{(A9)}$$

where A_{ij} and B_{ij} represent upgoing and downgoing compressional and rotational potentials in the layer immediately below the receiver. ν_1 is the corresponding vertical compressional wave number and α_n is the compressional velocity of the medium below the crustal layers.

When calculated seismograms are to be compared to observed data, a correction must be made for geometrical spreading. This is a frequency independent term which can be expressed in the form [Carpenter, 1966],

$$G = \frac{\alpha_S}{r_S r_R} \left(\frac{\rho_S \alpha_S}{\rho_R \alpha_R} \frac{1}{\sin \; \cos i_S \; \cos i_R} \frac{dT}{d\Delta} \left| \frac{d^2T}{d\Delta^2} \right| \right)^{1/2} \qquad \text{(A10)}$$

with

$$\sin i_S = \frac{\alpha_S}{r_S} \frac{dT}{d\Delta} \; , \; \sin i_R = \frac{\alpha_R}{r_R} \frac{dT}{d\Delta}$$

where α_S, ρ_S, α_R and ρ_R are the velocity and density of the material below the crustal layers at the source and receiver, respectively; i_S is the angle the ray makes with the vertical at the base of the crust below the source and i_R is the corresponding angle below the receiver; r_S and r_R denote the distance from the base of the crust at the source and receiver to the center of the earth; T is the P wave travel time; and Δ is the angular distance between the source and receiver.

The effect of attenuation in the mantle is introduced by the causal Q operator of Futterman [1962]. In the frequency domain the operator is given by

$$A(\omega) = \exp\left[-\frac{1}{2}\, t^* \left(\frac{\omega}{1+\frac{1}{\pi}\ell n\frac{\omega}{\omega_o}}\right)\right] \exp\left[i\, t^*\omega Q\left(\frac{1}{1+\frac{\pi}{Q}\ell n\frac{\omega}{\omega_1}} - \frac{1}{1+\frac{\pi}{Q}\ell n\frac{\omega}{\omega_o}}\right)\right] \qquad \text{(All}$$

for the angular frequency ω in the range $\omega_o \leq \omega \leq \omega_1$, ω_1 and ω_o being the highest and lowest frequencies resolved in the data. The quantity t^* is defined as T/Q where Q is the average quality factor along the path.

Finally, the seismogram must be convolved with the appropriate instrument response; for long period WWSSN stations we use the formula by Hagiwara [1958].

REFERENCES

Aki, K., Generation and propagation of G waves from the Niigata earthquake of June 16, 1964, Bull. Earthquake Res. Inst., Tokyo Univ., 44, 23-88, 1966.

Aki, K., and H. Patton, Determination of seismic moment tensor using surface waves, Tectonophysics, 43, 213-222, 1978.

Aki, K., and P. Richards, Methods of Quantitative Seismology, vol. 1, Freeman and Co., San Francisco, 1980.

Backus, G., and M. Mulcahy, Moment tensors and other phenomenological descriptions of seismic sources - I. continuous displacements, Geophys. J. Roy. Astron. Soc., 46, 341-361, 1976.

Ben-Menahem, A., and M. N. Toksöz, Source mechanism from spectra of long period seismic surface waves, 1, Mongolian earthquake of December 4, 1957, J. Geophys. Res., 67, 1943-1955, 1962.

Ben-Menahem, A., and M. N. Toksöz, Source mechanism from spectra of long period seismic surface waves, 3, The Alaska earthquake of July 10, 1958, Bull. Seis. Soc. Amer., 53, 905-919, 1963.

Bouchon, M., Teleseismic body wave radiation from a seismic source in a layered medium, Geophys. J. Roy. Astron. Soc., 47, 515-530, 1976.

Burdick, L. J. and D. D. Helmberger, The upper mantle P velocity structure of the western United States, J. Geophys. Res., 83, 1699-1712, 1978.

Burton, P. W., Estimation of Q_s^{-1} from seismic Rayleigh waves,

Geophys. J. Roy. Astron. Soc., 36, 167-189, 1974.

Calganile, G., and G. F. Panza, Crust and upper mantle structure under the Baltic shield and Barents Sea from dispersion of surface waves, Tectonophysics, 47, 59-71, 1978.

Carpenter, E. W., A qualitative evaluation of teleseismic explosion record, Proc. Roy. Soc. Lond., Ser. A, 290, 396-407, 1966.

Einarsson, P., Seismicity and earthquake focal mechanisms along the mid-Atlantic plate boundary between Iceland and the Azores, Tectonophysics, 55, 127-153, 1979.

Forsyth, D. W., The early structural evolution and anisotropy of the oceanic upper mantle, Geophys. J. Roy. Astron. Soc., 43, 102-162, 1975.

Francis, T. J. G., The seismicity of the Reykjanes Ridge, Earth Planet. Sci. Lett., 18, 119-124, 1973.

Futterman, W. I., Dispersive body waves, J. Geophys. Res., 67, 5279-5291, 1962.

Gilbert, F., Excitation of the normal modes of the earth by earthquake sources, Geophys. J. Roy. Astron. Soc., 22, 223-226, 1970.

Gilbert, F., and A. M. Dziewonski, An application of normal mode theory to the retrieval of structural parameters and source mechanism from seismic spectra, Phil. Trans. Roy. Soc. Lond. Ser. A, 278, 187-269, 1975.

Gregersen, S., Surface wave dispersion and crust structure in Greenland, Geophys. J. Roy. Astron. Soc., 22, 29-39, 1971.

Hagiwara, T., A note on the theory of the electromagnetic

seismograph, Bull. Earthquake Res. Inst., Tokyo Univ., 36, 139-164, 1958.

Hart, R., Body wave studies of the September, 1969, North Atlantic Ridge earthquake (abstract), EOS Trans. Am. Geophys. Un., 59, 1135, 1978.

Haskell, N. A., The dispersion of surface waves in multilayered media, Bull. Seismol. Soc. Am., 43, 17-34, 1953.

Herrin, E., Introduction to "1968 Seismological tables for P phases", Bull. Seismol. Soc. Am., 58, 1193-1241, 1968.

Kafka, A.L. and D.J. Weidner, The focal mechanisms and depths of small earthquakes as determined from rayleigh wave radiation patterns, Bull. Seis. Soc. of Am., 69, 1379-1390, 1979.

Kanamori, H., and D. L. Anderson, Theoretical basis of some empirical relations in seismology, Bull. Seis. Soc. Am., 65, 1073-1096, 1975.

Knopoff, L., Energy release in earthquakes, Geophys. J. Roy. Astron. Soc., 1, 44-52, 1958.

Knopoff, L., and J. Randall, The compensated linear vector dipole - a possible mechanism for deep earthquakes, J. Geophys. Res., 75, 4957-4963, 1970.

Landisman, M., A. Dziewonski, and Y. Sato, Recent improvements in the analysis of surface wave observations, Geophys. J. Roy. Astron. Soc., 17, 359-403, 1969.

Langston, C. A., Body wave inversion of the Koyna, India, earthquake of December 10, 1967, and some implications for body wave focal mechanisms, J. Geophys. Res., 81, 2571-2572, 1976.

Langston, C. A. and D. D. Helmberger, A procedure for modeling shallow dislocation sources, Geophys. J. Roy. Astron. Soc., 42, 117-130, 1975.

Laughton, A. S., R. C. Searle, and D. G. Roberts, The Reykjanes Ridge crest and the transition between its rifted and non-rifted regions, Tectonophysics, 55, 173-177, 1979.

Mathews, J. and R. Walker, Mathematical Methods of Physics, W.A. Benjamin, N.Y., N.Y., 273-275, 1964.

McCowan, D. W., Moment tensor representation of surface wave sources, Geophys. J. Roy. Astron. Soc., 44, 595-599, 1976.

McCowan, D. W., A moment tensor representation of body-wave displacement vectors on the focal sphere, Semi-annual technical summary, Lincoln Laboratory, M.I.T., 31 March, 9-11, 1977.

Mendiguren, J. A., Inversion of surface wave data in source mechanism studies, J. Geophys. Res., 82, 899-894, 1977.

Mitchell, B. J., Radiation and attenuation of Rayleigh waves from the southeastern Missouri earthquake of October 21, 1965, J. Geophys. Res., 78, 886-899, 1973.

Naponen, I., Surface wave phase velocities of Finland, Bull. Seis. Soc. Am., 56, 1093-1104, 1966.

Oliver, J., R. Kovach, J. Dorman, Crustal structure of the New York-Pennsylvania area, J. Geophys. Res., 66, 215-225, 1961.

Patton, H., A note on the source mechanism of the southeastern Missouri earthquake of October 21, 1965, J. Geophys. Res., 81, 1483-1486, 1976.

Patton, H. J., Source and propagation effects of Rayleigh waves from central Asian earthquakes, Ph.D. Thesis, M.I.T., Cambridge, MA, 342 pp., 1978.

Patton, H. and K. Aki, Bias in the estimate of seismic moment tensor by the linear inversion method, Geophys. J. Roy. Astron. Soc., 59, 479-495, 1979.

Patton, H., Reference point method for determining the source and path effects of surface waves, J. Geophys. Res., 85, 821-848, 1980.

Robson, G. R., K. G. Barr, and L. C. Luna, Extension failure: an earthquake mechanism, Nature, 218, 28-32, 1968.

Saito, M., Excitation of free oscillations and surface waves by a point source in a vertically heterogeneous earth, J. Geophys. Res., 72, 3689-3699, 1967.

Sleep, N. H., Formation of oceanic crust: some thermal constraints, J. Geophys. Res., 80, 4037-4042, 1975.

Sleep, N. H., and B. R. Rosendahl, Topography and tectonics of mid-ocean ridge axes, J. Geophys. Res., 84, 6831-6839, 1979.

Solomon, S. C., Shear wave attenuation and melting beneath the mid-Atlantic Ridge, J. Geophys. Res., 78, 6044-6059, 1973.

Solomon, S. C., Earthquake source parameters, median valley faulting, and the depth of hydrothermal circulation for slow spreading ridges (abstract), EOS Trans. Am. Geophys. Un., 60, 376, 1979.

Solomon, S. C., and N. C. Burr, The relationship of source parameters of ridge-crest and transform earthquakes to the thermal structure of oceanic lithosphere, Tectonophysics, 55, 107-126, 1979.

Solomon, S. C., and B. R. Julian, Seismic constraints on ocean-ridge mantle structure: anomalous fault plane solutions from first motions, Geophys. J. Roy. Astron. Soc., 38, 265-285, 1974.

Strelitz, R. A., Moment tensor inversions and source models, Geophys. J. Roy. Astron. Soc., 52, 359-364, 1978.

Strelitz, R.A., The fate of the downgoing slab: a study of the moment tensors from body waves of complex deep focus earthquakes, Physics of the Earth and Plan. Int., 21, 83-96, 1980.

Stump, B. W., The determination of source mechanism by linear inversion of seismograms (abstract), EOS Trans. Am. Geophys. Un., 57, 953, 1976.

Suarez, G., Moment tensor inversion of the January 15, 1972 earthquake in the Tien Shan Mountains, China, General examination paper, M.I.T., Cambridge, MA, 1978.

Sykes, L. R., Mechanism of earthquakes and nature of faulting on the mid-ocean ridge, J. Geophys. Res., 72, 2131-2153, 1967.

Sykes, L. R., Earthquake swarms and sea-floor spreading, J. Geophys. Res., 75, 6598-6611, 1970.

Sykes, L. R., Focal mechanism solutions for earthquakes along the world rift system, Bull. Seis. Soc. Am., 60, 1749-1752, 1970.

Tsai, Y. B., and K. Aki, Simultaneous determination of the seismic moment and attenuation of seismic surface waves, Bull. Seis. Soc. Am., 59, 275-287, 1969.

Vogt, P. R., and G. L. Johnson, Transform faults and longitudinal flow below the mid-oceanic ridge, J. Geophys. Res., 80, 1399-1428, 1975.

Weidner, D. J., Rayleigh wave phase velocities in the Atlantic Ocean, Geophys. J. Roy. Astron. Soc., 36, 105-139, 1974.

Weidner, D. J., and K. Aki, Focal depth and mechanism of mid-ocean ridge earthquakes, J. Geophys. Res., 78, 1818-1831, 1973.

Table 1. Locations of Reykjanes Ridge Earthquakes Studied in This Paper (from the International Seismological Centre).

Date	Time hr	min	sec	Location lat.N	long. W	Magnitude* m_b	M_s†
April 24, 1970	1	23	17	55.64°	35.03°	5.3	5.4
April 3, 1972**	20	36	20	54.33°	35.20°	5.1	5.5

*Although the 1970 event is assigned a larger m_b by the ISC, an examination of seismograms recorded at the same station for the two events indicates that these values are erroneous as P-wave as well as surface wave arrivals are consistently of larger amplitude for the 1972 event.

†From USCGS and NEIC.

**This event was the second of a pair of events at the same location and of approximately the same magnitude which were separated in time by 1 hr, 43 min. Seismograms for the two events are remarkably similar. The second event was chosen for study because clear P wave arrivals were observable for a greater range of azimuths and distances. These two events were not accompanied by any smaller teleseismically recorded events, unlike the 1970 earthquake which was the largest event of a swarm sequence.

Table 2. Velocity Model for the Mid-Atlantic Ridge, from Weidner [1974].

Thickness km	ρ g/cm^3	α km/sec	β km/sec
3	1.03	1.52	0.0
6	3.05	6.40	3.70
11	3.40	8.10	4.60
10	3.40	8.10	4.33
10	3.38	8.00	4.33
20	3.38	7.92	4.33
20	3.38	7.68	4.33
20	3.36	7.65	4.33
20	3.36	7.76	4.00
20	3.36	7.82	4.00
20	3.36	8.10	4.00
100	3.36	8.15	4.00
20	3.37	8.15	4.00
20	3.38	8.15	4.00
20	3.39	8.15	4.00
20	3.40	8.15	4.44
20	3.41	8.22	4.51
20	3.45	8.27	4.55
20	3.50	8.32	4.58
300	3.68	8.70	4.80

Table 3a. Regionalization of Surface Wave Paths for the April 24, 1970 Event.

Station	Distance, degrees	Azimuth, degrees	Fraction of path by region I	II	III	IV	V	VI	VII
AKU	13.0	32.4	-	-	-		-	1.0	-
COL	49.2	328.8	-	.20	.66	-	-	.03	.11
GDH	16.0	335.8	-	.56	-	-	-	.16	.28
KTG	15.9	16.1	-	.20	-	-	-	.48	.32
MAL	28.0	119.5	-	-	-	.25	-	.15	.60
NAT	60.6	180.0	-	-	-	-	-	.44	.56
NOR	26.6	5.9	-	.60	-	-	-	.20	.20
NUR	30.9	56.1	.36	-	-	-	-	.18	.46
PDA	19.0	156.6	-	-	-	-	-	1.0	-
PTO	22.6	118.9	-	-	-	.08	-	.18	.74
SCH	18.0	280.6	-	-	-	.30	-	.06	.64
SJG	44.3	224.8	-	-	-	-	-	.09	.91
STJ	13.6	241.0	-	-	-	.22	-	.16	.62
STU	27.5	85.7	-	-	.60	-	-	.09	.31
TRN	49.5	215.1	-	-	-	-	-	.11	.89
VAL	15.0	93.9	-	-	.21	-	-	.17	.62

Table 3b. Regionalization of Surface Wave Paths for the April 3, 1972 Event.

Station	Distance, degrees	Azimuth, degrees	I	II	III	IV	V	VI	VII
BEC	30.3	235.7	-	-	-	.12	-	.12	.76
BLA	35.1	259.7	-	-	-	.39	.32	.08	.21
CAR	50.5	222.2	-	-	-	-	-	.09	.91
COL	50.3	329.3	-	.22	.63	-	-	.08	.07
ESK	18.3	73.8	-	-	.36	-	-	.17	.47
FRB	19.3	312.4	-	.20	-	.15	-	.16	.49
KEV	31.2	36.4	.12	-	-	-	-	.53	.35
KTG	17.2	15.1	-	.19	-	-	-	.53	.28
MAL	27.5	117.1	-	-	-	.25	-	.13	.62
NAT	59.3	179.8	-	-	-	-	-	.35	.65
NOR	27.9	5.7	-	.56	-	-	-	.24	.20
NUR	31.7	54.2	.37	-	-	-	-	.11	.52
PDA	17.8	154.6	-	-	-	-	-	1.0	-
PTO	22.0	115.8	-	-	-	.06	-	.15	.79
SCH	18.2	284.5	-	-	-	.26	-	.15	.59
SJG	43.3	225.6	-	-	-	-	-	.10	.90
STJ	12.9	245.6	-	-	-	.19	-	.25	.56
STU	27.7	83.0	-	-	.59	-	-	.11	.30
TOL	25.4	111.8	-	-	-	.23	-	.13	.64

Table 4a. Results of the Moment Tensor Inversion for the April 24, 1970 Event

	Depth below sea floor (constraint)									
	4 km(4)	4 km(3)	4 km(2)	4 km(1)	1 km(4)	1 km(2)	7 km(4)	7 km(2)	77 km(4)	77 km(2)
	Moment tensor components, 10^{24} dyne-cm									
M_{xx}	4.83±0.10	4.94±5.11	3.88±0.17	4.74±8.68	3.86±0.08	3.14±0.14	5.71±0.12	4.58±0.20	-13.9±0.4	-12.1±0.7
M_{xy}	-1.03±0.09	-1.03±0.09	-0.46±0.15	-0.46±0.16	-0.37±0.08	-0.39±0.13	-1.22±0.11	-0.55±0.19	4.2±0.4	1.9±0.7
M_{yy}	0.47±0.10	0.58±5.13	-0.54±0.17	0.33±8.73	0.20±0.08	-0.58±0.14	0.45±0.12	-0.70±0.20	4.2±0.4	6.1±0.7
M_{xz}	---	---	2.67±0.65	2.67±0.65	---	10.3 ±2.50	---	2.53±0.61	---	0.7±0.2
M_{yz}	---	---	-4.47±0.66	-4.47±0.66	---	-17.3 ±2.56	---	-4.24±0.62	---	-1.1±0.2
M_{zz}	-5.30±0.09	-4.81±23.8	-3.34±0.15	0.67±40.40	-4.05±0.07	-2.56±0.12	-6.16±0.10	-3.88±0.18	9.6±0.2	6.1±0.3
	Eigenvalues, 10^{24} dyne-cm									
Tension	5.06±0.10	5.17±4.87	5.53±0.53	7.21±14.11	4.05±0.09	19.39±2.53	5.98±0.12	5.83±0.46	9.6±0.2	7.3 0.4
Intermediate	0.24±0.10	0.34±4.89	1.43±0.49	2.78±8.35	0.00±0.09	1.79±0.48	0.18±0.12	1.27±0.51	5.2±0.4	5.1 0.4
Compression	-5.30±0.09	-4.81±23.80	-6.96±0.63	-4.25±20.95	-4.05±0.07	-21.18±2.54	-6.16±0.10	-7.09±0.59	-14.8±0.4	-12.14 0.7
	Eigenvectors (strike°/dip°)									
Tension	-77±1/0	-77±19/0	-64±6/26±2	-59±218/35±26	-77±1/0	37±8/42±4	-78±1/0	-70±5/21±1	0/90	4±5/43±8
Intermediate	13±1/0	13±19/0	37±3/22±6	49±251/24±82	13±1/0	58±3/5±6	12±1/0	30±3/25±5	12±1/0	-171±2/48±8
Compression	0/90	0/90	162±2/54±4	165±156/45±81	0/90	154±3/47±5	0/90	164±2/56±4	-78±1/0	96±2/2±2
	Percent									
double couple	91	91	59	53	100	83	94	64	30	18
CLVD	9	4	41	21	0	17	6	36	70	82
explosion	-	5	-	26	-	-	-	-	-	-
	Double-couple scalar moment, 10^{24} dyne-cm									
	4.8	4.7	4.1	3.8	4.1	17.6	5.8	4.5	4.4	2.2

Table 4b. Results of the Moment Tensor Inversion for the April 3, 1972 Event

	Depth below sea floor (constraint)									
	4 km(4)	4 km(3)	4 km(2)	4 km(1)	1 km(4)	1 km(2)	7 km(4)	7 km(2)	77 km(4)	77 km(2)
	Moment tensor components, 10^{24} dyne-cm									
M_{xx}	7.84±0.16	7.99±7.73	7.32±0.18	7.12±8.90	6.43±0.14	6.08±0.16	9.04±0.19	8.46±0.21	-23.3±0.7	-24.3±0.8
M_{xy}	-0.71±0.12	-0.71±0.12	-1.60±0.14	-1.60±0.14	-0.61±0.11	-1.37±0.12	-0.83±0.15	-1.87±0.17	3.1±0.6	6.9±0.6
M_{yy}	0.49±0.16	0.64±0.12	-1.28±0.18	-1.48±9.35	0.21±0.14	-1.27±0.16	0.35±0.19	-1.64±0.21	8.0±0.7	12.7±0.8
M_{xz}	---	---	-8.85±0.81	-8.85±0.81	---	-34.30±3.15	---	-8.35±0.76	---	-2.0±0.2
M_{yz}	---	---	-5.96±0.99	-5.96±0.99	---	-23.2±3.87	---	-5.59±0.81	---	-1.3±0.2
M_{zz}	-8.33±0.13	-7.69±33.6	-6.04±0.15	-6.90±38.6	-6.64±0.11	-4.80±0.13	-9.39±0.15	-6.82±0.17	15.4±0.3	11.6±0.3
	Eigenvalues, 10^{24} dyne-cm									
Tension	7.91±0.16	8.06±7.66	11.86±0.69	11.52±10.67	6.49±0.14	40.64±3.31	9.12±0.19	12.16±0.60	15.4±0.3	14.7±0.6
Intermediate	0.42±0.16	0.57±8.05	1.60±0.66	1.33±8.85	0.15±0.14	2.24±0.71	0.27±0.19	1.26±0.61	8.3±0.7	10.9±0.3
Compression	-8.33±0.13	-7.69±33.60	-13.47±0.88	-14.10±26.01	-6.64±0.11	-42.88±3.44	-9.39±0.15	-13.42±0.75	-23.7±0.7	-25.6±0.8
	Eigenvectors (strike°/dip°)									
Tension	95°1/0	95°8/0	83±3/28±1	83±67/27±12	96±1/0	62±5/42±2	95°1/0	87°3/24±1	0/90	12°1/27±1
Intermediate	5°1/0	5°8/0	-18±3/21±3	-17±45/20±37	6±1/0	-33±3/5±4	5°1/0	-14°3/23±2	6±1/0	-175±1/62±3
Compression	0/90	0/90	-140±3/54±3	-139±89/55±44	0/90	-129±4/47±3	0/90	-141°3/55±2	96°1/0	-80°2/3°3
	Percent									
double couple	90	90	76	75	95	90	94	81	30	15
CLVD	10	6	24	22	5	10	6	19	70	85
explosion	-	4	-	3	-	-	-	-	-	-
	Double couple scalar moment, 10^{24} dyne-cm									
	7.5	7.3	10.2	10.6	6.3	38.6	8.8	10.9	7.1	3.8

Table 5. Stations Used for the Body Wave Analysis of April 3, 1972 Earthquake.

Station	Azimuth, degrees	Distance, degrees	Magnification
	WWSSN Network		
ATU	87.5	42.6	1500
BKS	-67.6	58.6	3000
CAR	-137.8	50.5	3000
COL	-30.7	50.3	1500
DUG	-71.9	51.8	3000
IST	80.2	43.6	1500
JER	84.5	53.6	3000
KBL	58.1	70.1	6000
NUR	54.2	31.7	1500
OXF	-95.1	42.2	3000
QUE	62.4	72.5	6000
QUI	-130.7	65.0	3000
SCP	-97.8	31.2	1500
TRI	85.1	32.0	3000
TUC	-80.2	56.2	1500
	Canadian Network		
EDM	-57.9	43.8	4500
FFC	-61.5	37.0	4200
FSJ	-51.3	48.3	3400

FIGURE CAPTIONS

Figure 1. Bathymetric map of the southern Reykjanes Ridge and Gibbs Fracture Zone. Contours are at one kilometer intervals. Earthquakes of m_b greater than 5.0 recorded by the WWSSN from 1962 to 1978 are shown by dots. Fault plane solutions are from Einarsson [1979]. Bathymetry from NAVOCEANO WORLD RELIEF MAP, NA-4, May 1977.

Figure 2. Response curves calculated at different depths for the oceanic model of table 2. $G_1 = A\frac{kY_3(h,\omega)}{2}$;

$G_2 = A\frac{-Y_2(h,\omega)-\lambda(h)kY_3(h,\omega)}{\lambda(h) + 2\mu(h)}$; $G_3 = A\frac{Y_4(h,\omega)}{\mu(h)}$;

$A = \frac{Y_i(0,\omega)}{4U\omega^2 I}\sqrt{\frac{2k}{\pi r}}$ where r is the data equalization distance of 4000 km. For definition of other terms, see Appendix I.

Figure 3. Stations and regionalization used for the surface wave analysis plotted on an azimuthal equidistant projection centered on the April 3, 1972 event. Regions are labeled with Roman numerals and the corresponding phase velocity dispersion curves are displayed in Figure 4. Circles mark distances of 30° and 60° from the epicenter of the 1972 event.

Figure 4. Phase velocity dispersion curves for the regions shown in Figure 3. References: I. Naponen [1966], Calgagnile and Panza [1978]; II. Gregersen [1971]; III, IV. Wickens [1971]; V. Oliver et al. [1961]; VI. Forsyth [1975] (5-10 m.y. normalized to water depth of 3.2 km); VII. Weidner [1974] (normal ocean basin).

Figure 5a. Examples of seismograms and corrected source spectra for the April 24, 1970 event. Displayed seismograms were traced directly from WWSSN records and are not equalized to a common epicentral distance and station magnification. Open circles in the source spectra indicate points which were eliminated from the data set for the inversion during the visual inspection of the data. Δ - epicentral distance in degrees, az - station azimuth in degrees from north, mag-station magnification.

Figure 5b. Examples of seismograms and corrected source spectra for the April 3, 1972 event. Source spectra obtained from filtered records are also shown.

Figure 6a. Residuals vs. focal depth for the inversion of the Rayleigh wave radiation pattern to obtain the moment tensor for the April 24, 1970 event.

Figure 6b. Residuals vs. focal depth for the April 3, 1972 event.

Figure 7a. Fault plane solution for the April 24, 1970 event. Superimposed are the axes and double-couple fault plane solutions corresponding to the results of the moment tensor inversion under constraints (2) and (4) for a focal depth of 4 km below the sea floor. Dotted line and □ - constraint (2); solid line and ⬡ - constraint (4). T - tension; B-intermediate; C-compression. Closed circles indicate compressional first motion of the P-wave. Open circles indicate stations for which the first motion was originally thought to be compressional but for which this interpretation was subsequently modified when considering the moment tensor solution and the expected amplitude of the first motion as

predicted by synthetic seismograms. In the lower right hand corner is the fault plane solution presented by Einarsson [1979]. Large dots signifiy clear arrivals whereas small dots indicate less reliable picks. Arrows indicate S-wave polarization angles.

Figure 7b. Fault plane solution for the April 3, 1972 event. Superimposed are the axes and nodal planes corresponding to the results of the moment tensor inversion for a focal depth of 4 km below the sea floor. Closed circles indicate compressional first motion of the P-wave; open circles indicate dilatational first motion. Apparent nodal planes separated by approximately 60° are constrained by the data. In the lower right hand corner is the fault plane solution presented by Einarsson [1979]: closed circles - compression; open circles - dilatation; crosses - nodal.

Figure 8a. Examples at several periods of the fit of the moment tensor solution to the observed data for the April 24, 1970 event for a depth of 4 km below sea floor. Plots of the real and imaginary parts versus azimuth illustrate the fit when the inversion is performed under constraint (2); plots of negative amplitude versus azimuth show the result under constraint (4) (real part = amplitude, imaginary part = 0). Open circles indicate data that were weighted by zero during the visual inspection of the spectra.

Figure 8b. Fit of the model to the data recast into the form of amplitude and phase: the solution under constraint (2) is given by dashed lines, the solution under constraint

(4) is given by solid lines.

Figure 9. Examples of the fit to the data of the moment tensor solution for the April 3, 1972 event for a depth of 4 km below sea floor (see Figure caption 8).

Figure 10. Model parameters and fault geometry used in the example of P-wave synthesis for a shallow, finite earthquake source. Circles are successive rupture fronts. Rupture propagates from top to bottom (T-B), from the center (C), and from bottom to top (B-T) in the three cases shown.

Figure 11. Theoretical seismograms for models described in Figure 10. The dip of the fault is 55°. Also shown is the theoretical fault plane solution; points A, B, C, and D represent projections of ray paths for which seismograms were calculated. T-B, C, and B-T signify rupture propagation radiating from top-to-bottom, from the center, and from bottom-to-top, respectively.

Figure 12. Theoretical seismograms for case T-B in Figure 10 illustrating the apparent distortion of the fault plane solution due to interference between the direct and reflected phases. Solid line is the true fault plane solution whereas dashed line delimits the apparent dilatational quadrant. The dip of the fault is 45°.

Figure 13. Examples of long period P-wave seismograms (vertical component) observed for the April 3, 1972 event. Seismograms were equalized by correcting for geometrical spreading and for differences in the seismometer magnifications. Dots indicate projections

of ray paths to the given stations. Also shown is the preferred fault plane solution.

Figure 14. Theoretical seismograms (vertical component) compared to observed P-wave data for the April 3, 1972 event. Upper trace is observed; lower trace is calculated. Seismograms were equalized to a seismometer magnification of 3000. Numbers below the station names corresponded to moment (in units of 10^{24} dyne-cm) at the given station, and M_o is the average moment. Dotted lines on the observed seismograms indicate the time of the first motion observed on the short period vertical component.

Figure 15. Model parameters used for the calculation of the theoretical seismograms shown in Figure 14. The indicated fault width is measured down-dip and the fault is projected onto a vertical plane parallel to the strike of the fault. Dots represent individual point sources. Fault length is 13 km. The medium structure below the receivers is a homogeneous half-space with α = 6 km/sec, β = 3.46 km/sec and ρ = 3 g/cm^3.

Figure 16a. Theoretical P-wave seismograms calculated for several fault geometries compared to the observed data (seismogram I). Fault dimensions are 13 km length by 3 km width for seismograms II and III and 7 km length by 6 km width for IV and V. Seismograms II and IV were calculated for rupture initiating at the top of the fault whereas III and V were calculated for rupture initiating at the bottom. Other parameters are the same as in

Figure 15. Seismograms VI were calculated for a point source at a depth of 0.35 km below sea floor and a triangular time function with a 0.8 second rise and a 1.8 second roll-off.

Figure 16b. Theoretical P-wave seismograms (lower trace) calculated for the moment tensor obtained from the Rayleigh wave inversion under constraint 2 (Table 4b - 4km below sea floor) compared to the observed data at several representative stations (upper trace). The seismograms were calculated for a point source with the same depth and time function as in Figure 16a. The fit is worse than that for constraint 4 (Figure 14). For example, constraint 2 requires that station CAR be further within the dilitational quadrant than is indicated by the data and that KBL have the wrong first motion polarity.

Figure 17. Examples of short period P-wave seismograms (vertical component) for the April 3, 1972 event. Seismograms are direct copies of observed records.

Figure 18. Examples of long period P-wave seismograms recorded for the April 24, 1970 earthquake. Seismograms are direct copies of observed vertical component records. Mag-station magnification, Az-station azimuth, Δ-epicentral distance.

Figure 19. Depth to various isotherms at a distance of 10 km from the ridge axis vesus spreading rate, calculated for the thermal model of Sleep [1975]. Also indicated is the depth of faulting, 2.1-2.8 km, corresponding to the 3-4 km wide fault obtained for the April 3, 1972 event. Figure modified from Solomon and Burr [1979].

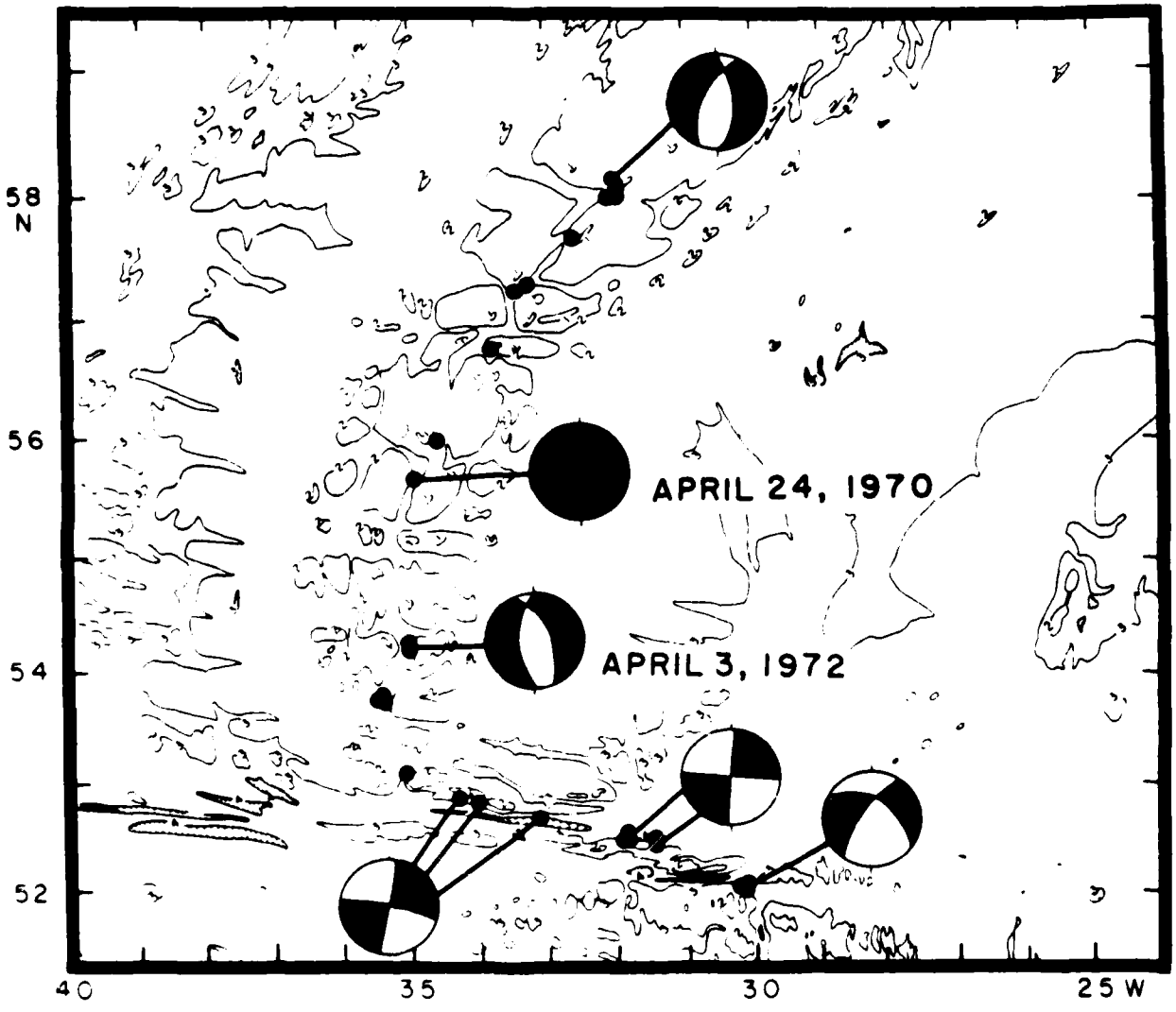

Figure 1

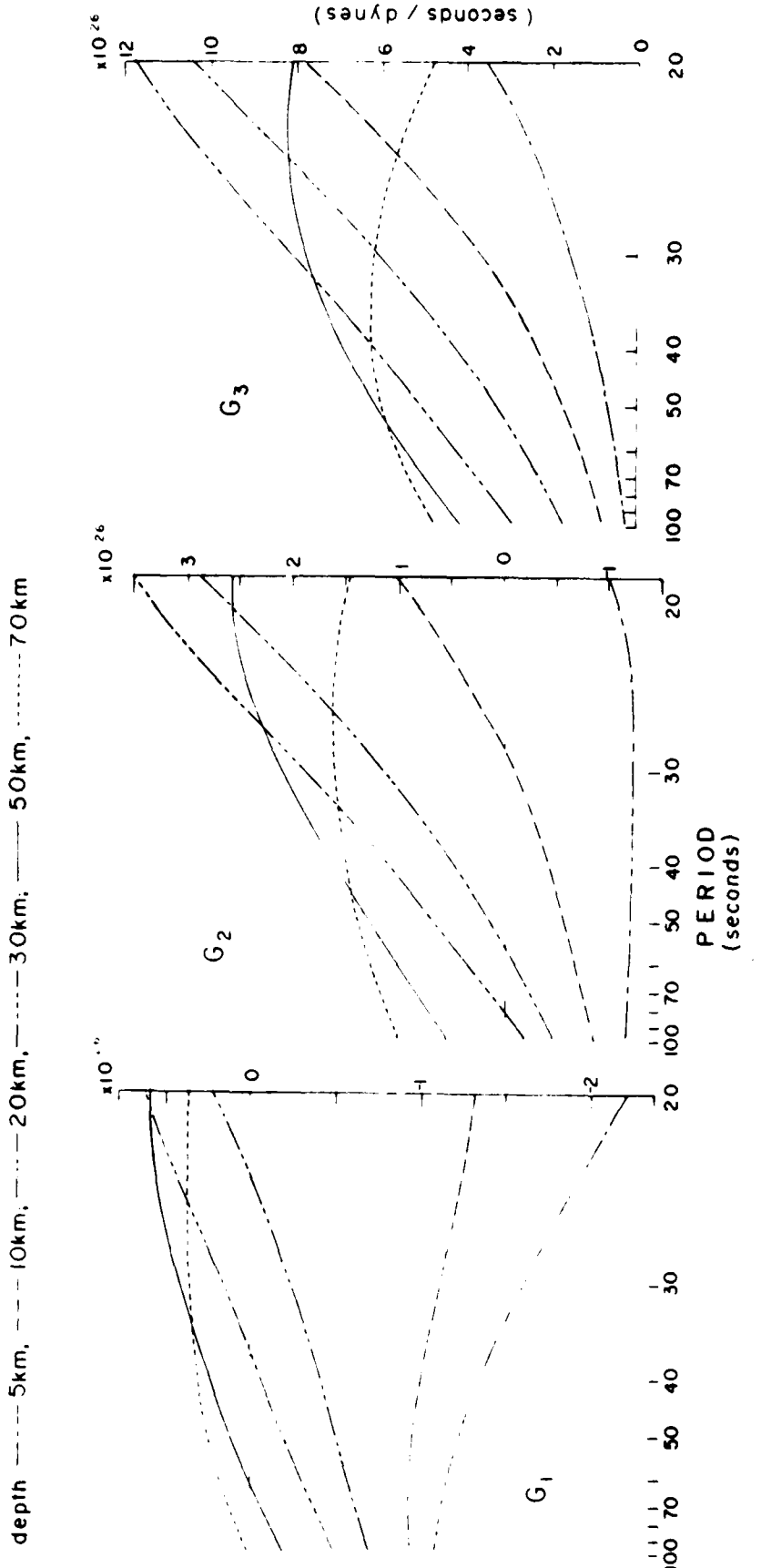
(seconds / dynes)
x10 26
12
10
8
6
4
2
0
20
30
40
50
70
100
1
G3
x10 26
3
2
1
0
G2
x10
0
-1
-2
G1
PERIOD
(seconds)
depth ---- 5km, - - - 10km, -·-·- 20km, ·····30km, —— 50km, ·····70km

Figure 2

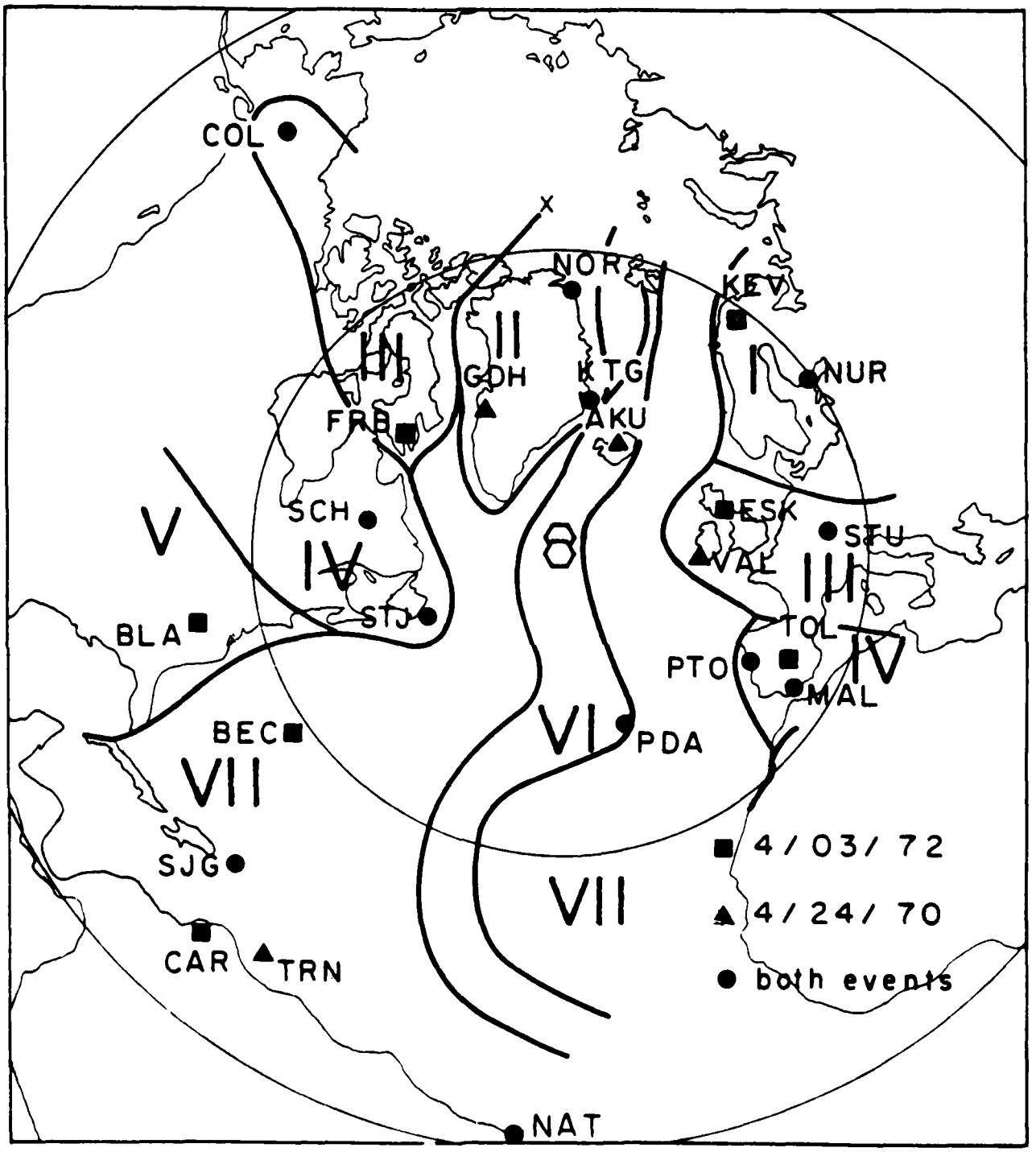
COL
NOR
KEV
NUR
GDH
KTG
AKU
FRB
SCH
ESK
STU
VAL
STJ
BLA
TOL
PTO
MAL
BEC
PDA
SJG
CAR
TRN
NAT
I
II
III
IV
V
VI
VII
VII
4/03/72
4/24/70
both events

Figure 3

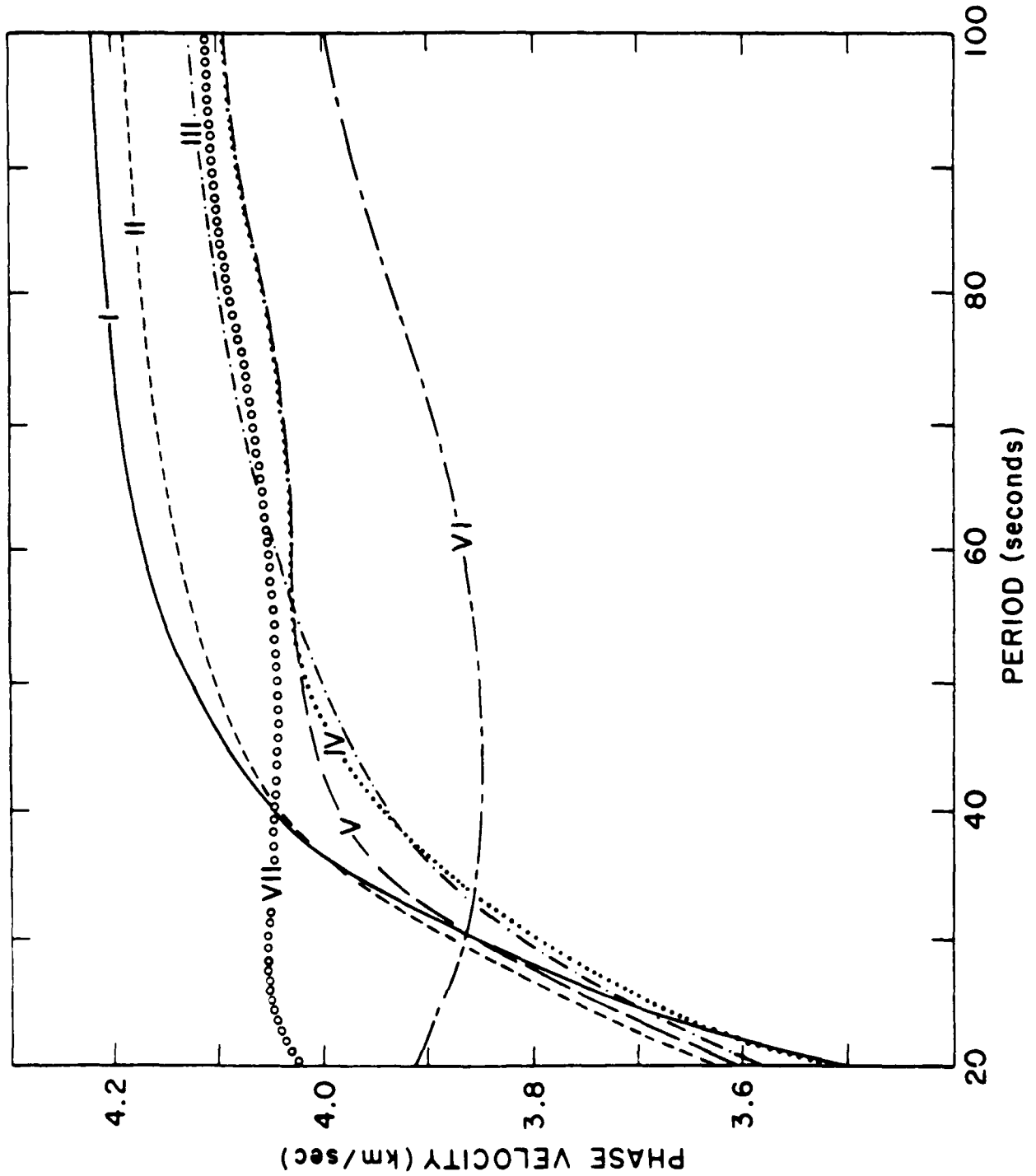
PERIOD (seconds)
20
40
60
80
100
PHASE VELOCITY (km/sec)
4.2
4.0
3.8
3.6
I
II
III
IV
V
VI
VII

Figure 4

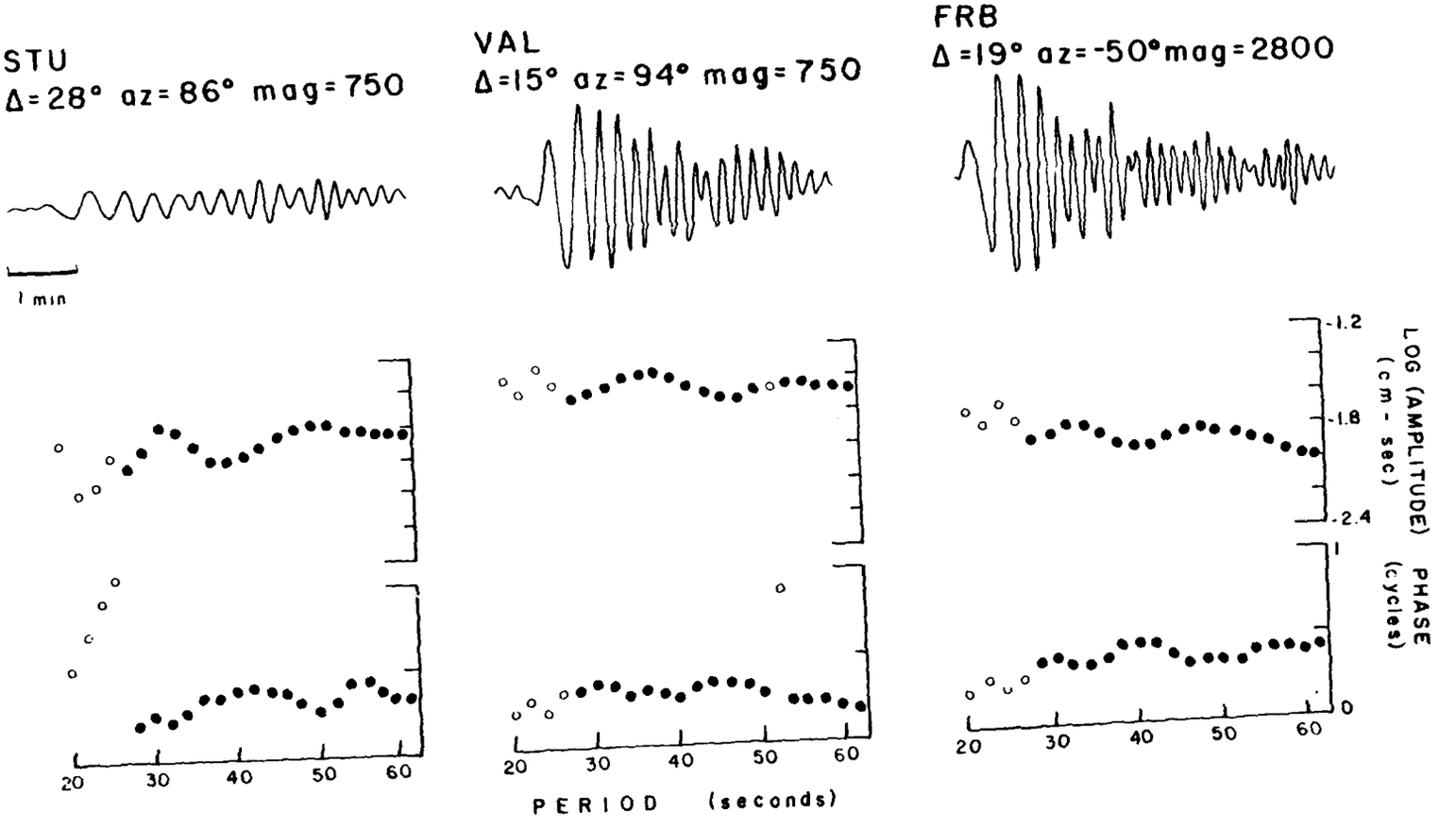
STU
Δ=28° az=86° mag=750
1 min
VAL
Δ=15° az=94° mag=750
FRB
Δ=19° az=-50°mag=2800
-1.2
-1.8
-2.4
LOG (AMPLITUDE) (cm - sec)
1
0
PHASE (cycles)
20
30
40
50
60
PERIOD (seconds)

Figure 5a

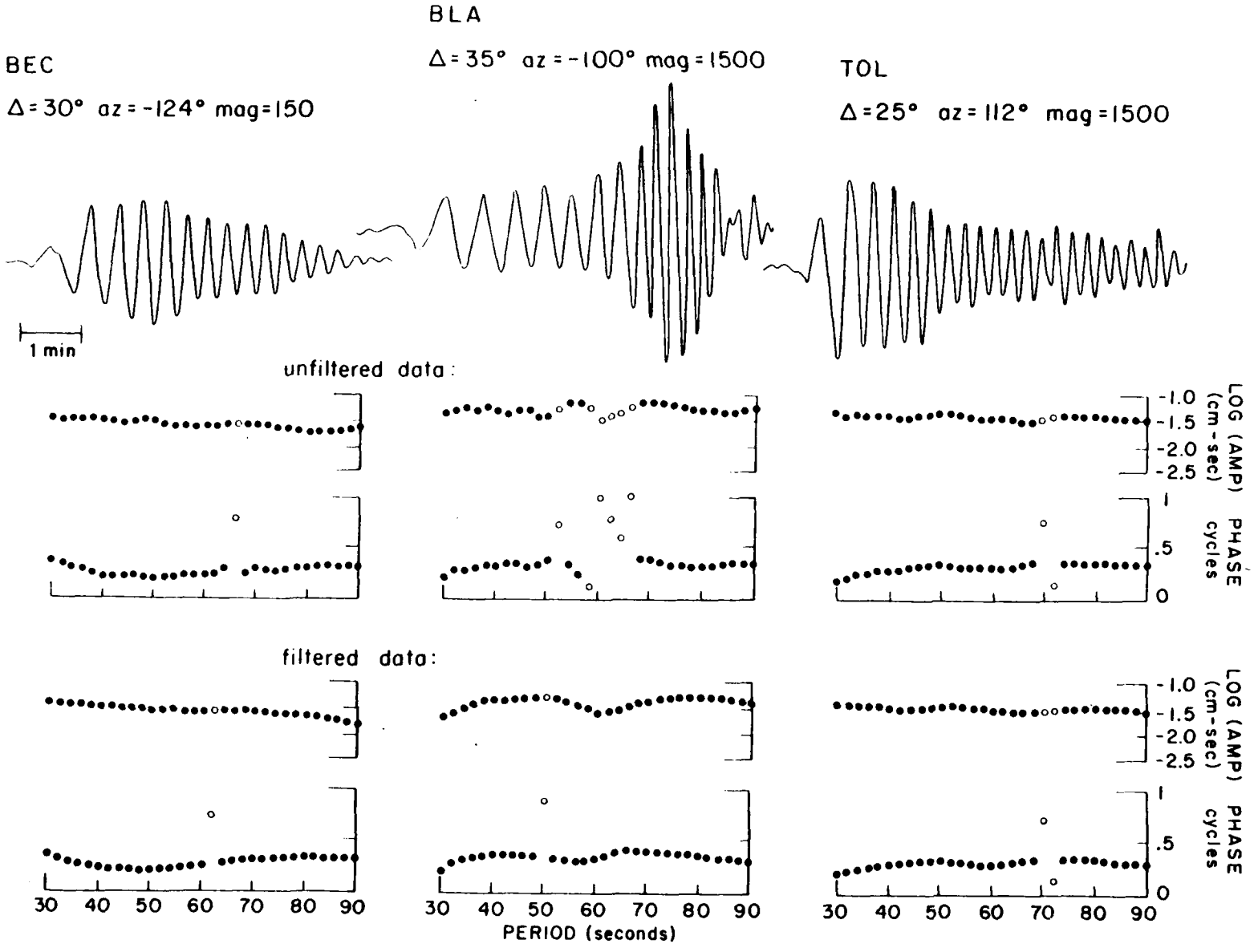
BEC
Δ = 30° az = -124° mag = 150
BLA
Δ = 35° az = -100° mag = 1500
TOL
Δ = 25° az = 112° mag = 1500
1 min
unfiltered data:
filtered data:
LOG (AMP) (cm-sec)
-1.0
-1.5
-2.0
-2.5
PHASE cycles
1
.5
0
30 40 50 60 70 80 90
PERIOD (seconds)

Figure 5b

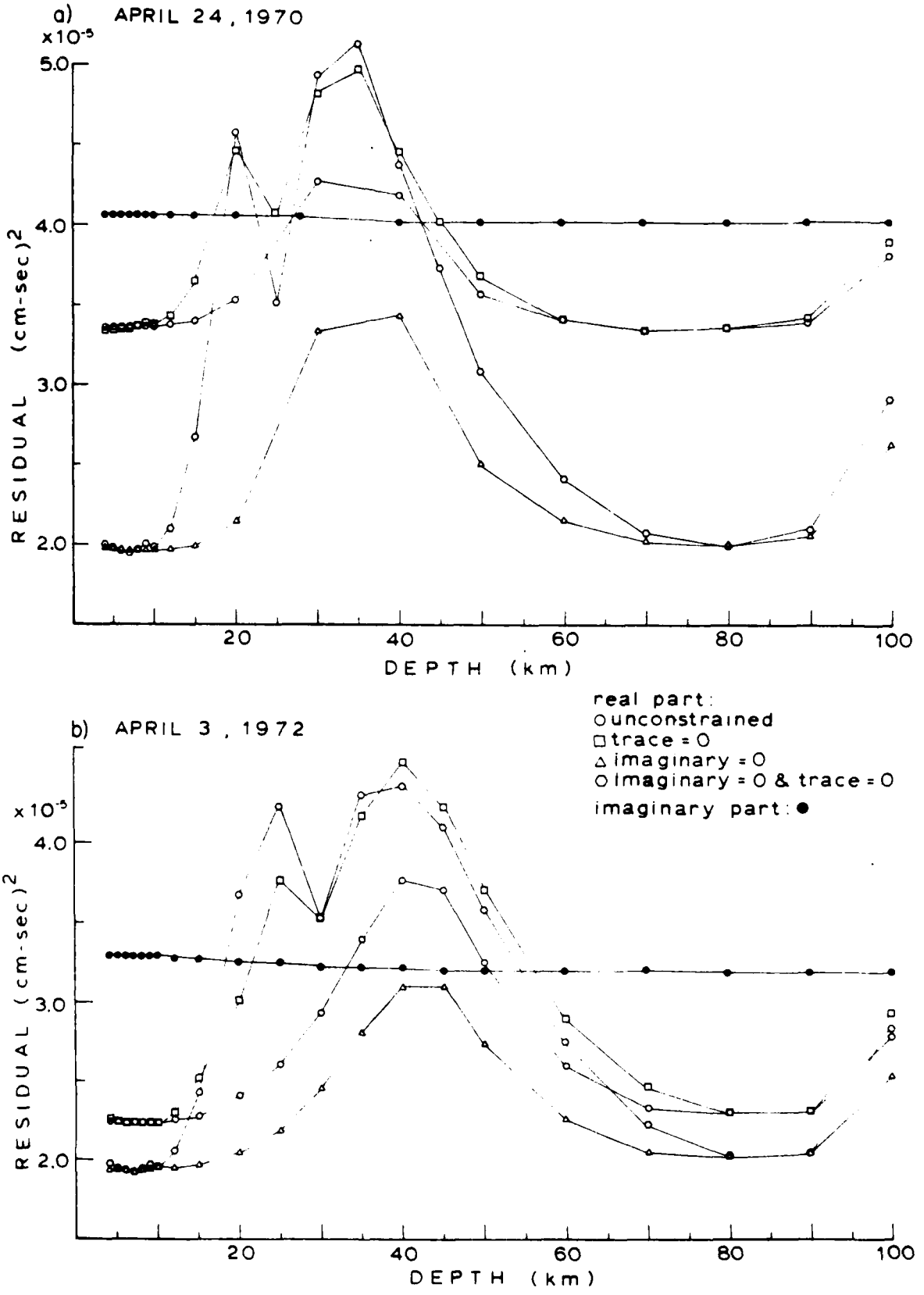
a) APRIL 24, 1970
x10⁻⁵
5.0
4.0
3.0
2.0
RESIDUAL (cm-sec)²
20
40
60
80
100
DEPTH (km)
real part:
○ unconstrained
□ trace = 0
△ imaginary = 0
○ imaginary = 0 & trace = 0
imaginary part: ●
b) APRIL 3, 1972
x10⁻⁵
4.0
3.0
2.0
RESIDUAL (cm-sec)²
20
40
60
80
100
DEPTH (km)

Figure 6

APRIL 24, 1970
55.6 N 35.0 W

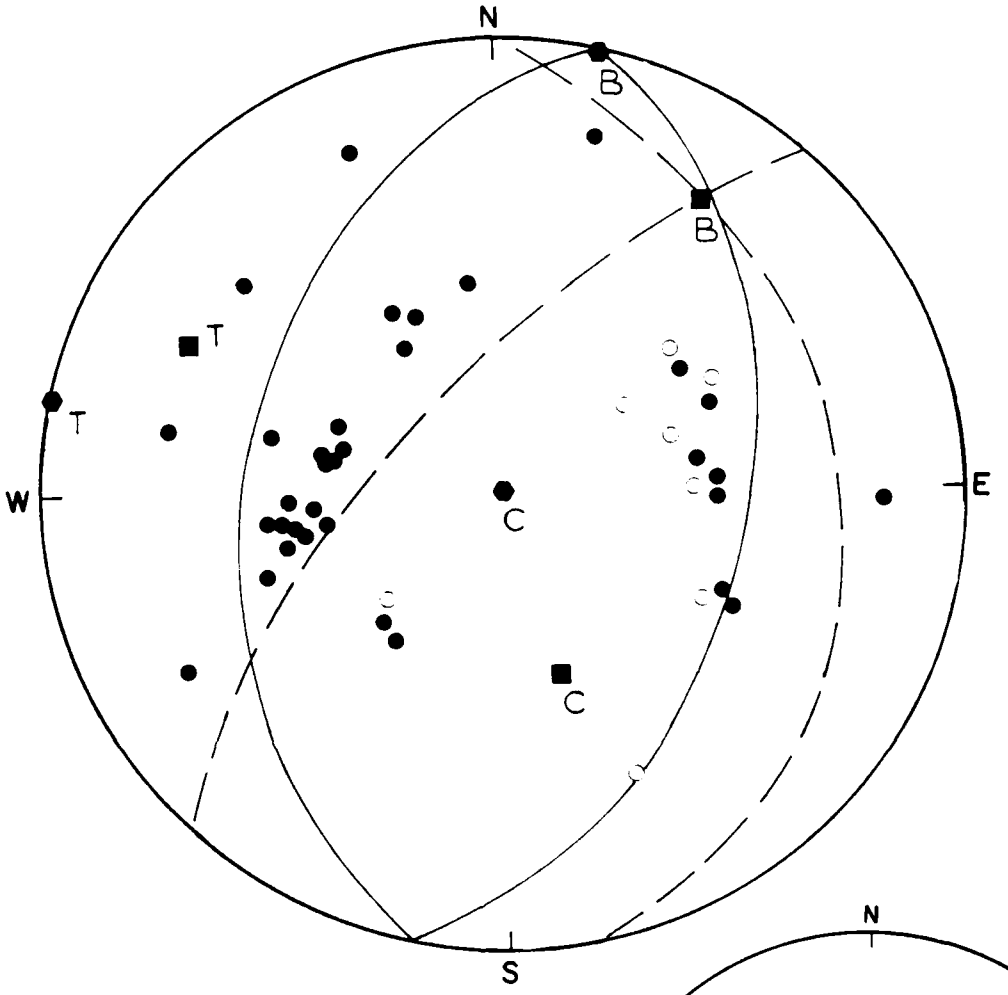

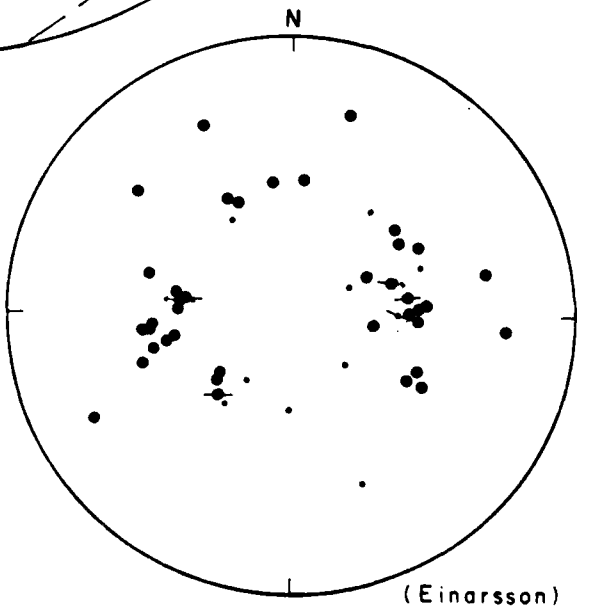

(Einarsson)

Figure 7a

APRIL 3, 1972

54.3 N 35.1W

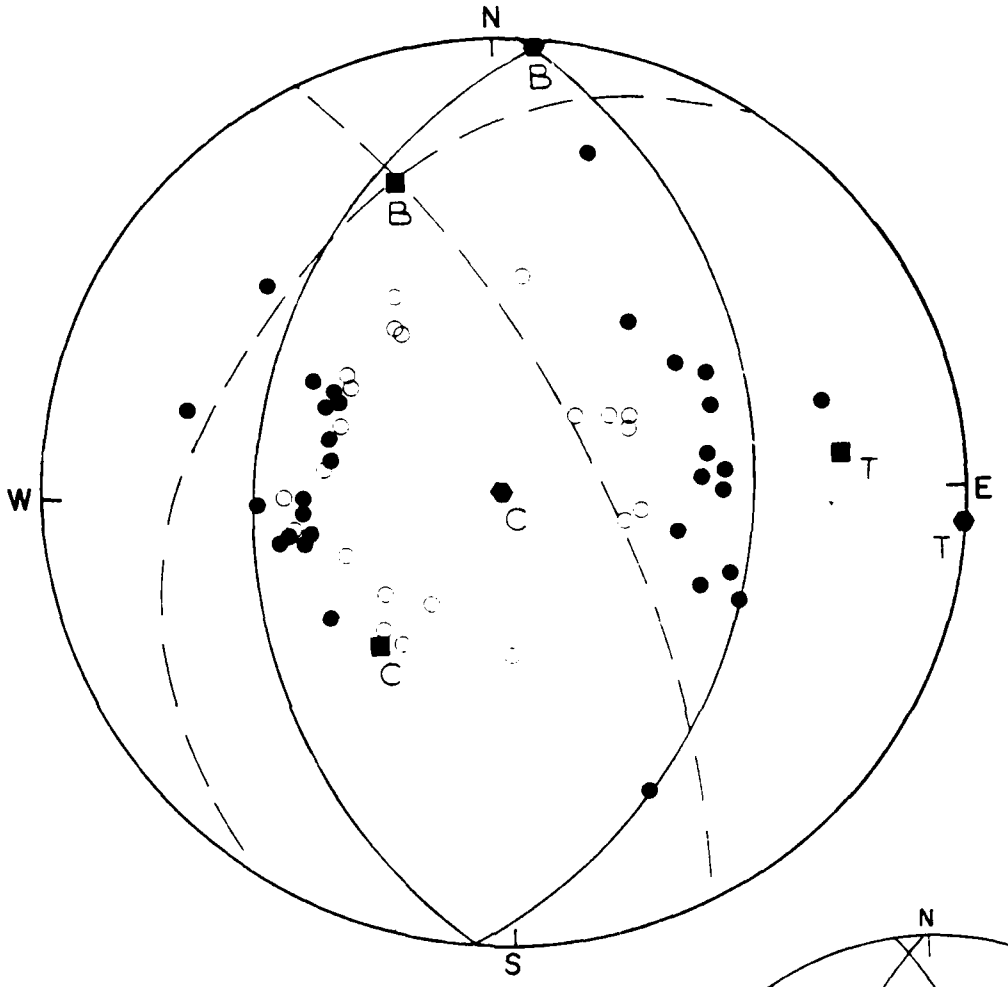

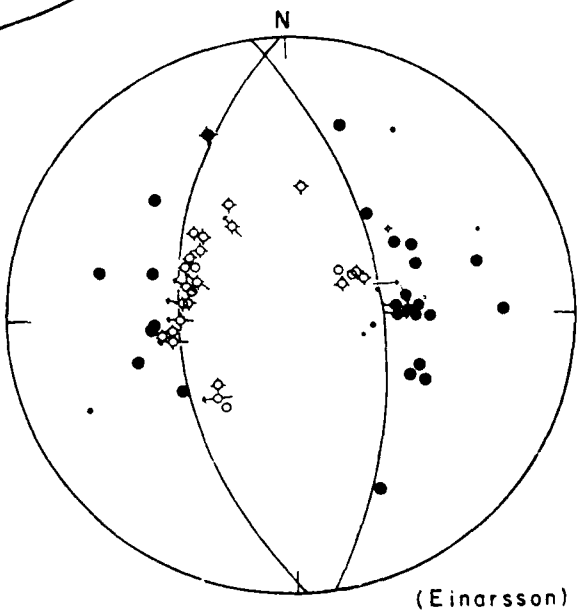

(Einarsson)

Figure 7b

APRIL 24, 1970

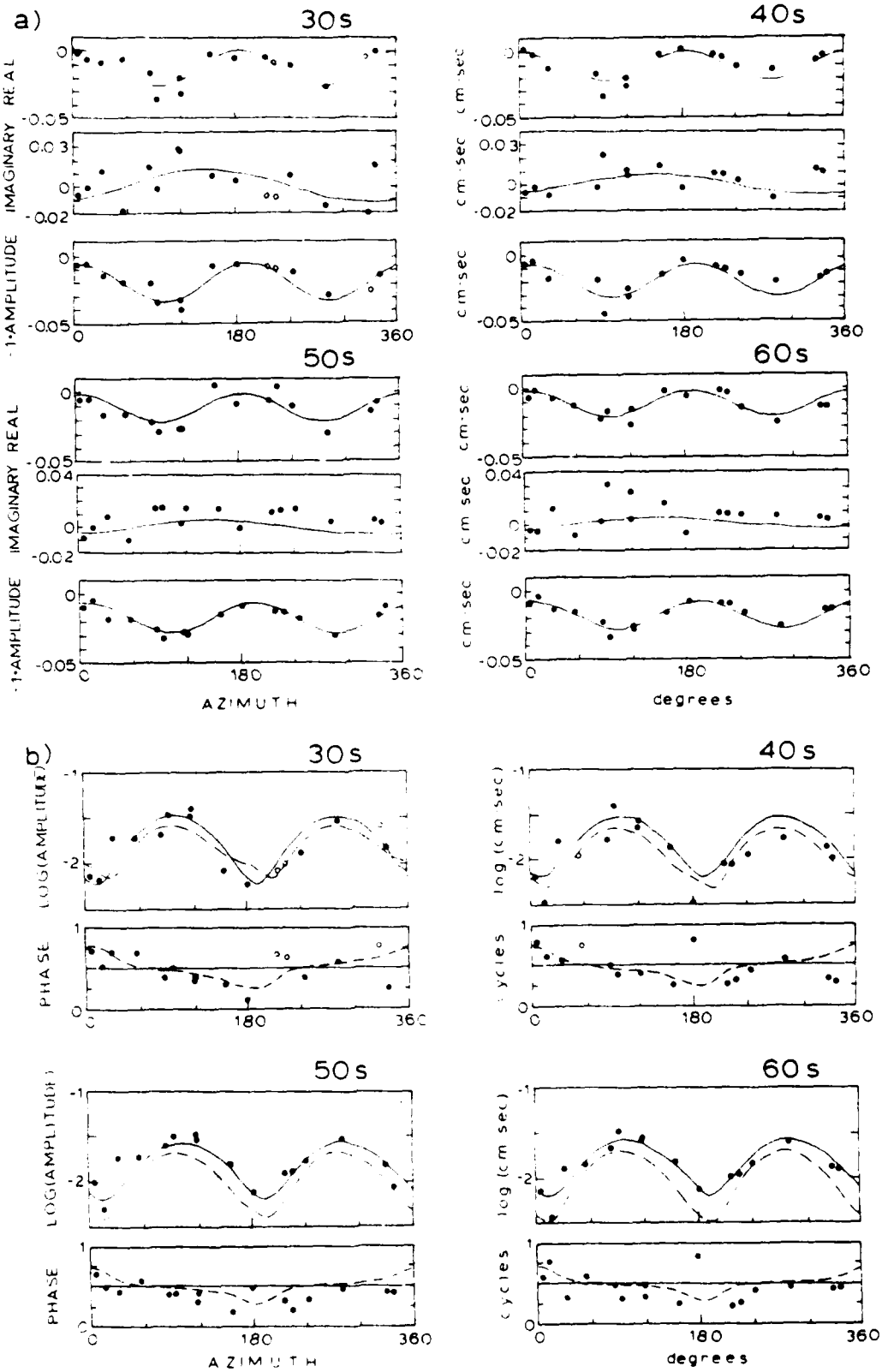

Figure 8

APRIL 3, 1972

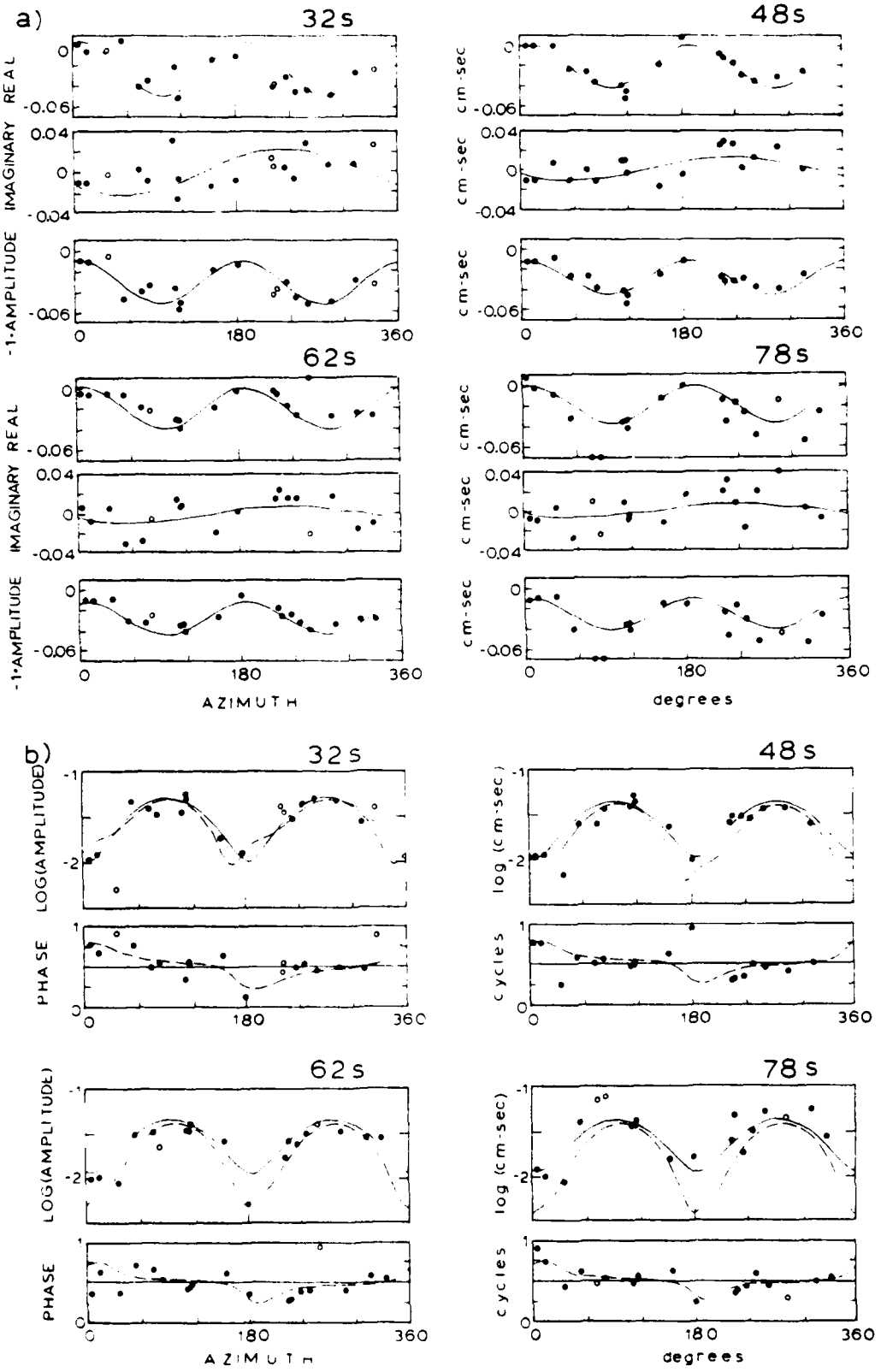

Figure 9

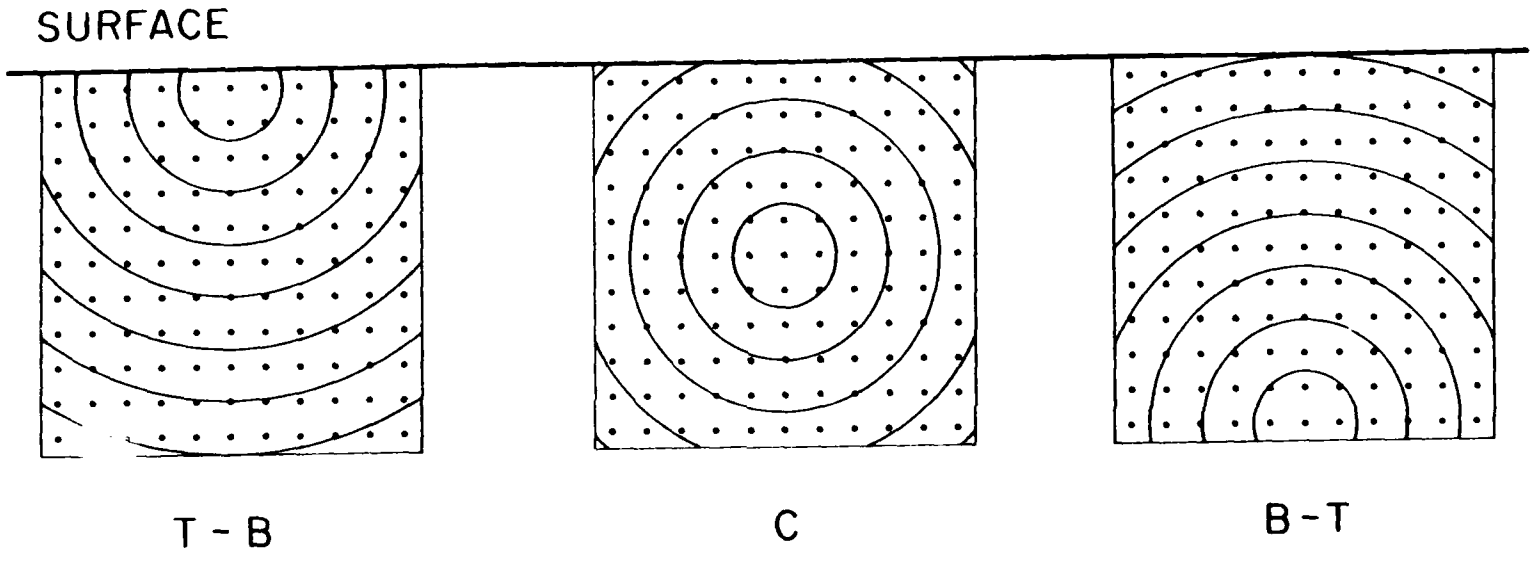

MODEL PARAMETERS:

FAULT SIZE = 11 x 11 km

RUPTURE VEL. = 2.5 km/sec RISE TIME = 0.3 sec

HALF - SPACE: α = 6.0 km/sec β = 3.3 km/sec ρ = 3 g /cm^3 t* = 1.2 sec

Figure 10

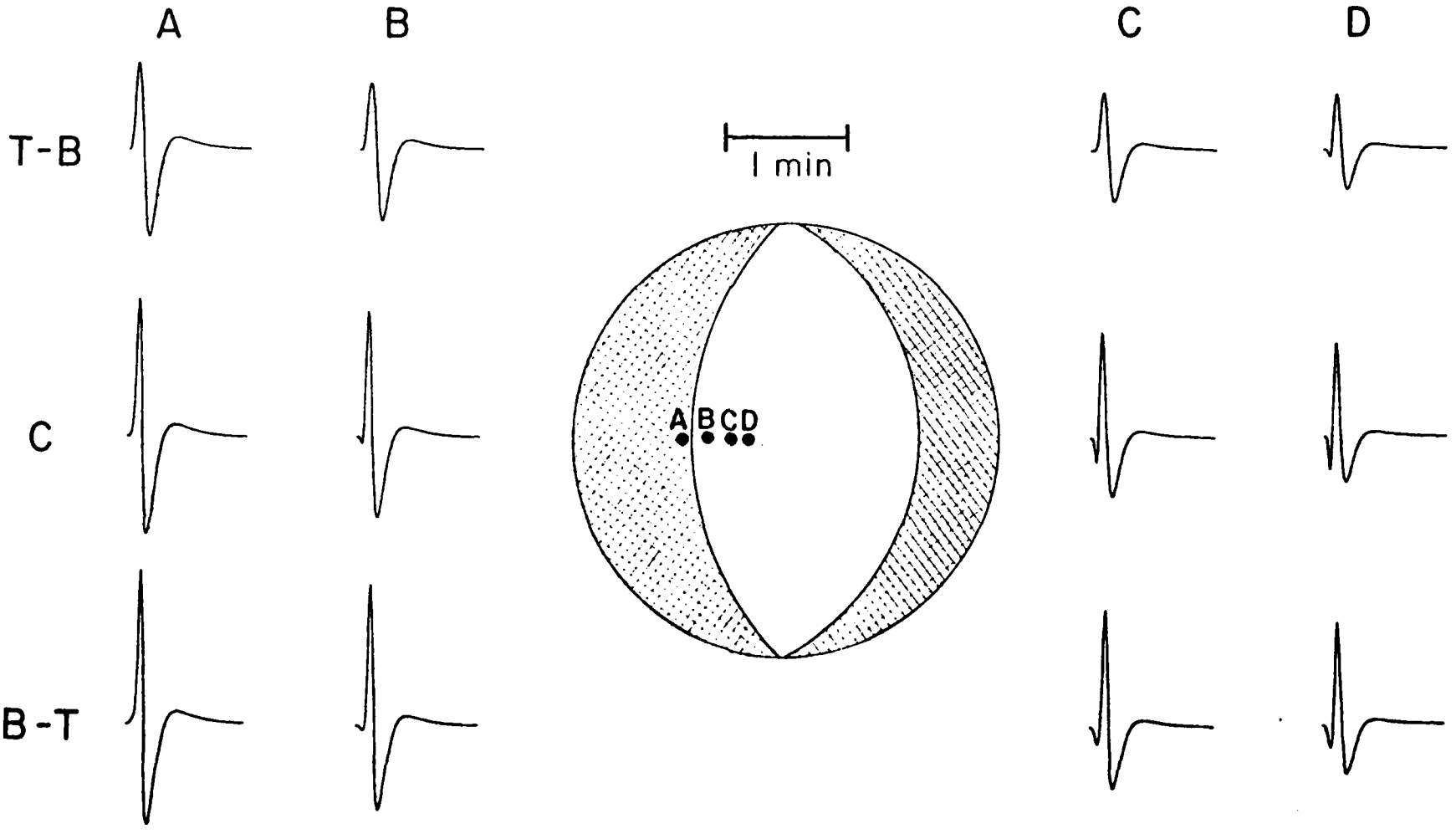
A
B
C
D
T-B
C
B-T
1 min
A B C D

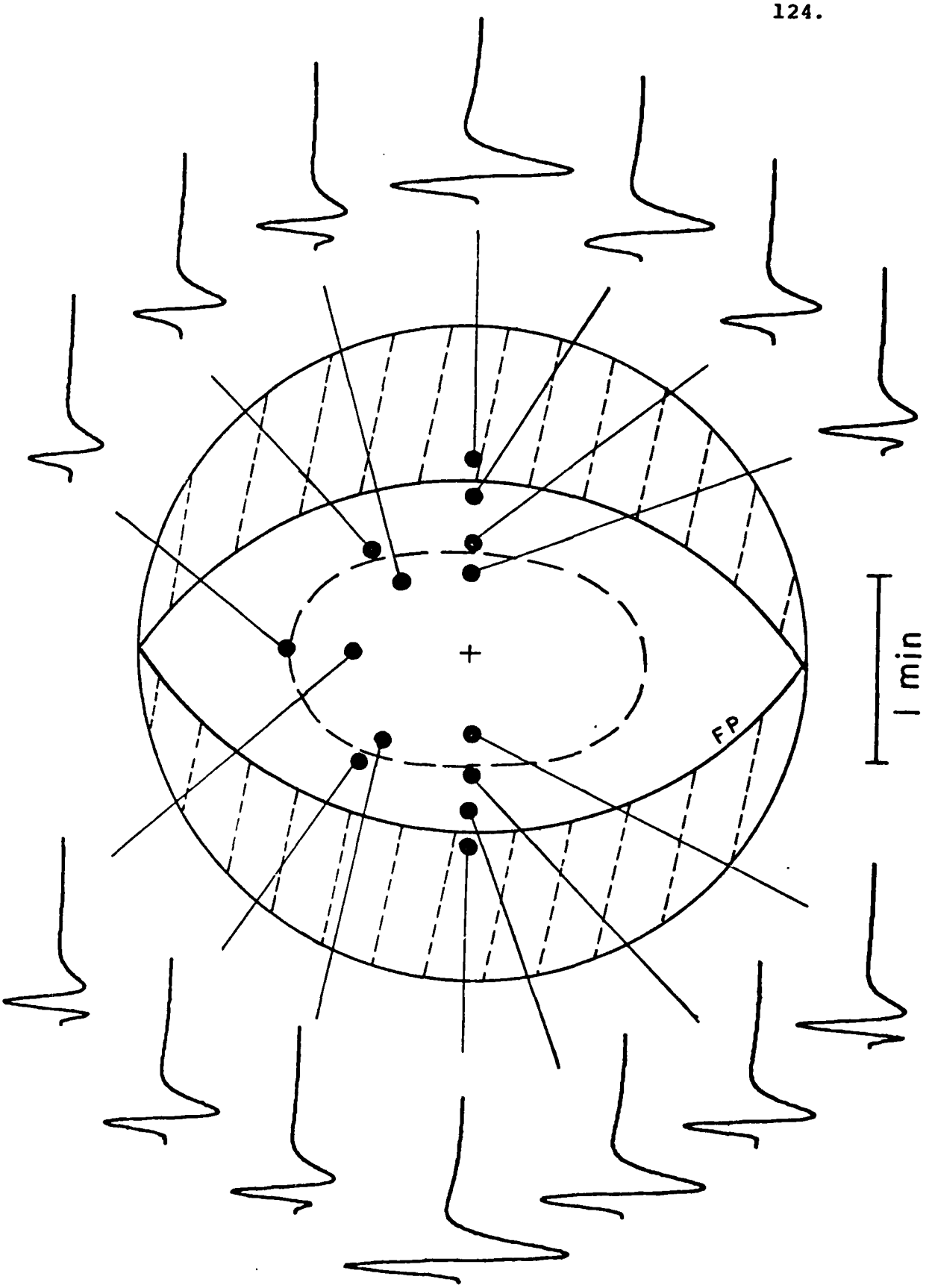

Figure 12

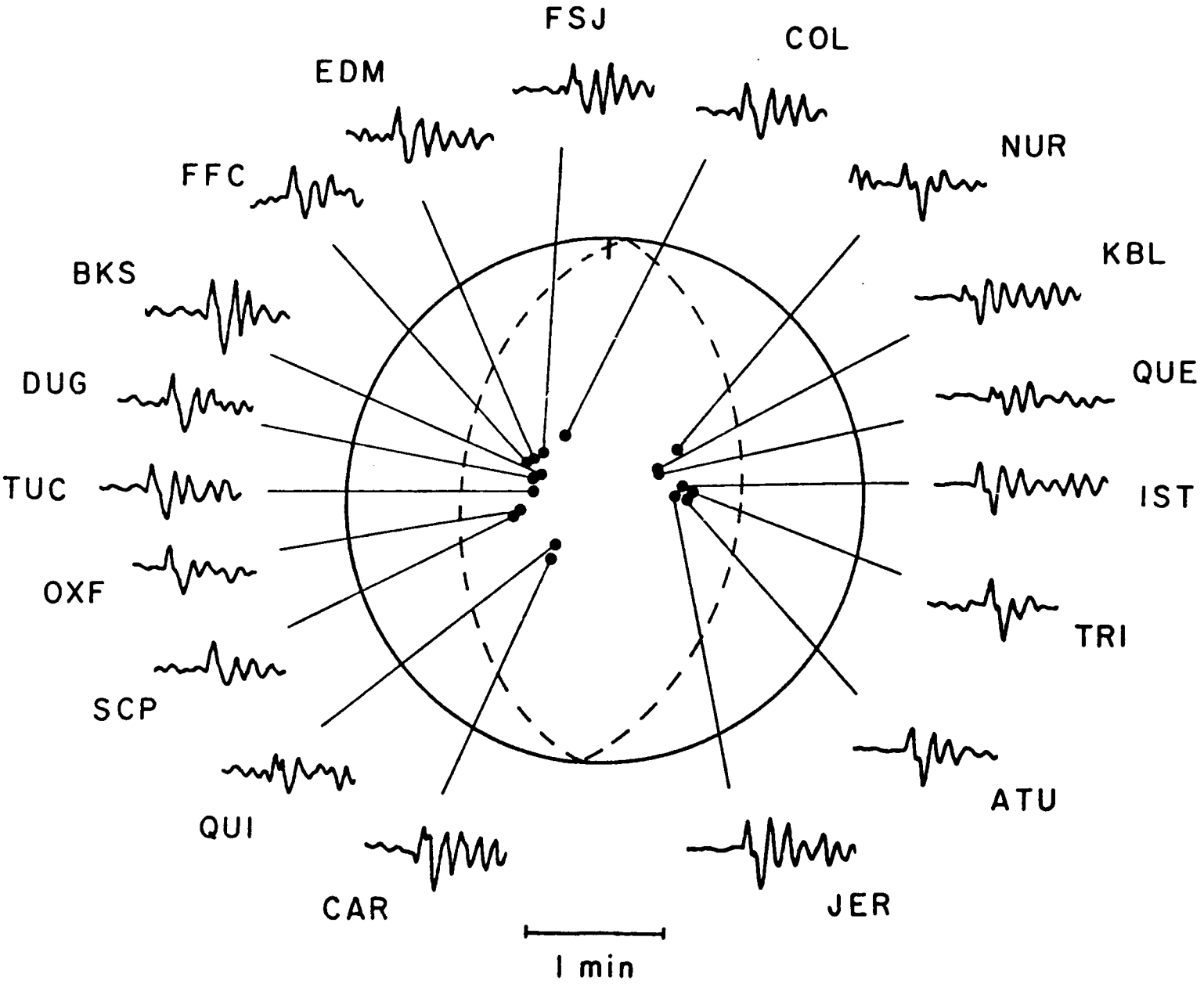
FSJ
COL
EDM
NUR
FFC
KBL
BKS
QUE
DUG
IST
TUC
TRI
OXF
ATU
SCP
QUI
CAR
JER
1 min

Figure 13

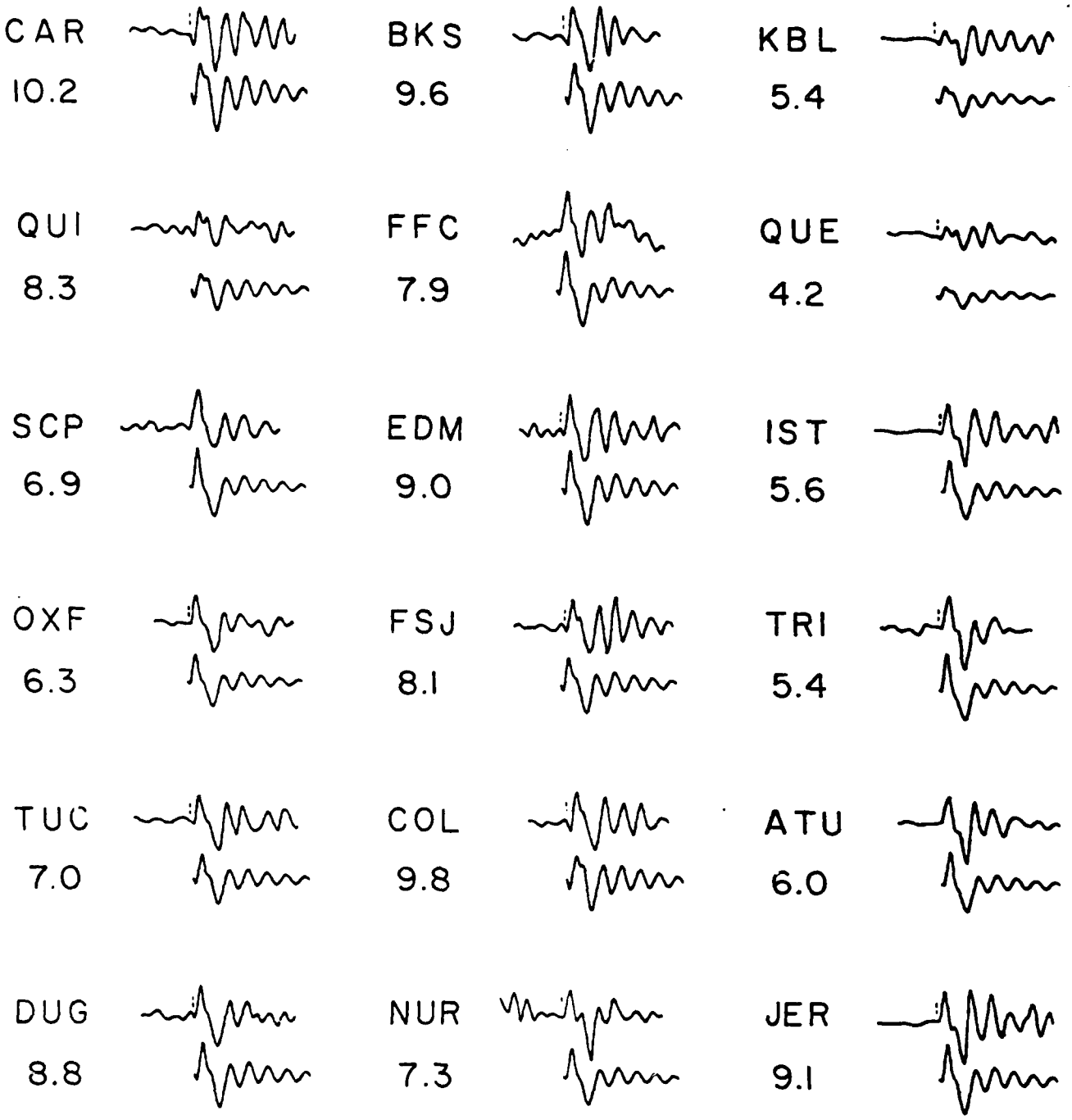
CAR
10.2
BKS
9.6
KBL
5.4
QUI
8.3
FFC
7.9
QUE
4.2
SCP
6.9
EDM
9.0
IST
5.6
OXF
6.3
FSJ
8.1
TRI
5.4
TUC
7.0
COL
9.8
ATU
6.0
DUG
8.8
NUR
7.3
JER
9.1
$M_o = 7.5 \times 10^{24}$ dyne-cm
1 min

Figure 14

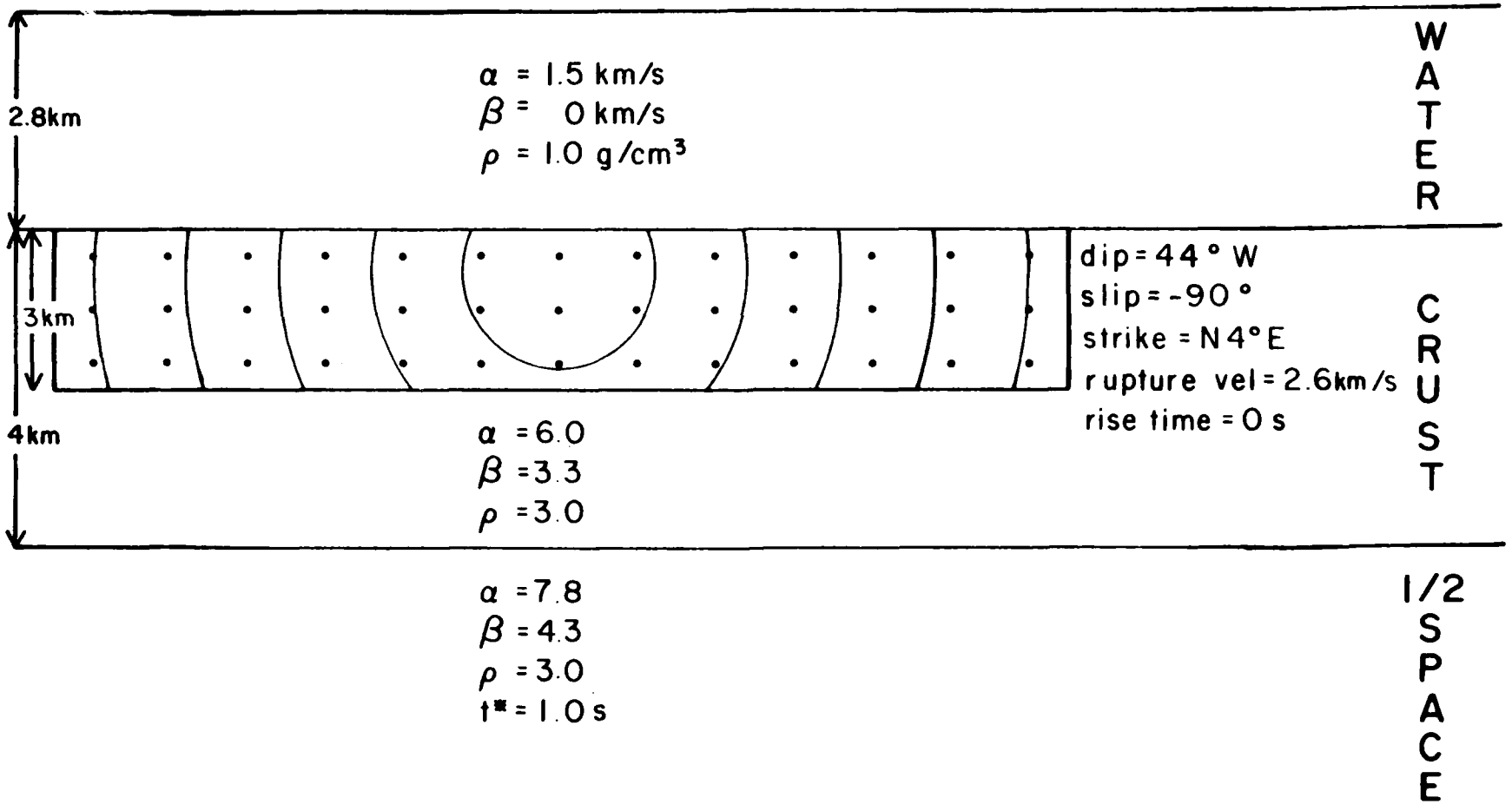
2.8km
α = 1.5 km/s
β = 0 km/s
ρ = 1.0 g/cm³
WATER
3km
dip = 44° W
slip = -90°
strike = N4°E
rupture vel = 2.6km/s
rise time = 0 s
CRUST
4km
α = 6.0
β = 3.3
ρ = 3.0
α = 7.8
β = 4.3
ρ = 3.0
t* = 1.0 s
1/2 SPACE

Figure 15

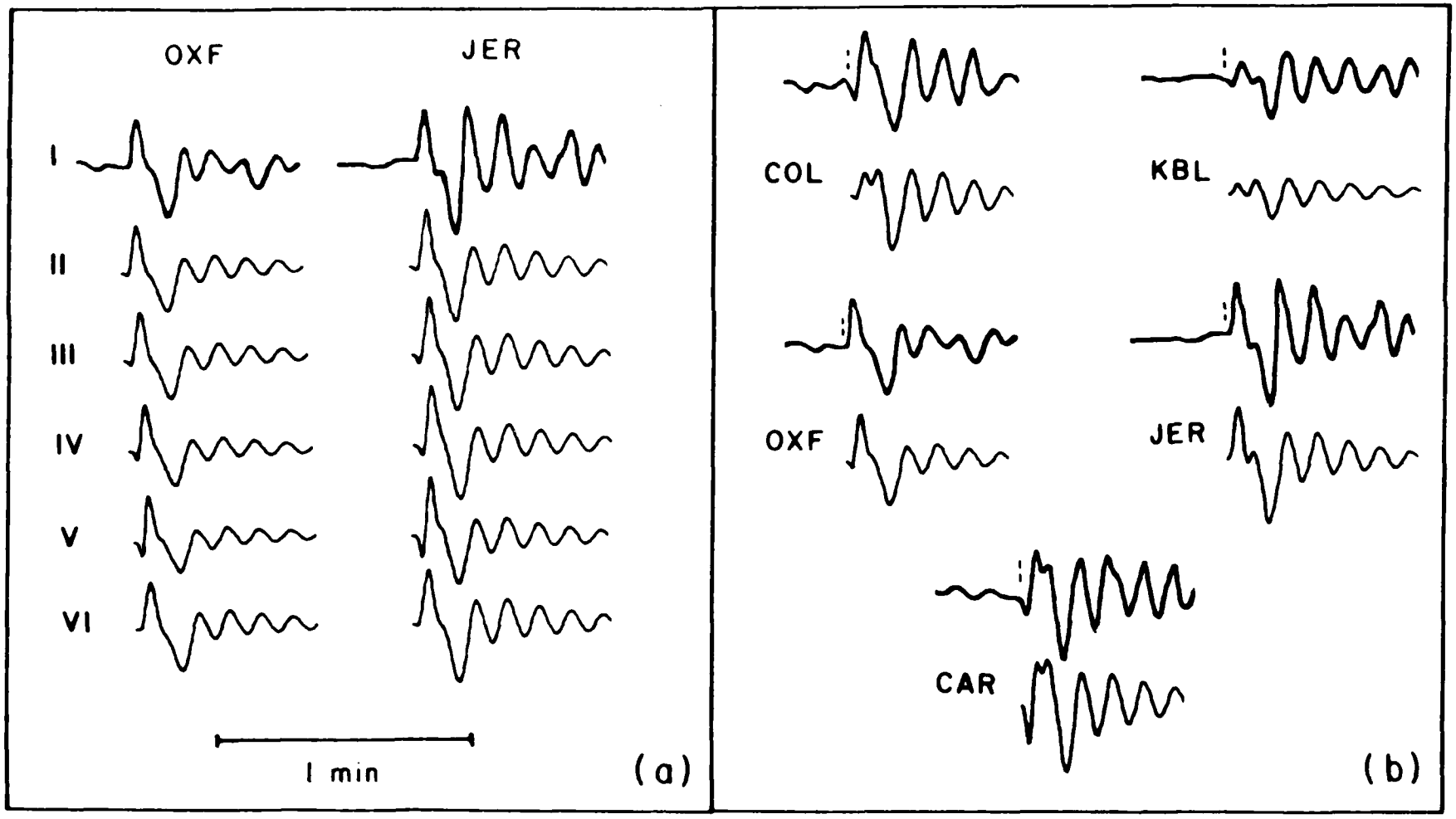

Figure 16

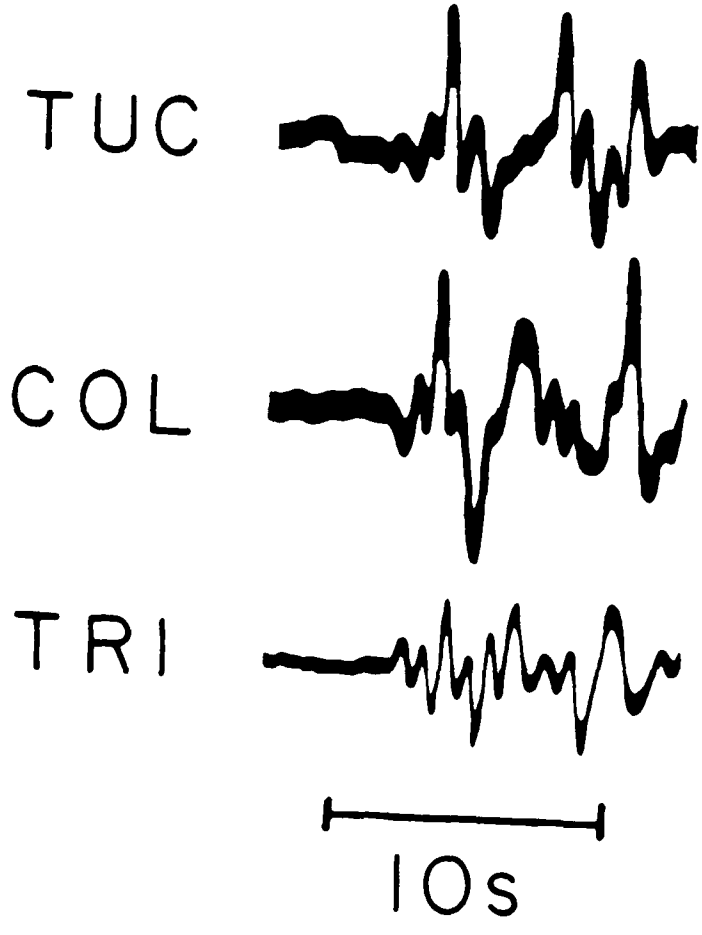

Figure 17

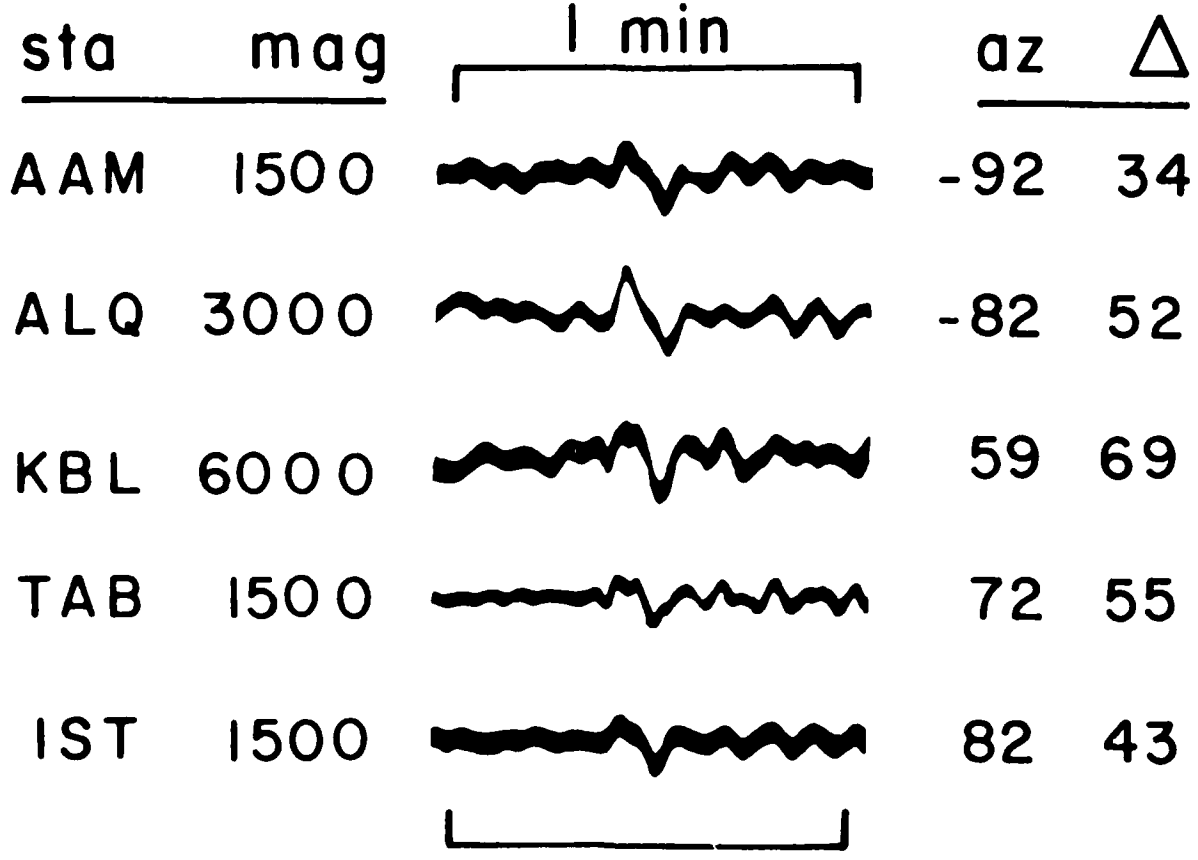
sta
mag
1 min
az
Δ
AAM 1500 -92 34
ALQ 3000 -82 52
KBL 6000 59 69
TAB 1500 72 55
IST 1500 82 43

Figure 18

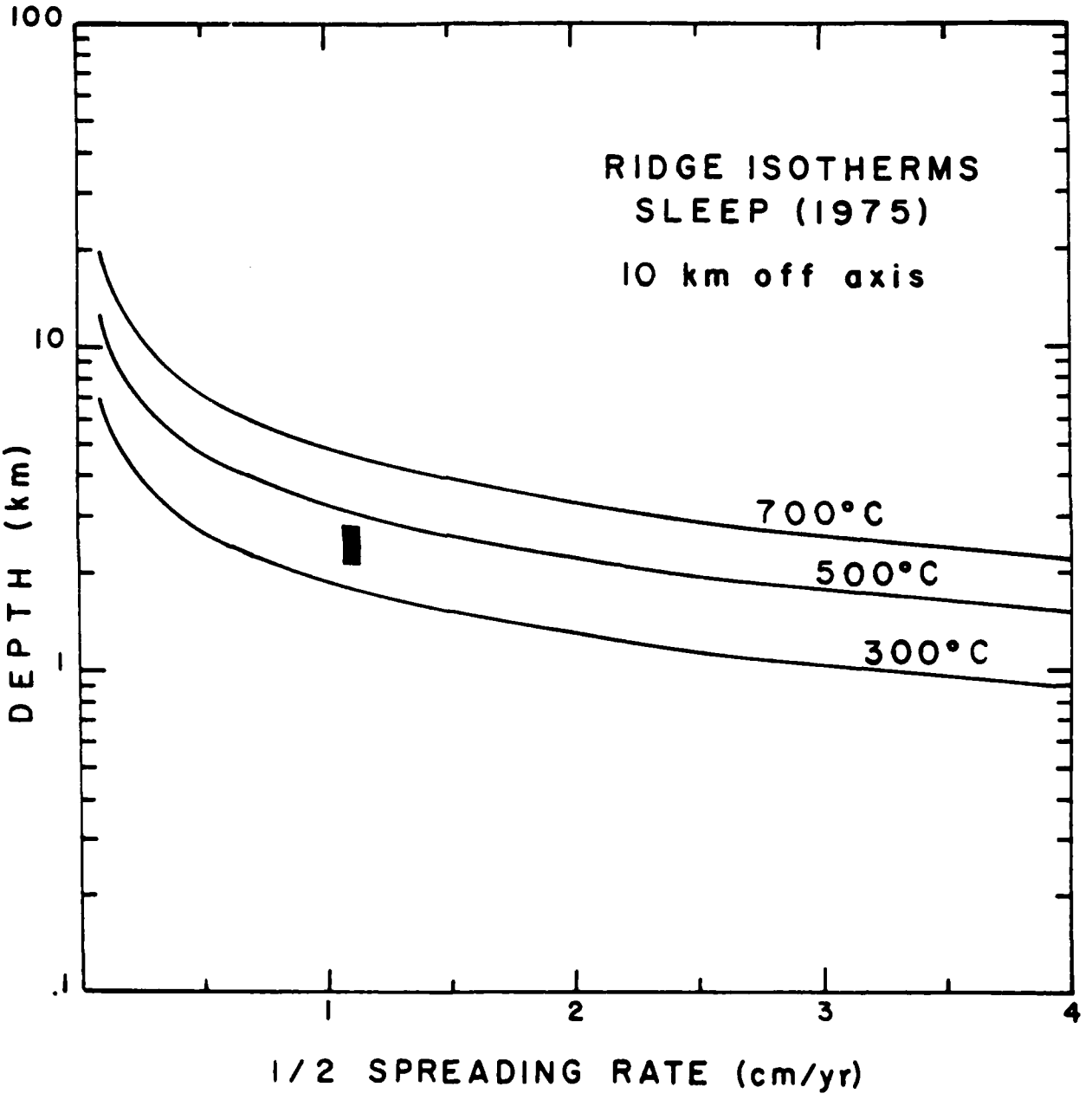
100
10
1
.1
DEPTH (km)
RIDGE ISOTHERMS
SLEEP (1975)
10 km off axis
700°C
500°C
300°C
1
2
3
4
1/2 SPREADING RATE (cm/yr)

Figure 19

V. THREE-DIMENSIONAL CRUST-UPPER MANTLE MODELS

Crust and Upper Mantle Velocity Structure in the Appalachian Orogenic Belt: Implications for Tectonic Evolution, S.R. Taylor and M.N. Toksöz, Geol. Soc. Am. Bull., submitted, 1980.

Abstract

The crust and upper mantle structure of the northeastern United States (NEUS) is studied by combining teleseismic and regional body wave observations with surface wave dispersion measurements. The velocity models suggest that structures down to 200 km and greater can be correlated with surficial geologic and tectonic features and that the Grenville and Appalachian orogenic belts show marked differences in crustal structure. This has the important implication that major orogenic belts have effects that reach well into the lithosphere which are stable for extended periods of time, perhaps as long as 1 b.y.

Regional travel times recorded across the NEUS seismic network indicate that the northern Appalachians are characterized by a well defined two-layer crust, with a relatively high velocity lower layer. The crust of the Grenville Province in New York State is slightly thinner than that of the New England Appalachians and vertically homogeneous with nearly constant P and S velocities.

Lateral variations in structure are studied using time

term analysis and teleseismic P wave residuals. The suture between the Grenville and Appalachian Province in the NEUS probably occurs along a north-northeast trending belt extending from northwestern Vermont to southwestern Connecticut. High crustal velocities and/or crustal thinning, a linear gravity high, a serpentinite belt, Precambrian uplifts, and the Taconic thrusts are found along much of this belt.

Comparison of seismic velocities with resistivity measurements suggests that the lower crust of the Grenville Province may be composed of rocks with hydrous mineral phases resulting in lowered velocities and a higher Poisson's ratio. Alternatively, the rocks of the lower crust beneath the Grenville Province may be similar to those found on the surface while higher velocity, mafic mineralogies are prevalent in the lower crust of the Appalachians. This is consistent with the hypothesis that the Grenville crust underwent substantial reactivation, thickened, and became vertically uniform during the Grenville orogeny. In contrast, the rocks of the Appalachian belt probably were associated with a cycle of oceanic opening and closure which suggests an ensimatic origin of the lower crust in this region.

Recent COCORP results indicate that the orogenic belt of the southern Appalachians is allochthonous and is underlain by a basal decollement that extends eastward to the coastal plain. However, contrasts in structural style and tectonic evolution between the northern and southern Appalachians suggest that it may not be possible to extrapolate the COCORP results to the northern Appalachians (north of about 41 degrees latitude) and that the suture between the Grenville Province and the Appalachian orogenic belt in New England is located in the vicinity of, or just east of the serpentinite belt.

INTRODUCTION

In previous papers (Taylor, 1980; Taylor and Toksoz, 1979; Taylor and others, 1980) we have combined seismic body wave data from measured blasts and regional and teleseismic earthquakes with surface wave dispersion measurements to determine the crust and upper mantle structure in the northeastern United States. Although the variations in regional structure are subtle (which is not unexpected in an ancient orogenic belt), the structural models derived using different measurement techniques are reasonably self-consistent. Along with the geology, the data provide some important constraints on the tectonic evolution of the northern Appalachians. In this paper, we combine our results with geologic and other geophysical information, and compare the New England Appalachians with the Grenville Province and the southern Appalachians. Finally, we interpret the results in a plate tectonic framework and present a model which satisfies the geologic and geophysical constraints.

GEOLOGIC SETTING OF THE APPALACHIAN MOUNTAIN BELT

In this section, we briefly review the geologic setting of

the northern and southern Appalachians and the Grenville Province. More detailed summaries can be found in McLelland and Isachsen (1980) and Dewey and Burke (1973) for the Grenville Province; Rodgers (1970), Bird and Dewey (1970), Osberg (1978), and Taylor and Toksoz (1979) for the northern Appalachians; and Rodgers (1970), Hatcher (1978) and Cook and others (1979), for the southern Appalachians. A generalized geologic map of eastern North America is shown in Figure 1. Table 1 lists the major Appalachian orogenic episodes, and their nature and extent of deformation.

The Precambrian (1.1 b.y.) Grenville Province, exposed in eastern Canada and the Adirondacks, extends southward in the subsurface to the west of the Appalachian mountain belt. The rocks of the Grenville Province are largely remobilized older basement of Superior or Hudsonian age and consist mainly of thick sequences of high-grade metasediments extensively intruded by granitic and anorthositic rocks.

The southern Appalachians extend from central Alabama to about 41 degrees latitude in southern-most New York state and can be divided across strike into three main

structural provinces (Rodgers, 1970). The westernmost section includes the marginal fold and thrust belt of the Valley and Ridge Province which involves Alleghanian (late Carboniferous-Permian; 270-220 m.y.) deformation of Paleozoic miogeoclinal rocks. The Blue Ridge Province is located to the east of the Valley and Ridge Province and consists of an allochthonous belt involving middle Precambrian (1.0 to 1.1 b.y.) basement. The late Precambrian and Paleozoic metasediments and metavolcanics become more intensely metamorphosed from west to east across the Blue Ridge Province which separates miogeoclinal rocks of the Valley and Ridge Province from eugeoclinal rocks and intrusives of the Piedmont Province. The allochthonous nature of the Blue Ridge is indicated by the existence of fensters in the Blue Ridge thrust sheet such as the Grandfather Mountain window in North Carolina where low grade platform sedimentary rocks and carbonates are found (Hatcher, 1978). Tectonic slivers of relatively unmetamorphosed carbonates have been observed in the Brevard fault zone which marks the southeast boundary of the Blue Ridge and gives additional evidence that lower Paleozoic continental margin deposits extend beneath the Blue Ridge (Hatcher, 1978; Cook and others, 1979).

The Piedmont Province is located to the east of the Brevard fault zone and can be sub-divided into a number of different zones based on differences in metamorphic grade and dominant lithology. In general, the Piedmont consists of metamorphosed eugeoclinal rocks of lower and middle Paleozoic age which are associated with Paleozoic plutons of variable composition. The southern Appalachians show two zones of ultramafic bodies; a well-defined belt associated with the Blue Ridge, and an eastern belt of irregularly distributed bodies in the Piedmont (Misra and Keller, 1978). Recent COCORP seismic-reflection profiling has shown that the platform rocks overlying the Grenville basement can be traced beneath the Blue Ridge and continue at least 150 km to the east beneath the crystalline Piedmont Province (Cook and others, 1979).

The northern Appalachians show a number of geologic dissimilarities to the southern Appalachians. The northern equivalent of the Valley and Ridge Province is older, less developed, and involved westward thrusting of eugeoclinal rocks (the Taconic klippen in New York State) over miogeoclinal rocks during the Ordovician Taconic orogeny. Precambrian uplifts such as the Green Mountains in Vermont and the Berkshires in western Massachusetts

involve Grenville basement and are located in the vicinity of the transition of the miogeocline to eugeocline. However, in the northern Appalachians, the uplifts are not as extensive as those in the Blue Ridge and Precambrian rocks are not exposed along the Sutton Mountain anticlinorium in Quebec. To the east of the Precambrian uplifts is a north to northeast trending belt of serpentinites which are located on strike with the Newfoundland ophiolites. In contrast to the southern Appalachians, few ultramafics are found to the east of the serpentinite belt in New England except along coastal Maine (Osberg, 1978). Rocks of the New England Appalachians are deformed into a number of broad structural warps containing Paleozoic eugeoclinal continental rise or back arc basin metasediments in the synclinoria and island arc metavolcanics and their associated intrusives in the anticlinoria (Rodgers, 1970). Except for a few exposures in coastal Maine, Paleozoic carbonate rocks typical of stable continental margins are rarely found to the east of the Precambrian inliers in the northern Appalachians (Williams, 1979; Osberg, 1978). Granites of the New Hampshire Plutonic series which were emplaced during the middle Devonian Acadian orogeny are exposed throughout much of the central orogenic belt of

New England and give age dates of about 360 m.y. (Naylor, 1975). On the eastern flank of the central orogenic belt of the New England Appalachians, a major northeast trending thrust belt (the Clinton--Newbury and Bloody Bluff fault zone in eastern Massachusetts) is found. Rocks which are probably correlative with those of the Avalon zone in Newfoundland are found to the east of this thrust belt in eastern Massachusetts and southeastern Maine (Bird and Dewey, 1970; Nelson, 1976).

SUMMARY OF REFRACTION MODELS IN EASTERN NORTH AMERICA

Velocity structures based on regional travel times suggest that significant differences in crustal structure exist between the Grenville and Appalachian Provinces. In this section, the models for the NEUS presented below will be compared with other refraction models measured in eastern North America. The tectonic implications of the structural differences will be examined in a later section.

Refraction models for the northern and southern Appalachians and the Grenville Province are contrasted in Table 2 and shown in Figure 1. The northern Appalachians

appear to be composed of a relatively thick, 40 km crust with two well-defined layers. The lower crust is characterized by relatively high velocities of 7 km/s. This is consistent with refraction models of Leet (1941) and Steinhart and others, (1962) in the NEUS, R.L. Street (pers. comm.) in central New Hampshire, and Dainty and others (1966) in Newfoundland. Two models presented by Chiburis and Ahner (1979) in southeastern New England and Nakamura and Howell (1964) in eastern Maine suggests crustal thinning and a missing high velocity lower layer along the Atlantic coast. The region where the Chiburis and Ahner (1979) model was compiled is located in a region characterized by a zone of negative time terms and apparent crustal thinning (Figure 4). Interestingly, these surveys may have sampled rocks of the eastern block (or Avalon zone) discussed above.

Refraction models from the Grenville Province appear to be fairly similar along its length from eastern Canada to the southeastern U.S. In eastern Canada the high velocity lower crustal layer is absent or weakly developed (Dainty and others, 1966; Berry and Fuchs, 1973). It also appears that the Grenville crust thickens from about 36 km at its eastern edge to about 45 km at its western edge in

the vicinity of the Grenville Front. Recent detailed seismic studies in the La Malbaie Region, Quebec indicate a 43 km thick crust with an average upper crustal velocity of about 6.5 km/s and lower crustal velocities of about 6.8 km/s with a thin 7.1 km/s layer at the base of the crust and Pn velocities of 8.1 km/s (Lyons and others, 1980). In New York state, the Grenville crust appears to be uniform, about 36 km thick, with velocities ranging from 6.4 to 6.6 km/s (Katz, 1955; Aggarwal in Schnerk and others, 1976).

Further south, west of the Blue Ridge, the Grenville crust appears to have two layers, but the lower crustal layer has a P velocity of about 6.7 km/s which is low relative to the northern Appalachians (Steinhart and Meyer, 1961). The 14 km thick upper layer could be composed in part of allochthonous miogeoclinal rocks.

The southern Appalachians appear to show velocity structures that are more like the Grenville models than those of the northern Appalachians because of the lack of the high velocity lower crustal layer (Long, 1979; Warren, 1968; Bollinger and others, 1980). This has very important implications that will be discussed below.

SEISMIC RESULTS IN THE NORTHEASTERN UNITED STATES

The cross-section of Figure 2 summarizes the structural features based on the velocity models derived from body and surface wave analysis in the northeastern United States (Taylor, 1980; Taylor and Toksoz, 1979; Taylor and others, 1980). The northern Appalachians are characterized by a two-layer, 40 km thick crust with a relatively high velocity lower crustal layer. To the west in the Grenville Province, the crust thins by a few kilometers and appears to be very homogeneous except in the vicinity of the Taconic thrust belt. This contrast in crustal structure between the Appalachians and the Grenville Province occurs across the north-northeast trending serpentinite belt. To the east, there also appears to be a contrast in crustal structure between the central orogenic belt of the Appalachians and the eastern block (Avalonia) described above. Because of the proximity to the coastline, this difference in structure (which may occur across the Clinton-Newbury - Bloody Bluff fault zone in eastern Massachusetts) is poorly defined.

The upper mantle velocities extending to depths of about

200 km beneath the Grenville Province are about 2 percent higher than those beneath the Appalachians.

Specific observations are outlined below in greater detail.

1. Regional travel times of P and S waves recorded across the NEUS seismic network indicate that (Taylor and others, 1980; Figure 3):

a. The northern Appalachians are characterized by a well-defined two layer crust, with a relatively high velocity lower layer. The upper crustal layer, approximately 15 km thick with P and S velocities of 6.1 and 3.6 km/s, respectively, overlies a high velocity lower crust with P and S velocities of 7.0 and 4.1 km/s. The average crustal thickness is approximately 40 km.

b. The crust of the Grenville Province is vertically homogeneous with nearly constant P and S velocities of 6.6 and 3.7 km/s, respectively, and an average crustal thickness of 37 km.

c. Pn velociities are 8.0 km/s for the Grenville and 8.1

km/s for the Appalachians.

2. A time term analysis (Taylor 1980; Figure 4) of the Pn branch of the travel time curve defines a region of thick or low-velocity crust trending northeast across eastern New York, western Massachusetts, southeast Vermont, central New Hampshire, and west-central Maine. Crustal thinning, or higher velocities are observed in northeastern New York and northwest Vermont and also along much of the coastline.

3. Analysis of Rayleigh wave phase and group velocities in the region yields structural models that are reasonably consistent with those described above (Taylor 1980; Figure 5). Interstation phase and group velocities were measured between selected long-period station pairs in eastern Canada and the northeastern United States. The phase and group velocities were inverted simultaneously to obtain regional crust and upper mantle models.

a. For a path along the strike of the Appalachians, between St. Johns, Newfoundland and southeastern New England, a 40 km thick crust with upper layer S velocities of about 3.6 km/s overlies a relatively high velocity lower layer with S velocities around 3.9 - 4.1 km/s (Path A1 in Figure 5).

b. The Grenville path, between Ogdensburg, New Jersey and Montreal, Quebec, appears to have a thinner 35 km crust with a slightly lower velocity lower-crust relative to the Appalachian paths (Path G in Figure 5). In contrast to the travel time models which show a homogeneous crust, a two layer crust is necessary to fit the observed phase and group velocities. However, part of the surface wave path crosses the Taconic thrust sheet in eastern New York where a two layer crust in not unexpected (Figure 2).

4. Analysis of teleseismic P-wave residuals delineates structures which correlate well with surface geology and is useful for studying lateral variations in structure (Taylor and Toksoz, 1979). Teleseismic P wave arrival times were collected from 50 stations which are part of the northeastern United States seismic network. Relative travel time residuals were calculated and used to invert for three-dimensional crust and upper mantle structure using the technique of Aki and others (1977).

a. Structures down to at least 200 km can be correlated with large-scale geologic and tectonic features.

b. The Grenville upper mantle is characterized by velocities

that are approximately 2 percent higher than those beneath the Appalachians. These velocities are maximum beneath the Adirondack dome.

c. A relatively low velocity anomaly dips to the northwest beneath the central mobile belt of the Appalachians and shows a spatial correlation with the Bronson Hill - Boundary Mountains Anticlinorium in New Hampshire and Maine.

d. By making assumptions on crustal velocities, the P wave residuals were used to estimate variations in crustal thickness. Crustal features are relatively consistent with those derived from the time term analysis (Figure 4), and the Appalachian crust appears to be slightly thicker than the Grenville (Figure 6).

e. Rapid crustal thinning or high velocities in the crust occur in northwestern Vermont and southwestern Connecticut.

f. Thick crust is observed below the Taconic thrusts in east-central New York and western Massachusetts.

g. There is some evidence that the crust [illegible] along the coastline.

CONTRASTS BETWEEN GRENVILLE AND APPALACHIAN PROVINCES IN THE NEUS

One of the most significant results of this study is the pronounced difference in crustal structure between the Precambrian Grenville Province and the Paleozoic Appalachian Province. The observed differences in crustal structure between the two orogenic belts are probably the result of variations in petrology, chemistry, water content, temperature, and tectonic evolution. These factors will be examined in this section.

Recent summaries of geophysical, geological, and geochemical information suggest that beneath the sedimentary layer, the upper crust is composed mainly of schists and gneisses of the amphibolite facies which grade downward into migmatites and finally into basic and intermediate granulites in the lower crust (Smithson, 1977). Because seismic velocities increase rapidly from amphibolite to granulite facies rocks, the depth to the Conrad discontinuity may mark the location of this change in metamorphic grade (Fountain, 1976). Numerous crustal layers characterized by low velocities, high and low

velocity gradients, etc., have been observed and/or postulated using deep seismic sounding techniques (cf. Mueller, 1977; Giese, 1976) and will not be reviewed here. Electrical measurements in the northeastern United States suggest the presence of a highly conductive lower crust in the Adirondack Mountains in New York State (Connerney and others, 1980), and a resistive lower crust underlying a slightly conductive 15 km thick upper crust in New England (Kasameyer, 1974). The slightly conductive 15 km thick upper layer in New England correlates well with the 15 km thick, upper layer observed in this study and probably corresponds to metamorphosed eugeoclinal rocks of the major synclinoria. This implies that the observed differences in velocity and conductivity of the lower crust between the two belts may be the result of a hydrated lower crust beneath the Grenville Province. Although the rocks of the lower crust may be compositionally similar, a hornblende-granulite petrology beneath the Grenville would yield lower velocities than a pyroxene-granulite petrology beneath the Appalachians (Christensen and Fountain, 1975).

The existence of a low velocity lower crust beneath the Grenville Province is also supported by the study of the Sp phase across eastern Canada by Jordan and Frazer (1975), who

found evidence for a lower crustal layer with a very high Poisson's ratio of 0.33. Because we only acquired travel times of first arrivals, it was not possible for us to positively identify a low velocity zone. We found shear velocity models with low velocity crustal layers that could fit the observed surface wave dispersion curves. However, in these models the resolution was inadequate and the model errors too large to positively identify a low velocity layer. Using the P and S wave velocity models derived from regional travel times and surface wave inversions, the Poisson's ratio of the lower crust beneath the Grenville is 0.27 which is slightly higher than the value of 0.25 - 0.26 found beneath the Appalachians.

The values of Poisson's ratio and shear velocity for the Grenville and Appalachian Provinces are shown on Figure 7 along with a plot of Poisson's ratio versus shear velocity at 10 kbar for a number of rocks that may exist in the lower crust (Christensen and Fountain, 1975; Christensen 1966; Manghnani and others, 1974). From Figure 7, it can be seen that the observed lower crustal velocities may be partially explained by an amphibole granulite beneath the Grenville Province and a pyroxene granulite beneath the Appalachians. Interestingly, the Grenville point on Figure 7 plots in the

vicinity of quartzo-feldspathic gneisses and has shear velocities similar to anorthosite. The Grenville Province is characterized by a number of large anorthosite intrusive bodies which, on the basis of gravity modelling, may be confined to the upper 10-15 km of the crust (Simmons, 1964).

The above interpretation of hydrous versus anhydrous mineral phases beneath the Grenville and Appalachian Provinces is also consistent with the observed resistivity models. At temperatures and pressures representative of the lower crust in shield areas, microcracks are generally closed or healed and conduction by pore fluids is probably small relative to that of hydrated mineral phases (Brace, 1971).

Field studies of granulite terrains in the Adirondacks indicate a fairly dehydrated crust (Buddington, 1939). Dewey and Burke (1973) suggest the Grenville Province is a deeply eroded zone of reactivated basement similar to a Tibetan platcau. Partial melting of a dioritic lower crust during the Grenville Orogeny may have resulted in potassic granitic melts which rose to higher crustal levels leaving a dehydrated refractory residue consisting of pyroxene granulites, charnockites, and anorthosites. However, there are exposures of amphibolite and hornblende granulite zones

with rocks containing scattered biotite in the Adirondacks (Buddington, 1939; Manghani and others, 1974) which agrees with observations that conditions with some degree of water saturation can exist during granulite facies metamorphism (Fyfe and others, 1958). Conductivity measurements on amphiboles at lower crustal conditions are lacking (Connerney and others, 1980) and it is not clear if the existence of hornblende granulites (which generally contain less than 1 percent water, Manghnani and others, 1974) in the lower crust will explain both the conductivity measurements and the observed seismic velocities.

As suggested by Jordan and Frazer (1975), the existence of serpentinite in the lower crust of the Grenville Province may explain their observations of a low velocity layer with a high Poisson's ratio and would be consistent with the observed high deep crustal conductivities. Although serpentinized peridotite does not exhibit seismic velocities comparible to those shown in Figure 3, a small degree of serpentinization may change the average lower crustal properties by increasing Poisson's ratio and increasing rock conductivities.

Temperature differences may affect the velocities observed in

the lower crust. However, at temperatures and pressures representative of the lower crust in older geologic belts (Blackwell, 1971), the effect of temperature on seismic velocities is small relative to pressure (Christensen, 1979). Christensen (1979) concluded that critical thermal gradients resulting in low velocity layers can be reached at temperatures and pressures representative of the upper and middle crust in shield areas. This is particularly apparent for coarse grained rocks with euhedral crystals such as granites, amphibolites, anorthosites, and granulites which have grain boundaries that open at higher temperatures. However, at greater pressures, the grain boundary cracks remain closed even at elevated temperatures and it is more difficult to reach critical thermal gradients in the lower crust. As discussed by Taylor and Toksoz (1979), temperature differences may be important in the upper mantle and may account for the observed teleseismic P-wave delays.

As an alternative explanation to those which are based on physical properties such as water content or temperature, the rocks of the Grenville and Appalachian Provinces may show contrasts in their chemistry and petrology that are caused by differences in their tectonic evolution. As was noted from Figure 7, rocks of the lower crust in the Grenville Province

may be very similar to the quartzo-feldspathic gneisses found on the surface. In contrast, the lower crust in the Appalachians exhibits velocities more representative of mafic rocks such as pyroxene-garnet granulites. Geochemical models suggest that some members of the White Mountain Plutonic series in central New Hampshire were formed by reaction of fractionated mantle derived alkali basalt with metamorphosed tholeiitic (oceanic) basalt at the base of the crust (Loiselle, 1978). At temperatures and pressures representative of the lower crust, a tholeiitic basalt will alter to a garnet or pyroxene granulite (Green and Ringwood, 1972).

From the cross-section of Figure 2, the upper 15 km layer in the northern Appalachians probably corresponds to rocks which have been subjected to a high degree of compression and crustal shortening during the Taconic and Acadian orogenies. The metasediments exposed in the central orogenic belt of the northern Appalachians were probably subduction melanges and backarc and forearc basin deposits from an island arc regime. As discussed by Dickerson and Seely (1979), oceanic crust may often be trapped beneath a forearc basin, and it is expected that these and backarc basin mafic rocks will be caught up in the crust during collision episodes. Thus, involvement of

ocean floor within the Appalachians would account for the higher velocities found in the lower crust relative to the predominantly ensialic crust of the Grenville Province.

The homogeneous character of the crust in this portion of the Grenville Province is consistent with the hypothesis that the crust underwent substantial reactivation, thickened, and became vertically uniform during the Grenville orogeny (Dewey and Burke, 1973). Subsequent to the thickening, the crust was eroded to relatively deep levels, as evidenced by the surface exposure of granulite terrains (Putman and Sullivan, 1979).

Based on teleseismic P-wave residuals and Pn residuals (Taylor and Toksoz, 1979; Figures 4 and 6), it appears that the transition zone between the Grenville and Appalachian Province in the NEUS occurs in the vicinity of the Precambrian uplifts and the serpentinite belt (Figure 2). This north-northeast trending belt may mark the suture zone between the two orogenic belts. At many locations along this postulated suture, particularly in northwest Vermont, geological and geophysical features such as high crustal velocities, a linear gravity high, a serpentinite belt, Precambrian uplifts, and the Taconic thrusts show many

similarities to the Ivera zone in northern Italy (Giese and Prodehl, 1976, Fountain, 1976).

There is also the possibility of a second suture located in the eastern section of the study area. This feature is marked by the Clinton-Newbury - Bloody Bluff fault zone (CN - BB F.Z.) in eastern Massachusetts (see Figure 2) and other structures such as the Norumbega fault zone in eastern Maine (Loiselle and Ayuso, 1979). In eastern Massachusetts, the CN - BB F.Z. separates rocks that are probably correlative with Avalon rocks from those of the central mobile belt. The northwest-dipping fault zone is also well-marked by such features as the offset of metamorphic isograds, a strong magnetic signature, and a cataclastic zone containing mylonite that is up to 1.5 km thick. A pronounced gravity anomaly is also associated with the fault zone (Taylor and others, 1980b), and the Bouguer gravity is relatively high over the eastern basement. Loiselle and Ayuso (1979), present evidence suggesting that post-Acadian strike slip faulting along the Norumbega fault has juxtaposed plutonic rocks of differing geochemistry, texture, and mode of emplacement.

The deep crustal structure of the eastern block appears to

differ from that of the central belt. Refraction models, Pn and teleseismic P-wave residuals indicate that the crust of the eastern block is probably thinner than that of the central belt and may be missing a high velocity lower crustal layer.

Although there are a few localities along the CN - BB F.Z. where mafics and ultramafics are exposed that resemble highly altered ophiolites (P. Osberg, personal communication, 1980), the paucity of ophiolites along this zone is problematical. As discussed by Dewey (1977), zones of intense suturing undergo the most uplift and subsequent erosion and may exhibit few ophiolite exposures. This is [illegible] thrust in [illegible] stages of orogeny and occupy high structural levels. Thus, a deeply eroded suture zone may be observed as a narrow high-strain or thrust zone with little evidence of any ophiolites. For example, few ophiolite bodies are observed along the eastern portion of the Indus suture of the Himalayas where the collision appears to have been more intense (LeFort, 1975). Additionally, the CN - BB F.Z. may have become a transform fault in late Paleozoic time (Ballard and Uchupi, 1975) which may have obliterated any evidence of ophiolites.

Alternatively, the suture may be located further west and the CN - BB F. Z. may have had a history similar to the Main Central Thrust or the Boundary Fault of the Himalayas. This hypothesis is supported by recent paleomagnetic results which suggest that Lower Devonian volcanics from north-central Maine have paleopoles closer to Avalonia than to North America (Brown, 1980). Even in this case, however, the suture remains cryptic and numerous other tectonic problems are encountered. Regardless of its mode of emplacement, the eastern block has undergone a significantly different orogenic history than that of the central belt, and differences in deep crustal structure across the CN - BB F. Z. are not unexpected.

Three dimensional inversion of travel time data illustrates that structures down to perhaps 200 km and greater can be correlated with large scale geologic features (Taylor and Toksoz, 1979). This has the important implication that major orogenic belts have effects extending well into the lithosphere which are stable for extended periods of time, perhaps as long as 1 billion years. The lateral variations in seismic properties of the crust and upper mantle beneath the northeastern United States are very small relative to those observed over similar distances in active tectonic

regions such as central Asia or the western United States. Poupinet (1979) showed that absolute P-residuals are a linear function of the square root of age inside stable continental plates. This indicates that the crust and upper mantle become increasingly more uniform with age during evolution toward a state of equilibrium.

In addition to the regional differences existing between the two structural provinces in the northeastern U.S., we see smaller scale features that are related to specific segments of each orogenic belt and to the intervening suture zone. As discussed previously, the Taconide belt, the eastward-lying Precambrian uplifts (The Berkshire Highlands and Green Mountains), and serpentinite belt are Lower Ordovician structures that may be related to the closure of an inner-arc basin and to a continent-island arc collision. This region is extensively deformed and is also characterized by apparent crustal thinning and geophysical anomalies such high crustal velocities, and large positive Bouguer gravity anomalies. It is possible that these features are related to deep-seated thrusts emplaced near the end of the Taconic orogeny which carried oceanic crust and upper mantle material to higher levels within the crust. This material would have high velocities and densities relative to the surrounding

eugeoclinal lithologies and would provide a model consistent with the observed geophysical anomalies.

CONTRASTS BETWEEN NORTHERN AND SOUTHERN APPALACHIANS

Recent COCORP seismic reflection profiling in the southern Appalachians indicates that the platform rocks overlying the Grenville basement can be traced beneath the Blue Ridge and continue at least 150 km to the east (Cook and others, 1979; Figure 8). Because the northern and southern Appalachians show many contrasts in structural style and tectonic history, it may not be possible to extrapolate the COCORP results to the northern Appalachians (north of about 41 degrees latitude). The tectonic evolution of the northern and southern Appalachians is very similar up through the mid-Devonian Acadian orogeny. However, the southern Appalachians have an additional late Paleozoic orogenic episode (the Alleghenian orogeny) which resulted in the westward thrusting of the Blue Ridge, Inner Piedmont, and Carolina Slate Belt (Cook and others, 1979). In the northern Appalachians, the Alleghenian orogeny was only felt in southeastern New England and by strike slip faulting farther north. It has been suggested that the Alleghenian deformational belt truncates the Appalachian-Caledonian belt

in southern Connecticut and Rhode Island and is correlative with the Hercynian belt in central Europe (Dewey and Kidd, 1974). The extensive crustal shortening of the late Paleozoic Alleghenian marginal fold and thrust belt of the Valley and Ridge Province is confined mainly to the southern Appalachians. Slices of relatively unmetamorphosed carbonates are found to the east of the Blue Ridge in the Brevard zone and the Grandfather Mountain window (Cook and others, 1979). The ultramafics found in the southern Appalachians are diffuse and are irregularly distributed throughout the Piedmont zone indicating their involvment in the numerous thrusts of the allochthonous crystalline belt (Misra and Keller, 1978). In contrast, the ultramafics of the northern Appalachians form a narrow north-northeast trending belt and lower Paleozoic platform rocks are rarely found east of the Precambrian outliers in the northern Appalachians.

As pointed out by Williams (1980), Alleghanian deformation involves Carboniferous rocks in the Piedmont of the southern Appalachians. In contrast, autochthonous Silurian and younger cover rocks unconformably overlie rocks of the Ordovician [illegible] into the central orogenic belt of the northern Appalachians.

This implies that any major decollement in the northern Appalachians would have to be a pre-Silurian structure.

The COCORP results indicate that the suture between proto-Africa and North America is located at least 150 km to the east of the Blue Ridge. However, by combining gravity and geologic information, Diment and others (1972) suggested that the suture (which would actually separate North America from Avalonia) cuts across southern New England and trends north-northeast up the coast of New England (boundary EF in Figure 12 of Diment and others, 1972). In the southern Appalachians, boundary EF is actually on a thin-skinned allochthonous belt. Reconstruction of the westward-directed thrusts may allign the two segments of boundary EF.

Seismic refraction data also suggests differences in crustal structure between the northern and southern Appalachians. The structure to the west of the Blue Ridge in the southern Appalachians (Table 2 and Figure 1) is similar to that west of the Precambrian outliers in the northern Appalachians. Both regions are missing a high velocity lower crustal layer and are composed of the homogeneous Grenville basement. However, to the east of the Precambrian outliers, the southern Appalachians continue to show a relatively

homogeneous, low velocity crust in marked contrast to the two-layer crust of the northern Appalachians. These similarities in crustal structure across the Blue Ridge are consistent with the interpretation that the crystalline rocks of the Blue Ridge, Inner Piedmont, and the Carolina slate belt are allochthonous and overlie Grenville basement. The contrasts in crustal structure across the serpentinites in the northern Appalachians suggest that they are located in the vicinity of the suture separating the Grenville from the Appalachian Province.

PALEOZOIC EVOLUTION OF THE NORTHERN APPALACHIANS

A possible scenario for the evolution of the northern Appalachians will be briefly outlined in this section. Figure 9 shows cross-sections (taken approximately across line AA' in Figure 2) illustrating the possible tectonic evolution of the northern Appalachians. Table 1 lists major orogenic episodes in the Appalachians and the maximum manifestation in the area of influence (from Rodgers, 1970).

It is currently thought that a continental rifting stage initiated approximately 820 m.y. ago leading to the formation of the Iapetus Ocean (proto-Atlantic) (Rankin,

1976). The late Precambrian and Cambrian geology of the western belt is characterized by the establishment of an Atlantic-type, stable continental margin (Figure 9a).

Late Precambrian lithologies on the eastern belt also indicate a rifting stage with the development of an active continental margin (Kennedy, 1976). Geochemical, paleomagnetic, and paleontological evidence suggests that the western and eastern belts were located on opposite sides of the Iapetus Ocean (Strong and others, 1974; McKerrow and Cocks, 1976; Kent and Opdyke, 1978).

Early or Mid-Ordovician through Permian times are characterized by the episodic closing of the Iapetus Ocean (Figure 9b). The Bronson Hill Anticlinorium was a site of major volcanic activity in this time period as shown by the presence of thick volcanic sequences. The curvature of the Bronson Hill Anticlinorium (convex to the northwest) and the asymmetrical distribution of volcanics (Osberg, 1978) in the central mobile belt suggest an eastward dipping Benioff zone existed at this time.

Major deformation occuring in Middle and Late Ordovician time marked the climax of the Taconic orogeny which affected rocks

within and west of the Bronson Hill Anticlinorium (Figure 9c). Evidence based on styles of deformation and metamorphism indicates that the Taconic orogeny in New England probably was an episode of arc-continent collision. Numerous island arc segments and inner-arc basins now located within the central mobile belt were probably involved in the deformation. On the basis of teleseismic P-wave residuals, Taylor and Toksoz (1979) present evidence for an upper mantle low-velocity anomaly dipping to the northwest beneath the Bronson Hill Anticlinorium. If this upper mantle anomaly was caused by subduction prior to the Acadian orogeny, then it is possible that a reversal of subduction polarity from southeast to northwest occured following the Taconic orogeny.

The Silurian to Early Devonian time was a period of relative quiescence and erosion of the Taconic highlands (Boucot, 1968). In the Early Devonian era there is evidence of increased tectonic activity as indicated by the deposition of vast thicknesses of turbidite sequences across the major synclinoria (Littleton Formation of New Hampshire) and renewed volcanism along arcs in the central mobile belt (Figure 9d). This episode of major deformation climaxed in mid-Devonian time and is called the Acadian orogeny spanning a period of approximately 30 m.y. (Naylor, 1971; Figure

9e). The styles of deformation associated with the Acadian orogeny show many parallels with those documented in other continental convergence zones (Dewey, 1977). Thus, the Acadian orogeny was probably a period of continental collision between North America and the Avalon block which is now exposed in southeastern New England and eastern Newfoundland.

Three major events following the Acadian orogény are recorded in New England. Alleghenian deformation in Pennsylvanian to Permian times strongly affected rocks in southeastern New England. The Allegheny orogeny probably represents the final closure of the Iapetus Ocean by the collision of Africa with North America. It has been suggested (Dewey and Kidd, 1974) that the Alleghenian deformational belt truncates the Appalachian-Caledonian belt in southern Connecticut and Rhode Island and is correlative with the Hercynian belt in central Europe. Strike slip faulting in the northern Appalachians may have been important in the late Paleozoic (Rodgers, 1970; Arthand and Matte, 1977; Ballard and Uchupi, 1975) although the sense of motion is not well defined.

ACKNOWLEDGMENTS

We wish to thank B.C. Burchfiel, Frank Spear, and Pat Barosh for interesting and valuable discussions. Careful review by Martin Kane and Richard Goldsmith is also appreciated. This research was supported by Nuclear Regulatory Commission contract NRC-04-76-209 and in part by the Advanced Research Projects Agency, monitored by the Air Force Office of Scientific Research, under contract F44620-75-C-0064.

REFERENCES

Aki, K., A. Christoffersson, and E.S. Husebye, Determination of the three-dimensional seismic structure of the lithosphere, J. Geophys. Res., 82, 277-296, 1977.

Arthand, F. and P. Matte, Late Paleozoic strike-slip faulting in southern Europe and northern Africa: Result of a right-lateral shear zone between the Appalachians and the Urals, Geol. Soc. Am. Bull., 88, 1305-1320; 1977.

Ballard, R.D. and E. Uchupi, Triassic rift structure in Gulf of Maine, Am. Assoc. Pet. Geol. Bull., 59, 1041-1072, 1975.

Berry, M.J. and K. Fuchs, crustal structure of the superior and Grenville Provinces of the northeastern Canadian Shield, Bull. Seism. Soc. Am., 63, 1393-1432, 1973.

Bird, G.P., Thermal and mechanical evolution of continental convergence zones: Zagros and Himalayas, unpublished Ph.D. Thesis, Massachusetts Institute of Technology, 1976.

Bird, J.M., and J.F. Dewey, Lithosphere plate-continental margin tectonics and the evolution of the Appalachian orogen,

America Bull., 81, 1031-1060, 1970.

Blackwell, D.D., The thermal structure of the continental crust, AGU Mono. 14, Washington D.C., J.G. Heacock (ed), 169-184, 1971.

Bollinger, G.A., M.C. Chapman, and T.P. Moore, Central Virginia Regional Seismic Network: Crustal velocity structure in central and southwestern Virginia, NUREG CR-1217, 187pp., 1980.

Boucot, A.J., Silurian and Devonian of the northern Appalachians, in Studies of Appalachian Geology-Northern and Maritime, E. Zen, ed., Interscience, New York, 83-94, 1968.

Brace, W.F., Resistivity of saturated crustal rocks to 40 km based on laboratory measurements, AGU Mono. 14, Washington D.C., J.G. Heacock (ed), 243-255, 1971.

Brown, L., Paleomagnetic results from northern Maine and the western limit of "Avalon" in the mid Paleozoic, (abstract), in abstracts with programs, Geol. Soc. Am., 12, 26, 1980.

Burchfiel, B.C., and G.A. Davis, Nature and controls of

Cordilleran orogenesis, western United States: extensions of an synthesis, American J. of Sc., 275-A, 363-396, 1975.

Chapman, C.A. Structural evolution of the White Mountain Magma series, GSA mem 146, 281-300, 1976.

Chiburis, E.F., and R.O. Ahner, Northeastern U.S. Seismic Network, Bull. 15, 1979.

Chidester, A.H., Evolution of the ultramafic complexes of northwest New England, in studies of Appalachian Geology - Northern and Maritime, E. Zen, ed., Interscience, New York, 343-354, 1968.

Christensen, N.I., Shear wave velocities in metamorphic rocks at pressures to 10 Kilobars, J. Geophys. Res., 71, 3549-3556, 1966.

Christensen, N.I., Compressional wave velocities in rocks at high temperatures and pressures, critical thermal gradients, and crustal low-velocity zones, J. Geophys. Res., 84, 6849-6857, 1979.

Christensen, N.I. and D.M. Fountain, Constitution of the

lower continental crust based on experimental studies of seismic velocities in granite, Geol. Soc. Am. Bull., 86, 227-236, 1975.

Connerney, J.E.P., T. Nekut, and A.F. Kuckes, Deep crustal electrical conductivity in the Adirondacks, J. Geophys. Res., 85, 2603-2614, 1980.

Cook, F.A., D.S. Albough, L.D. Brown, S. Kaufman, J.E. Oliver, R.D. Hatcher, Thin-skinned tectonics in the crystalline southern Appalachians; COCORP seismic-reflection profiling of the Blue Ridge and Piedmont, Geol., 7, 563-567, 1979.

Dainty, A.M., C.E. Keen, M.J. Keen, and C.E. Blanchard, Review of geophysical evidence on crust and upper mantle structure on the eastern seaboard of Canada, AGU Mono. 10, Washington D.C., 349-369, 1966.

Delong, S.E., P.J. Fox, and F.W. McDowell, Subduction of the Kula Ridge at the Aleutian Trench, Geol. Soc. Amer. Bull., 89, 83-95, 1978.

Dewey, J.F., Suture zone complexities: a

review, Tectonophysics, 40, 53-67, 1977.

Dewey, J.F. and K.C.A. Burke, Tibetan, Variscan, and Precambrian basement reactivation: products of continental collision, J. Geol., 81, 683-692, 1973.

Dewey, J.F., and W.S. Kidd, Continental collisions in the Appalachian Caledonian Orogenic belt. Variations related to complete and incomplete suturing, Geology, 2, 543-546, 1974.

Dickinson, W.R. and D.R. Seely, Structure and Stratigraphy of Forearc Regions, Am. Assoc. Pet. Geol. Bull., 63, 2-31, 1979.

Diment, W.H., T.C. Urban, and F.A. Revetta, Some geophysical anomalies in the eastern United States: in the Nature of the Solid Earth, Robertson, E., ed., McGraw Hill, New York, p. 544-574, 1972.

Fountain, D.M., The Ivrea-Verbano and Strona-Ceneri Zones, northern Italy: a cross-section of the continental crust - New evidence from seismic velocities of rock samples, Tectonophys., 33, 145-165, 1976.

Fyfe, W.S., F.J. Turner, and J. Verhoogen, Metamorphic Reactions and Metamorphic Facies, Geol. Soc. Am. Mem., 73, 259pp., 1958.

Giese, P. and C. Prodehl, Main features of crustal structure in the Alps, in Explosion Seismology in Central Europe - Data and Results, P. Giese, C. Prodehl, and A. Stein, eds., Springer, New York, 347-375, 1976.

Giese, P., Models of crustal structure and main wave groups, in Explosion Seismology in Central Europe - Data and Results, P. Giese, C. Prodehl, and A. Stein, eds., Springer, New York, 196-200, 1976.

Green, D.H. and A.E. Ringwood, A comparison of recent experimental data on the gabbro-garnet granlite-eclogite transition, J. Geol., 80, 277-288, 1972.

Hatcher, R.D., Tectonics of the western Piedmont and Blue Ridge, southern Appalachians: review and speculation, Am. J. Sci., 278, 276-304, 1978.

Jordan, T.H. and L.N. Frazer, Crustal and upper mantle structure from Sp phases, J. Geophys. Res., 80, 1504-1518,

1975.

Kane, M.F., M.J. Yellin, K.G. Bell, and I. Zietz, Gravity and magnetic evidence of lithology and structure in the Gulf of Maine region, U.S. Geol. Survey Geophys. Inv., 726-B, 1972.

Kasameyer, P.W., Low-frequency magnetotelluric survey of New England, unpublished Ph.D. thesis, Massachusetts Institute of Technology, 1974.

Katz, S., Seismic study of crustal structure in Pennsylvania and New York, Bull. Seism. Soc. Am., 45, 303-325, 1955.

Kennedy, M.J., Southeastern margin of the Northeastern Appalachians: late Precambrian orogeny on a continental margin, Geol. Soc. America Bull., 87, 1317-1325, 1976.

Kent, D.V. and N.D. Opdyke, Paleomagnetism of the Devonian Catskill red beds: evidence for motion of the coastal New England-Canadian Maritime region relative to cratonic North America, J. Geophy. Res., 83, 441-450, 1978.

King, P.B., Tectonic map of North America, scale 1:5,000,000,

U.S. Geol. Surv., Washington, D.C., 1969.

Leet, D., Trial travel times for northeastern America, Bull. Seism. Soc. Am., 31, 325-334, 1941.

LeFort, P., Himalayas: The collided range. Present knowledge of the continental arc, Am. J. Sci., 275-A, 1-44, 1975.

Loiselle, M., Geochemistry and petrogenesis of the Belknap Mountains Complex and Plinz Range, White Mountain Series, New Hampshire, unpublished Ph.D. thesis, Massachusetts Institute of Technology, 1978.

Loiselle, M.C., and R.A. Ayuso, Geochemical characteristics of granitoids across the Merrimack Synclinorium eastern and central Maine, in The Caledonides in the U.S.A., I.A.C.P., Blacksburg, VA, 117-121, 1979.

Long, L.T., The Carolina slate belt - evidence of a continental rift zone, Geol., 7, 180-184, 1979.

Lyons, J.A., D.A. Forsyth, and J.A. Mair, Crustal studies in the La Malbaie region, Quebec, Can. J. Earth Sci.,

17, 478, 490, 1980.

Manghnani, M.H., R. Ramananantoandro, and S.P. Clark, Compressional and shear wave velocities in granulite facies rocks and eclogites to 10 kbar, J. Geophys. Res., 79, 5427-5446, 1974.

McKerrow, W.S., and L.R.M. Cocks, The location of the Iapetus Ocean suture in Newfoundland, Can. J. Earth Sci., 14, 488-495, 1977.

McLelland, J. and Y. Isachsen, Structural synthesis of the southern and central Adirondacks: A model for the Adirondacks as a whole and plate-tectonics interpretations, Geol. Soc. Am. Bull., 91, 68-72 and 208-292, 1980.

Misra, K.C. and F.B. Keller, Ultramafic bodies in the southern Appalachians: A review, Am. J. Sci., 278, 389-418, 1978.

Moench, R.H., and R.E. Zartman, Chronology and styles of multiple deformation, plutonism, and [illegible] in the Merrimack Synclinorum of western Maine, Geol. Soc. of America, Mem 146, 203-238, 1976.

Mueller, S., A new model of the continental crust, in The Earth's Crust, AGU mono. 20, J.G. Heacock ed., AGU, Washington, D.C., 289-317, 1977.

Nakamura, Y. and B.F. Howell, Maine seismic experiment frequency spectra of refraction arrivals and the nature of the Mohorovicic discontinuity, Bull. Seism. Soc. Am., 54, 9-18, 1964.

Naylor, R.S., Acadian Orogeny: an abrupt and brief event, Science, 172: 558-560, 1971.

Naylor, R.S., Age Provinces in the Northern Appalachians, Ann. Rev. Earth and Planetary Sci., 3, 387-400, 1975.

Nelson, A.E., Structural elements and deformational history of rocks in eastern Massachusetts, Geol. Soc. America Bull., 87, 1377-1383, 1976.

Osberg, P.H., Synthesis of the geology of the northeastern Appalachians, U.S.A., IGCP Project 27, Geol. Surv. Com. Pap., 78-13, 137-147, 1978.

Poupinet, G., On the relation between P wave travel time residuals and the age of continental plates, Earth Planet. Sci. Lett., 43, 149-161, 1979.

Pulli, J.J., and T. Graham, The earthquake mechanism in New England (abstract), Earthquake Notes, 49, 86, 1979.

Putman, G.W. and J.W. Sullivan, Granitic pegmatites as estimators of crustal pressures - A test in the eastern Adirondacks, New York, Geol., 7, 549-553, 1979.

Rankin, D.W., Appalachian salients and recesses: Late Precambrian continental breakup and the opening of the Iapetus Ocean, J. Geop. Res., 81, 5605-5619, 1976.

Ratcliffe, N.M., Cross section of the Berkshire massif at 42 N.: Profile of a basement reactivation zone, in N.E.I.G.C. Guidebook for field trips in western Massachusetts, northern Connecticut and adjacent areas of New York, N.M. Ratcliffe, ed., 1975.

Rodgers, J., The Tectonics of the Appalac[illegible] Interscience, N.Y., 271pp., 1970.

Sbar, M.L. and L.B. Sykes, Seismicity and lithospheric stress in New York and adjacent areas, J. Geop. Res., 82, 5771-5784, 1977.

Schenk, P.E., Synthesis of the Canadian Appalachians, IGCP Project 23, Geol. Surv. Canada, Paper 78-13, 111-136, 1978.

Schnerk, R., Y.P. Aggarwal, M. Golisono, and F. England, Reg. Seism. Bull. of the Lamont-Doherty Network, Lamont-Doherty Geological Observatory, Palisades, N.Y., 1976.

Simmons, G., Gravity survey and geological interpretation, northern New York, Geol. Soc. Am. Bull., 75, 81-98, 1964.

Skehan, J.W., Fracture tectonics of southeastern New England as illustrated by the Wachusett-Marlborough Tunnel, Studies in Appalachian Geology: Northern and Maritime: New York, Interscience Publs., 281-290, 1968.

Smithson, S.B., A model for lower continental crust, Earth planet. Sci. Lett., 35, 134-144, 1977.

Steinhart, J.S., and R.P. Meyer, Explosion Studies of

Continental Structure, Carnegie Inst. of Washington, Publ. 622, Wash., D.C., 409pp., 1961.

Steinhart, J.S., R. Green, T. Asada, B.A. Rodriguez, L.T. Aldrich, and M.A. Tuve, Seismic studies: Carnegie Inst. Washington Year Book 61, 1961-1962, 221-234, 1962.

Strong, D.F., Dickson, W.L., O'Driscoll, L.F., Kean, B.F., and R.K. Stevens, Geochemical evidence for an east-dipping Appalachian subduction zone in Newfoundland: Nature, 248, 37-39, 1974.

Taylor, S.R., Crust and Upper Mantle Structure of the Northeastern United States, Ph.D. thesis, Massachusetts Institute of Technology, 1980.

Taylor, S.R. and M.N. Toksoz, Three-dimensional crust and upper mantle structure of the northeastern United States, J. Geophys. Res., 84, 7627-7644, 1979.

Taylor, S.R., M.N. Toksoz, and M.P. Chaplin, Crustal structure of the northeastern United States: Contrasts between the Grenville and Appalachian Provinces, Science, 208, 595-597, 1980a.

Taylor, S.R., G. Simmons, and P. Barosh, A gravity survey of the Clinton-Newbury and Bloody Bluff fault zones in eastern Massachusetts, (abstract), in abstracts with programs, Geol. Soc. Am., 12, 86, 1980b.

Toksoz, M.N. and P. Bird, Modelling of temperatures in continental convergence zones, Tectonophysics, 41, 181-193, 1977.

Warren, D.J., Transcontinental geophysical survey (35 -39 N) seismic refraction profiles of the crust and upper mantle from 74 to 87 W longitude, Misc. Geol. Inv. Map I-535-D, U.S.G.S., Washington D.C., 1968.

Williams, H., Appalachian orogen in Canada, Can. J. Earth Sci., 16, 792-807, 1979.

Williams, H., Comments on 'Thin-skinned tectonics in the crystalline southern Appalachians: COCORP seismic-reflection profiling of the Blue Ridge and Piedmont by Cook and others', Geology, 8, 211-212, 1980.

Williams, H., and A.F. King, Geologic development of the

Appalachians, Newfoundland J. Geol. Educ., 3, 17-35, 1977.

FIGURE CAPTIONS

Figure 1 Generalized geologic map of the Appalachian orogen (after Schenk, 1978; Williams and King, 1977) and summary of refraction models in eastern North America. Key to refraction models: 1,2,3,4 Dainty and others (1966); 5 Berry and Fuchs (1973); 6 Katz (1954) and Aggarwal in Schnerk and others (1976); 7 Taylor and others (1980); 8,9 Bollinger and others (1980); 10,11 Warren (1968); 12 Long (1979).

Figure 2 Generalized geologic map of the northeastern United States (modified from King, 1969) and schematic structural cross section along profile AA'. Abbreviations: T, Taconic thrust belt; GM, Green Mountains; CVS, Connecticut Valley synclinorium; BHA, Bronson Hill anticlinorium; MS, Merrimac synclinorium; and CN-BB, Clinton-Newbury - Bloody Bluff fault zone.

Figure 3 Reduced P and S travel times from regional earthquakes for stations in the Grenville and Appalachian Provinces (top). Lines correspond to calculated travel times from velocity models (bottom) for the Grenville and Appalachian Provinces. Solid and dashed lines (bottom) correspond to P- and S-wave velocity models for the

Appalachian and Grenville Provinces, respectively, derived from an inversion of travel times from regional earthquakes.

Figure 4 Variations in crustal thickness (kilometers) from relative station time terms (Taylor 1980).

Figure 5 Shear velocity with depth from simultaneous inversion of Rayleigh wave phase and group velocities for two paths across New England and Canada (Taylor 1980). The Appalachian path (Path A1) is located between St. Johns, Newfoundland and Ogdensburg, New Jersey. The Grenville path (Path G) is located between Ogdensburg, New Jersey and Montreal, Quebec. Horizontal bars indicate model standard errors for each layer.

Figure 6 Crustal thickness (kilometers) variations across the [illegible] States derived from teleseismic P-wave residuals (Taylor and Toksoz, 1979).

Figure 7 Poisson's ratio versus shear velocity at 10 kbar for a number of rocks that are possible constituents of the lower crust (from Christersen, 1966; Christensen and Fountain, 1975; Manghnani and others, 1974). Symbol A corresponds to Poisson's ratio and shear velocity for the New England

Appalachians and G for the Grenville Province in New York state. Solid line derived from velocity-density relationships at 10 kbar for granulites and eclogites given by Manghnani and others (1974) with mean atomic weights of about 22.

Figure 8 Generalized cross section based on COCORP data of the southeastern United States taken across Tennessee, North Carolina, and Georgia (taken from Cook and others, 1979).

Figure 9 Schematic illustration of plate tectonic model for the evolution of the New England Appalachians. Profile is taken approximately across line AA′ in Figure 2.

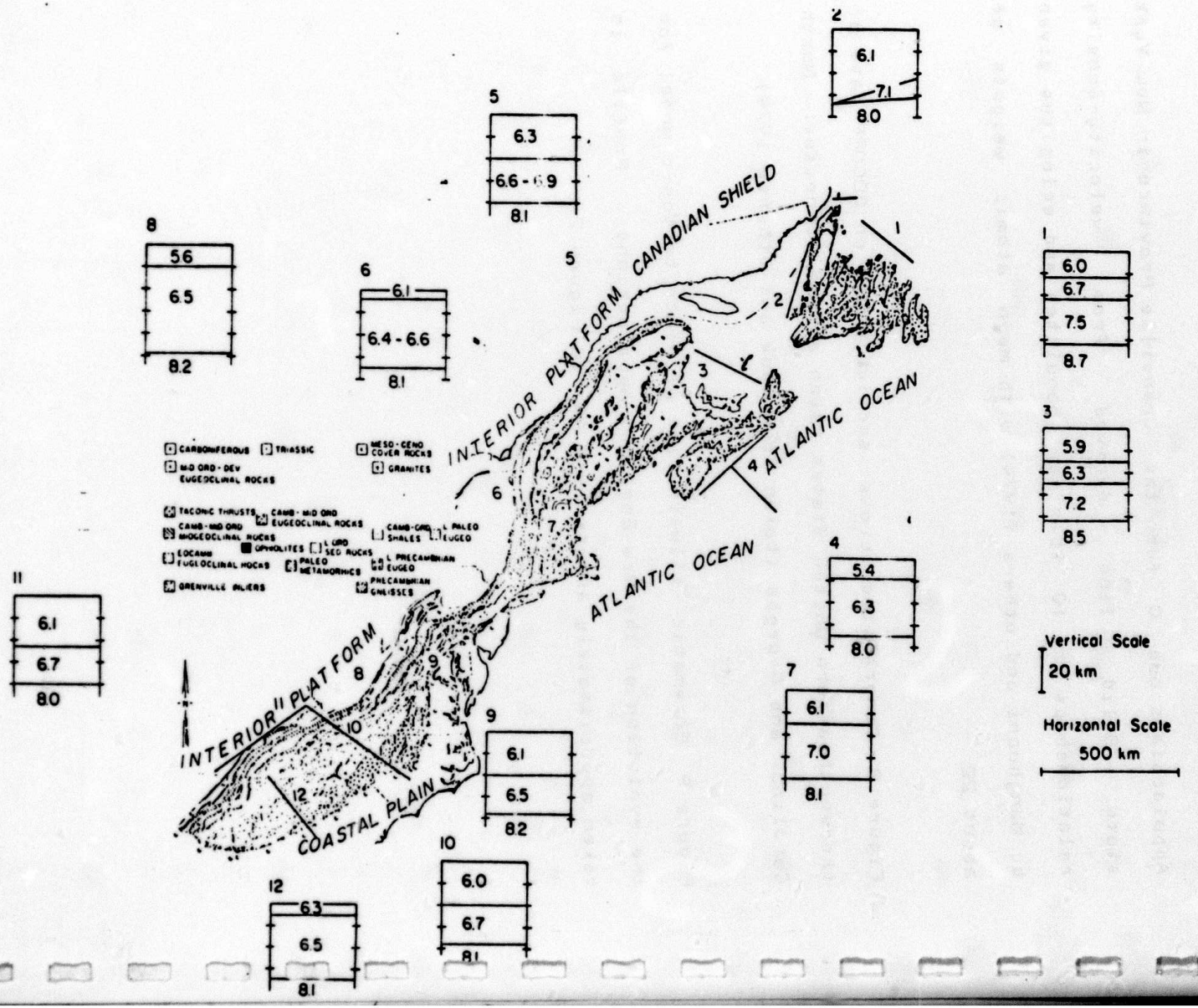
INTERIOR PLATFORM
CANADIAN SHIELD
ATLANTIC OCEAN
ATLANTIC OCEAN
INTERIOR II PLATFORM
COASTAL PLAIN
CARBONIFEROUS
TRIASSIC
MESO-CENO COVER ROCKS
MID ORD - DEV EUGEOCLINAL ROCKS
GRANITES
TACONIC THRUSTS
CAMB - MID ORD EUGEOCLINAL ROCKS
CAMB - MID ORD MIOGEOCLINAL ROCKS
CAMB-ORD SHALES
L PALEO EUGEO
OPHIOLITES
L ORD SED ROCKS
LOCAMB EUGEOCLINAL ROCKS
PALEO METAMORPHICS
L PRECAMBRIAN & EUGEO
GRENVILLE ALIERS
PRECAMBRIAN GNEISSES
Vertical Scale
20 km
Horizontal Scale
500 km

186.

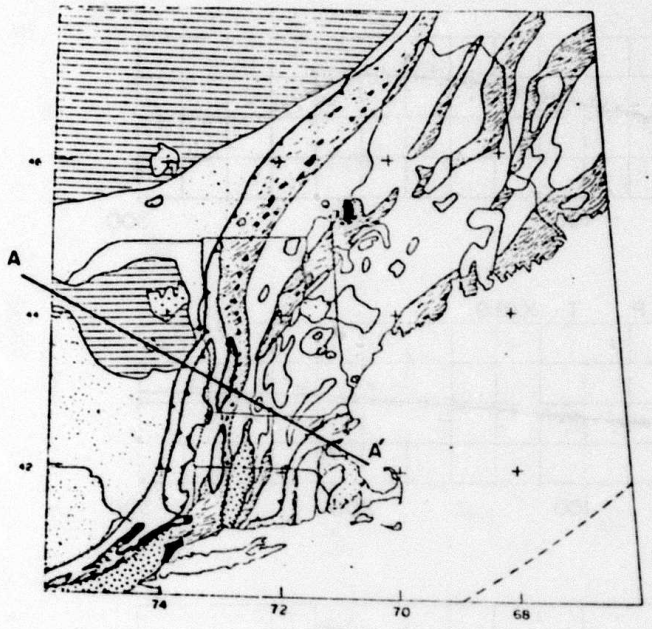

EXPLANATION

Thrust fault, barbs on upper block

Normal fault, hachures on downthrown side

STRATIFIED ROCKS

- Cenozoic glacial deposits
- Triassic red beds
- Carboniferous
- Silurian – Devonian eugeoclinal rocks
- Cambrian – Ordovician foreland rocks
- Cambrian – Ordovician deformed miogeoclinal rocks
- Cambrian – Ordovician eugeoclinal rocks
- Precambrian rocks of the eastern block
- Precambrian uplifts, Grenville basement
- Precambrian Grenville basement

IGNEOUS ROCKS

- Mesozoic White Mountain Plutonic Series
- Devonian New Hampshire Plutonic Series
- Cambrian – Ordovician serpentinites, ultramafics
- Precambrain anorthosites

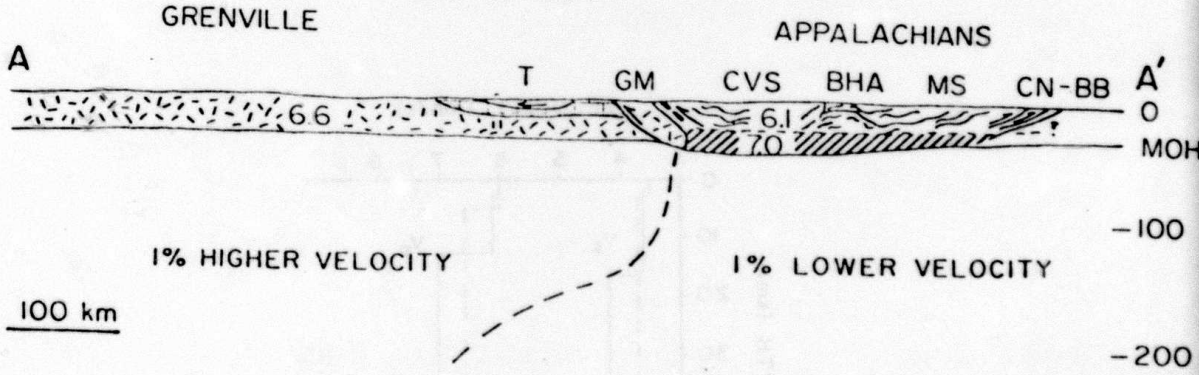

Figure 2

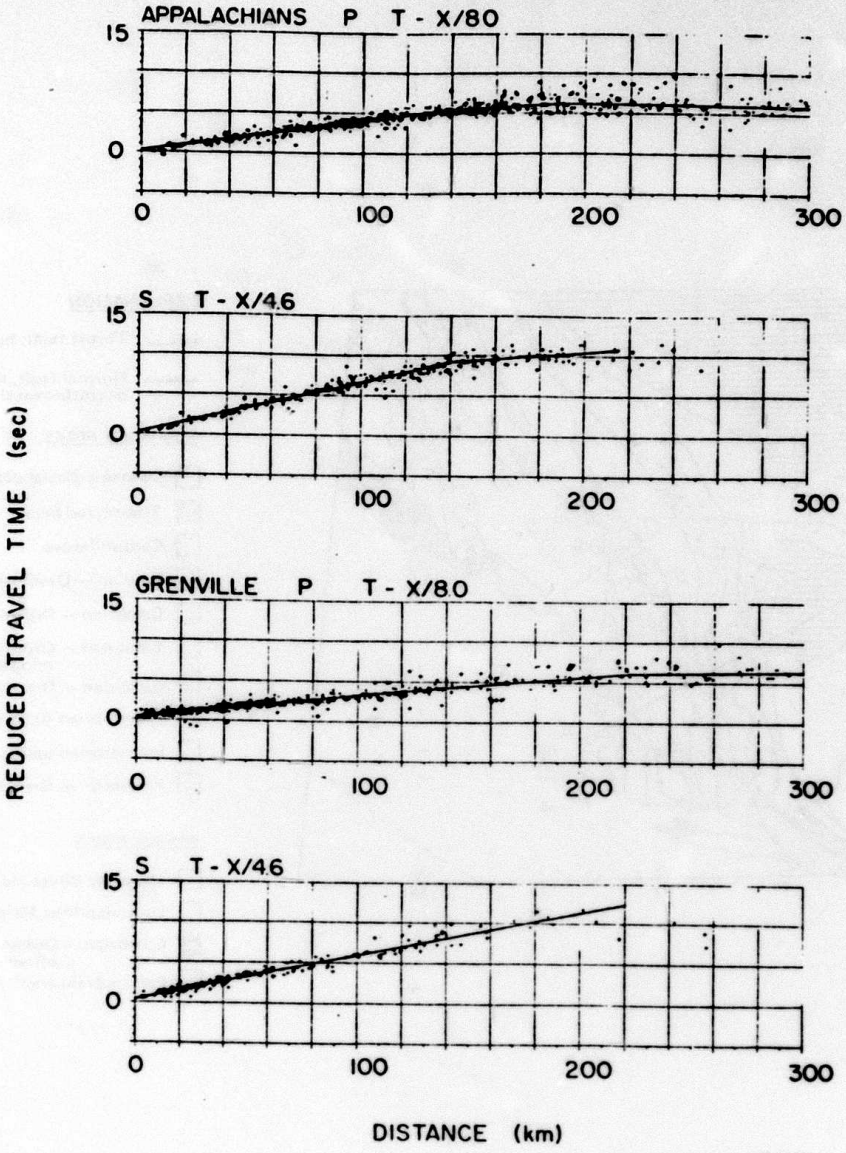
APPALACHIANS P T - X/8.0
S T - X/4.6
GRENVILLE P T - X/8.0
S T - X/4.6
15
0
0
100
200
300
REDUCED TRAVEL TIME (sec)
DISTANCE (km)

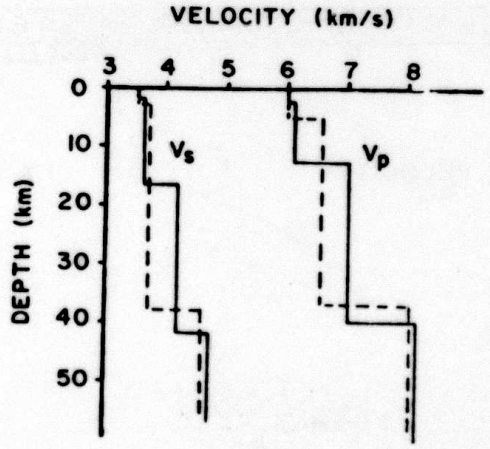
VELOCITY (km/s)
3
4
5
6
7
8
0
10
20
30
40
50
DEPTH (km)
V_s
V_p

Figure 3

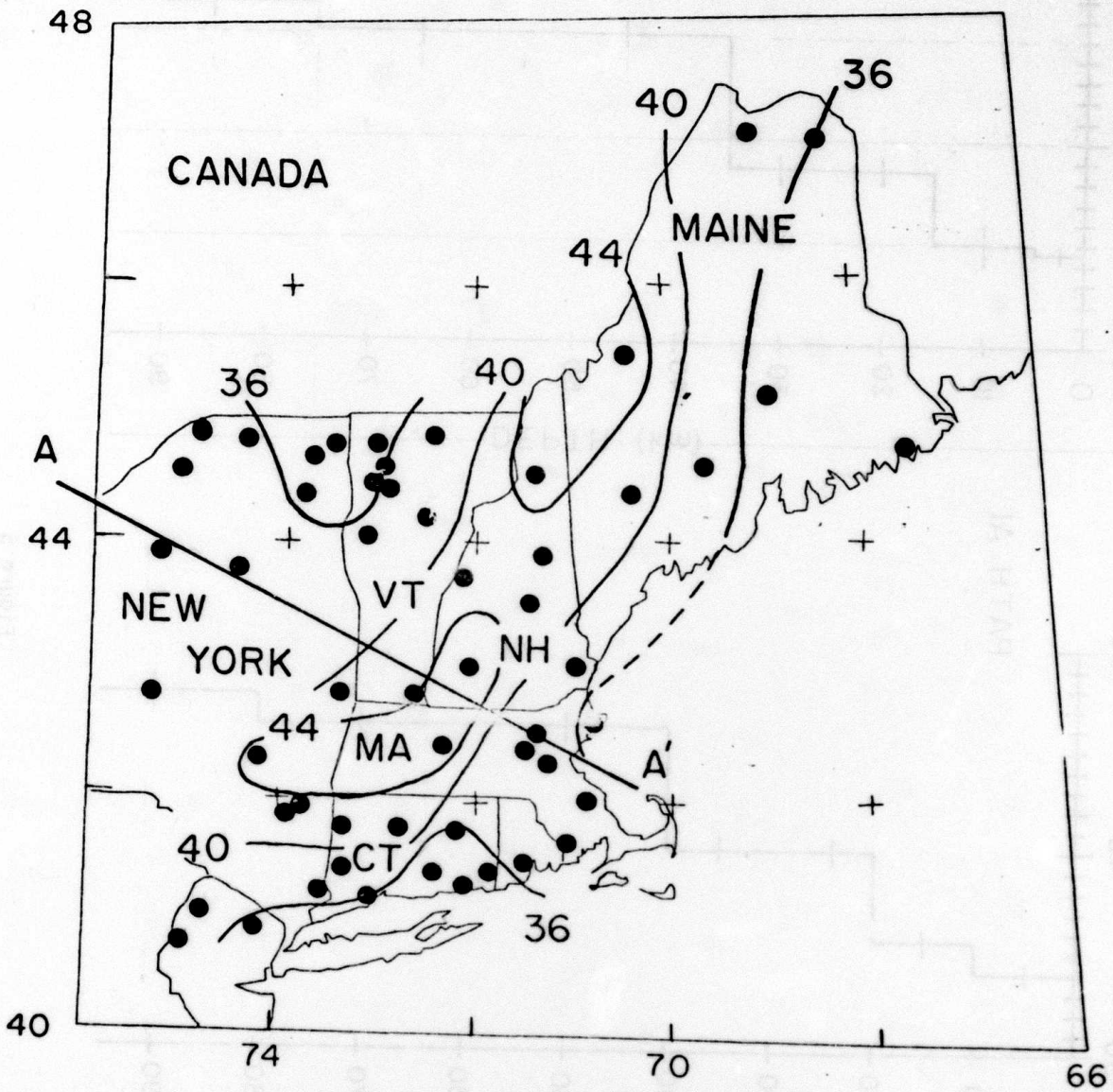
48
40
36
CANADA
MAINE
44
36
40
A
44
NEW
YORK
VT
NH
44
MA
A'
40
CT
36
40
74
70
66

Figure 4

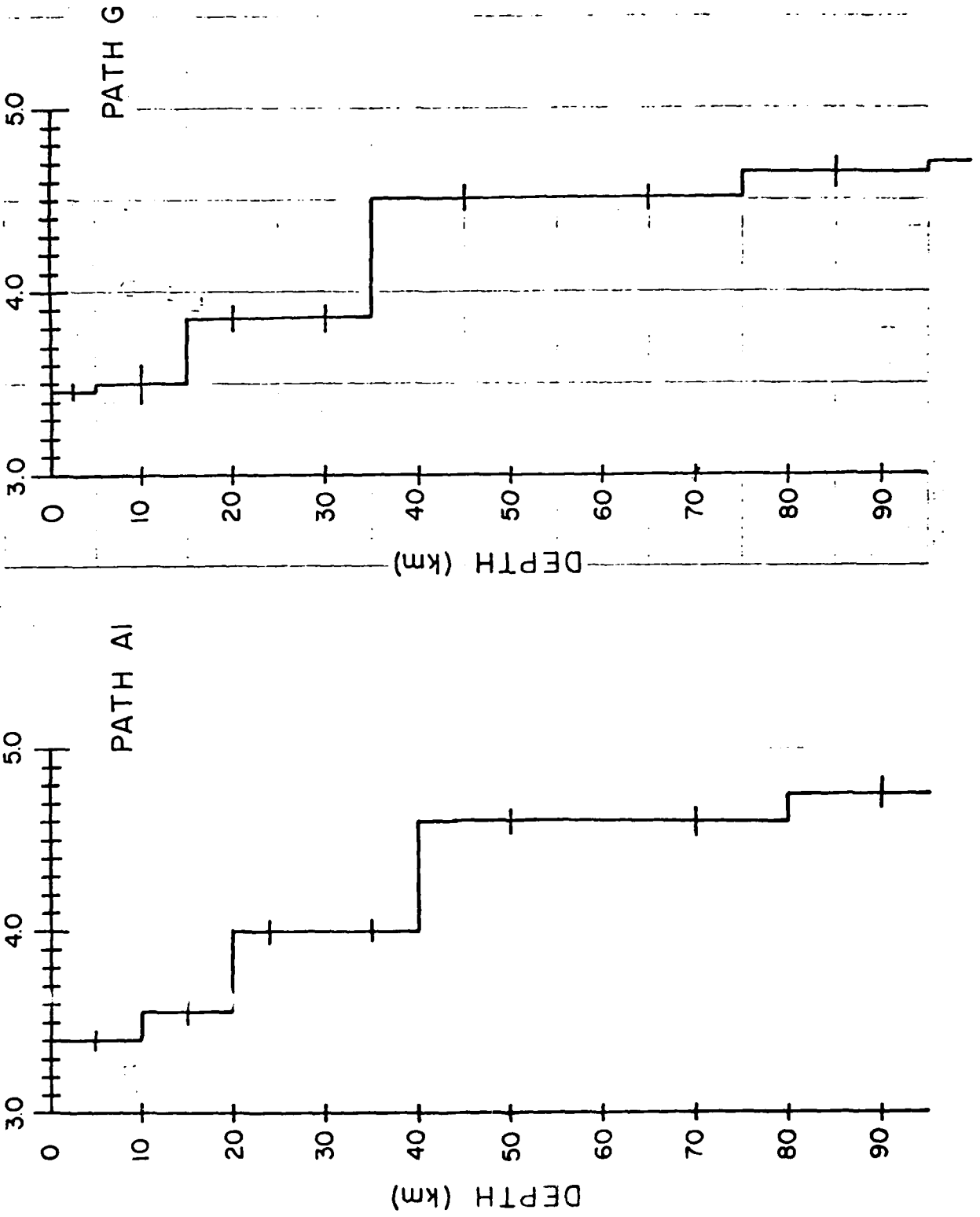
PATH G'
5.0
4.0
3.0
0
10
20
30
40
50
60
70
80
90
DEPTH (km)
PATH AI
5.0
4.0
3.0
0
10
20
30
40
50
60
70
80
90
DEPTH (km)

Figure 5

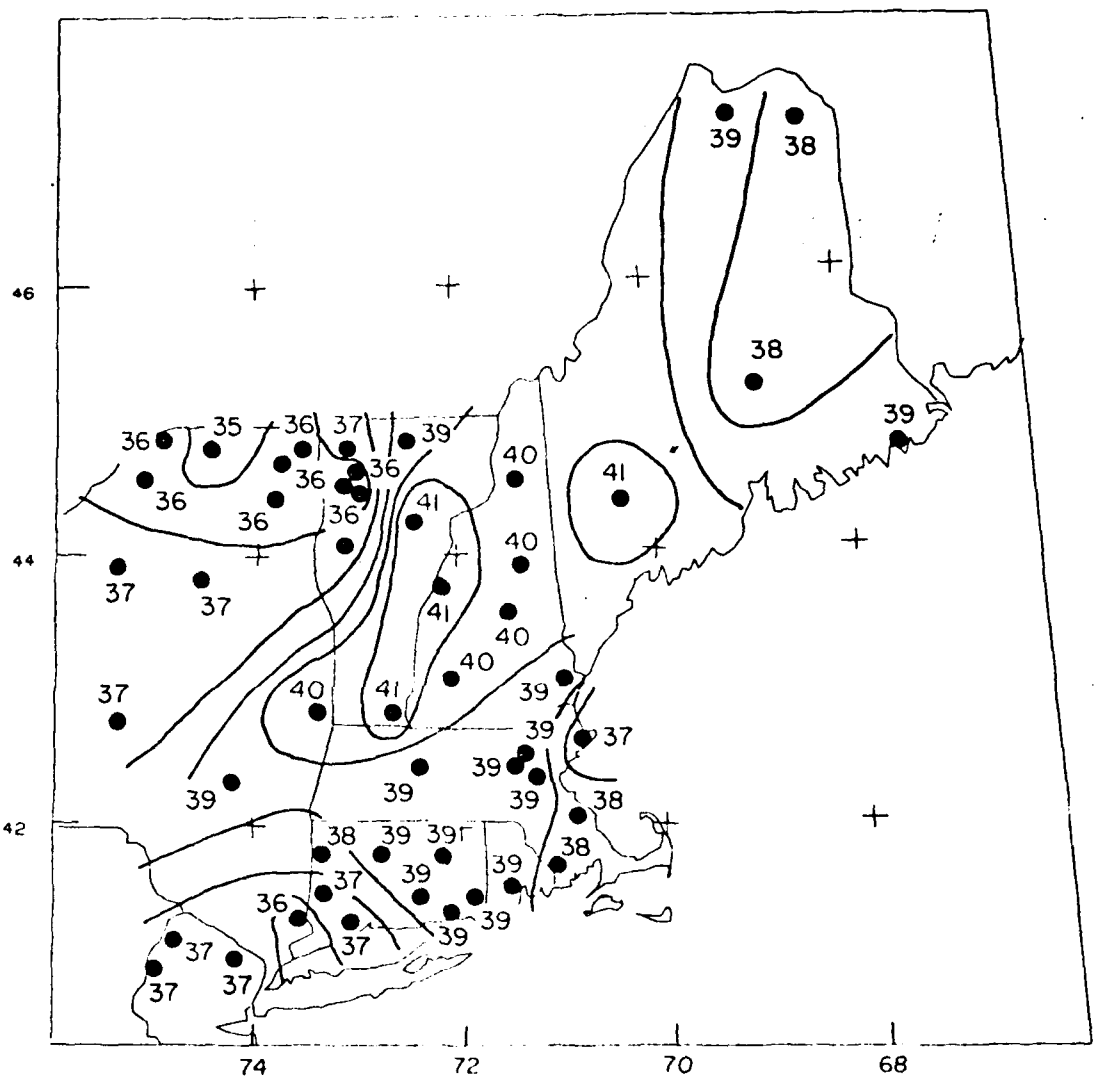
46
44
42
74
72
70
68
39
38
38
39
36
35
36
37
39
36
36
36
36
36
41
40
41
40
37
37
41
40
37
40
41
39
39
37
39
39
39
38
39
38
39
39
39
37
39
36
37
39
37
37
37

Figure 6

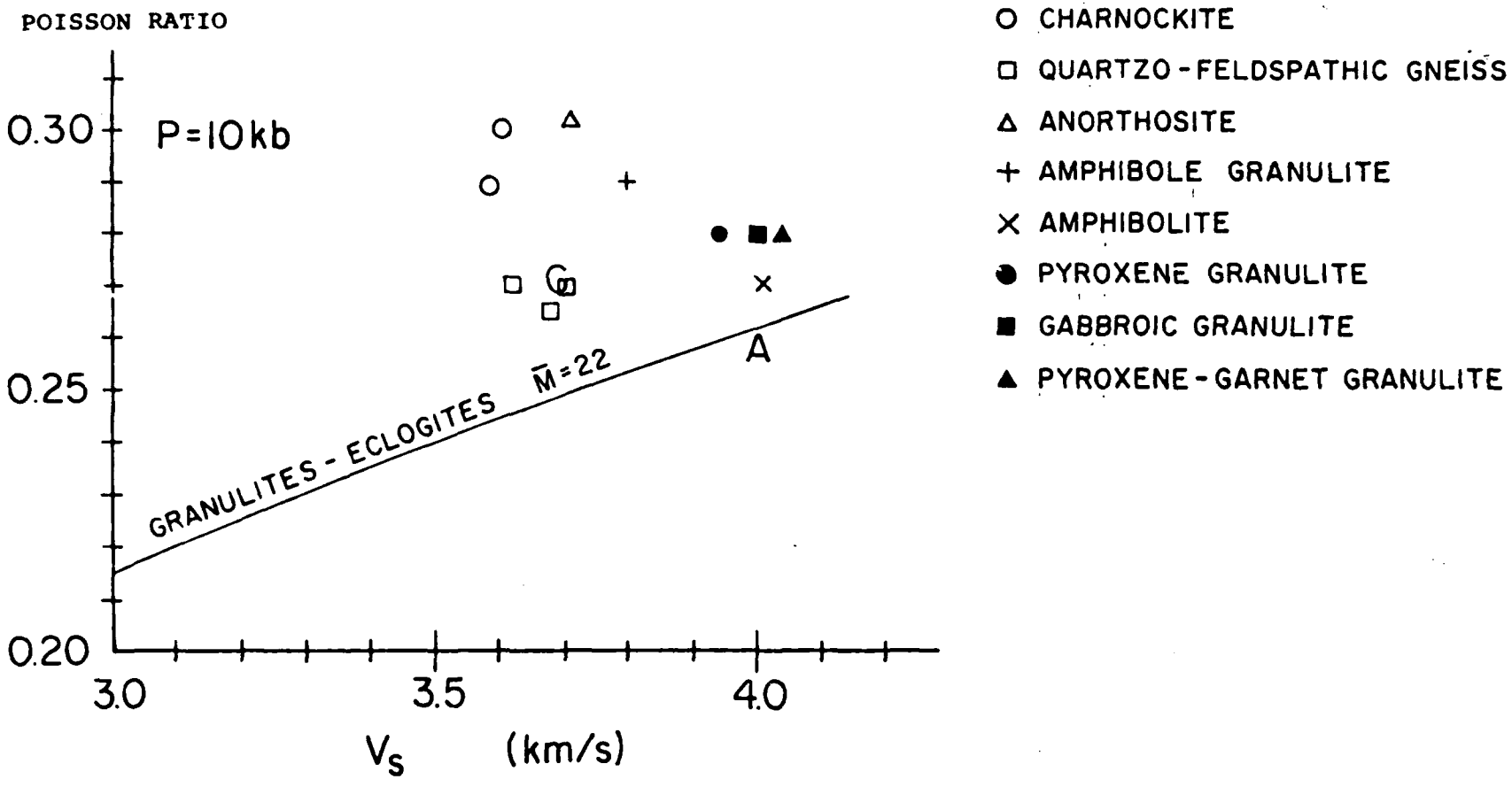
POISSON RATIO
0.30
0.25
0.20
P=10kb
GRANULITES - ECLOGITES
M=22
A
3.0
3.5
4.0
Vs (km/s)
CHARNOCKITE
QUARTZO-FELDSPATHIC GNEISS
ANORTHOSITE
AMPHIBOLE GRANULITE
AMPHIBOLITE
PYROXENE GRANULITE
GABBROIC GRANULITE
PYROXENE-GARNET GRANULITE

Figure 7

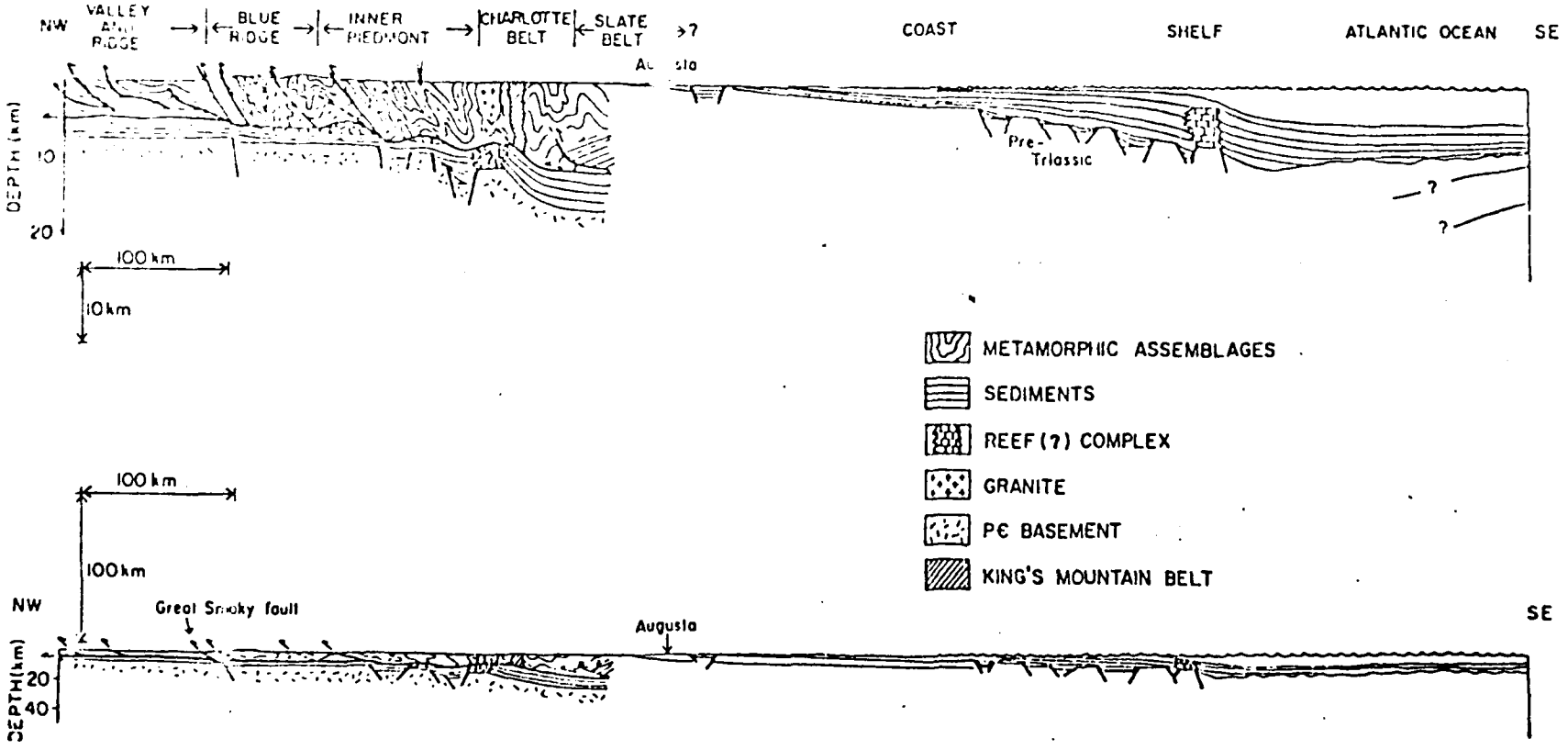
NW
VALLEY AND RIDGE
BLUE RIDGE
INNER PIEDMONT
CHARLOTTE BELT
SLATE BELT
>?
COAST
SHELF
ATLANTIC OCEAN
SE
Augusta
DEPTH (km)
10
20
Pre-Triassic
?
?
100 km
10km
METAMORPHIC ASSEMBLAGES
SEDIMENTS
REEF (?) COMPLEX
GRANITE
Pε BASEMENT
KING'S MOUNTAIN BELT
100 km
100km
NW
Great Smoky fault
Augusta
SE
DEPTH(km)
20
40

Figure 8

EOCAMBRIAN - EARLY ORDOVICIAN

a.

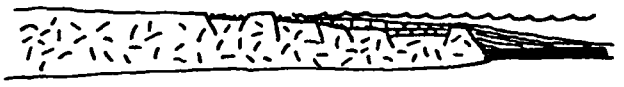

EARLY - MIDDLE ORDOVICIAN

b.

MIDDLE ORDOVICIAN TACONIC OROGENY

c.

SILURIAN - EARLY DEVONIAN

d.

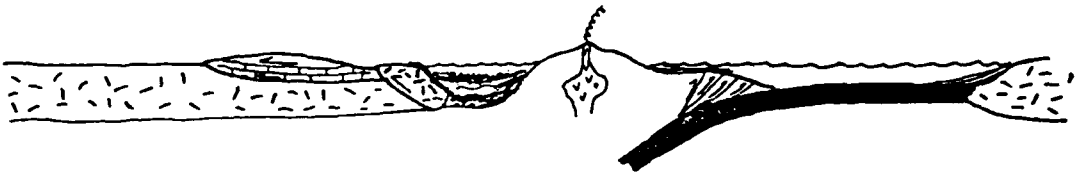

MIDDLE DEVONIAN ACADIAN OROGENY

e.

Figure 9

Table 1*

Orogenic Movements in the Appalachian Region

Orogenic episode and approximate date	*Known area of influence*	*Maximum manifestation*
Appalachian movements		
Palisades Late Triassic (Carnian-Norian) 190–200 m.y.	Belt along central axis of already completed mountain chain	Fault troughs, broad warping, basaltic lava, dike swarm
Alleghany Pennsylvanian and/or Permian (Westphalian and later) 230–260 m.y.	West side of central and southern Appalachians, southeast side of northern Appalachians, perhaps also in Carolina Piedmont	Strong folding, also middle-grade metamorphism and granite intrusion at least in southern New England
Early Ouachita Mid-Mississippian through early Pennsylvanian (Viséan to early Westphalian)	Only in southernmost Appalachians in central Alabama	Clastic wedge, also possibly broad east-west structures that influenced later deformation
Acadian Devonian, mainly Middle but episodic into Mississippian (Emsian-Eifelian) 360–400 m.y.	Whole of northern Appalachians, except along northwest edge; as far southwest as Pennsylvania	Medium- to high-grade metamorphism, granite intrusion
Salinic Late Silurian (Ludlow)	Local on northwest side of northern Appalachians	Mild angular unconformity, minor clastic wedge
Taconic Middle (and Late) Ordovician (Caradoc, locally probably older) 450–500 m.y.	General on northwest side of northern Appalachians, local elsewhere; an early phase in Carolinas and Virginia, perhaps general in Piedmont province	Strong angular unconformity, gravity slides (?), at least low-grade metamorphism, granodioritic and ultramafic intrusion
Penobscot Early Ordovician or older (Arenig or older)	Local on northwest side of northern Appalachians	Strong angular unconformity, slaty cleavage, possibly some intrusion
Avalonian Latest Precambrian	Southeastern Newfoundland, Cape Breton Island, southern New Brunswick; probably also central and southern Appalachians (Florida?)	Probably some deformation, uplift of sources of coarse arkosic debris, gravity slides(?)
Late Precambrian about 580 m.y.	Southeastern Newfoundland, Cape Breton Island, southern New Brunswick; perhaps eastern Massachusetts	Mostly low-grade metamorphism, granitic intrusion
Grenville (pre-Appalachian) movements Late Precambrian 800–1100 m.y.	Eastern North America including western part of Appalachian region	High-grade metamorphism, granitic and other intrusion

* From Rodgers (1970)

TABLE 2

GENERALIZED REFRACTION MODELS IN EASTERN NORTH AMERICA

Canadian Appalachians

Grenville		Appalachians		Cont. Margin	
Berry and Fuchs (1973)		Dainty et al. (1966)		Dainty et al. (1	
Depth (km)	Vp (km/s)	Depth	Vp	Depth	Vp
0.-20.	6.3	0.-15.	5.9	0.-9.	5.4
20.-40.	6.6-6.9	15.-25.	6.3	9.-35.	6.25
Moho	8.06	25.-42.	7.2	Moho	8.0
		Moho	8.1		
Dainty et al. (1966)					
0.-37.	6.25				
Moho	8.18				
Lyons et al. (1980)					
0.-22.	6.5				
22.-38.	6.8				
38.-43.	7.1				
Moho	8.1				

Northeastern United States

Grenville		Appalachians		Cont. Margin	
Katz (1954)		Street (1976)		Nakamura and Howe (1964)	
0.-35.	6.4	0.-2.5	5.76	0.-30.	6.0
Moho	8.14	2.5-26.0	6.40	Moho	8.1
		26.0-42.1	7.47		
		Moho	8.13		
Aggarwal in (Schnerk et al. 1976)		Taylor et al. (1980)		Chiburus and Ahne (1979)	
0.-4.0	6.1	0.-15.	6.1	0.-13.0	6.1
4.0-35.0	6.6	15.-40.	7.0		
Moho	8.1	Moho	8.1	Moho	8.1

TABLE 2 (continued)

Leet (1941)

0.-16.0	6.13
16.0-29.0	6.77
29.0-36.0	7.17
Moho	8.43

Steinhart et al. (1962)++
(Gulf of Me. to Me. interior)

0.-20.	6.0
20.-40.	7.0
Moho	8.0

Southern Appalachians

Grenville

Steinhart and Meyer (1961)

Depth (km)	Vp (km/s)
0.-13.7	6.20
13.7-45.3	6.73
Moho	8.06

Warren (1968)

0.-23.0	6.1
23.0-40.0	6.7
Moho	8.0

Bollinger et al. (1980)

0.-10.0	5.63
10.0-49.0	6.53
Moho	8.18

Appalachians (east of Blue Ridge)

Bollinger et al. (1980)*

Depth (km)	Vp (km/s)
0.-15.0	6.09
15.0-39.0	6.50
Moho	8.18

Warren (1968)

0.-20.0	6.0
20.0-38.0	6.7
Moho	8.1

Long (1979)+

0.-5.0	6.3
5.0-35.0	6.5
Moho	8.1

* Crust thins to 31 km to the east beneath central Piedmont
\+ Crust varies from 30-37 km thickness
++ Average velocities reported in Kane and others (1972)

V. CUMULATIVE LIST OF PUBLICATIONS UNDER THIS PROJECT

Abe, K., Re-examination of the fault model for the Niigata earthquake of 1964, J. Phys. Earth, 23, 349-366, 1975.

Aki, K., Scattering and attenuation of shear waves in the lithosphere, J. Geophys. Res., 85, 6496-6504, 1980.

Aki, K., Attenuation and scattering of high frequency seismic waves in the lithosphere, Proc. NATO Advanced Study Institute, Identification of Seismic Sources - Earthquakes or Underground Explosions, in press, 1981.

Aki, K., A. Christoffersson and E. Husebye, Three-dimensional seismic structure of the lithosphere under Montana LASA, Bull. Seism. Soc. Am., 66, 501-524, 1976.

Aki, K., A. Christoffersson and E. Husebye, Determination of the three-dimensional seismic structure of the lithosphere, J. Geophys. Res., 82, 277-296, 1977.

Bird, P., Thermal and mechanical evolution of continental convergence zones, Ph.D. Thesis, M.I.T., Cambridge, MA, 1976.

Bird, P. and M.N. Toksöz, Strong attenuation of Rayleigh waves in Tibet, Nature, 266, 161-163, 1977.

Bird, P., M.N. Toksöz and N.H. Sleep, Thermal and mechanical models of continent-continent convergence zones, J. Geophys. Res., 80, 4405-4416, 1975.

Burr, N.C., The relationship of source parameters of oceanic transform earthquakes to plate velocity and transform length, M.S. Thesis, M.I.T., Cambridge, MA, 1977.

Burr, N.C. and S.C. Solomon, The relationship of source parameters of oceanic transform earthquakes to plate velocity and transform length, J. Geophys. Res., 83, 1193-1205, 1978.

Canitez, N., Optimum filter for surface-wave group velocity determination, Bull. Seism. Soc. Am., 67, 79-85, 1977.

Chapman, M.E. and S.C. Solomon, North American-Eurasian plate boundary in northeast Asia, J. Geophys. Res., 81, 921-930, 1976.

Husebye, E., A. Christoffersson, K. Aki and C. Powell, Preliminary results on the three-dimensional seismic structure of the lithosphere under the USGS central California seismic array, Geophys. J. R. Astr. Soc., 46, 319-340, 1976.

Johnston, D.H., The attenuation of seismic waves in dry and saturated rocks, Ph.D. Thesis, M.I.T., Cambridge, MA, 1978.

Johnston, D.H., M.N. Toksöz and A. Timur, Attenuation of seismic waves in dry and saturated rocks, II. Mechanisms, Geophysics, 44, 691-711, 1979.

Johnston, D.H. and M.N. Toksöz, Thermal cracking and amplitude dependent attenuation, J. Geophys. Res., 85, 937-942, 1980.

Johnston, D.H. and M.N. Toksöz, Ultrasonic P and S wave attenuation in dry and saturated rocks under pressure, J. Geophys. Res., 85, 925-936, 1980.

Lee, W.B., Simultaneous inversion of surface wave phase velocity and attenuation for continental and oceanic paths, Ph.D. Thesis, M.I.T., Cambridge, MA, 1977.

Lee, W.B. and S.C. Solomon, Inversion schemes for surface wave attenuation and Q in the crust and the mantle, Geophys. J. R. Astr. Soc., 43, 47-71, 1975.

Lee, W.B. and S.C. Solomon, Simultaneous inversion of surface wave phase velocity and attenuation: Love waves in western North America, J. Geophys. Res., 83, 3389-3400, 1978.

Lee, W.B. and S.C. Solomon, Simultaneous inversion of surface wave phase velocity and attenuation: Rayleigh and Love waves over continental and oceanic paths, Bull. Seism. Soc. Am., 69, 65-95, 1979.

Madariaga, R., Dynamics of an expanding circular fault, Bull. Seism. Soc. Am., 66, 639-666, 1976.

Patton, H.J., Source and propagation effects of Rayleigh waves from central Asian earthquakes, Ph.D. Thesis, M.I.T., Cambridge, MA, 1978.

Patton, H.J., Crust and upper mantle structure of the Eurasian continent from the phase velocity and Q of surface waves, Rev. Geophys. Space Phys., 18, 605-625, 1980.

Sengupta, M.K. and B.R. Julian, P-wave travel times for deep earthquakes, Bull. Seism. Soc. Am., 66, 1555-1579, 1976.

Sengupta, M.K. and M.N. Toksöz, Three dimensional model of seismic velocity variation in the earth's mantle, Geophys. Res. Lett., 3, 84-86, 1976.

Sengupta, M.K. and M.N. Toksöz, The amplitudes of P waves and magnitude corrections for deep focus earthquakes, J. Geophys. Res., 82, 2971-2980, 1977.

Solomon, S.C., Geophysical constraints on radial and lateral temperature variations in the upper mantle, Am. Mineral., 61, 788-803, 1976.

Solomon, S.C. and K.T. Paw U, Elevation of the olivine-spinel transition in subducted lithosphere: seismic evidence, Phys. Earth Planet. Int., 11, 97-108, 1975.

Taylor, S.R., Crust and upper mantle structure of the Northeastern United States, Ph.D. Thesis, M.I.T., Cambridge, MA, 1980.

Taylor, S.R. and M.N. Toksöz, Three-dimensional crust and upper mantle structure of the northeastern United States, J. Geophys. Res., 84, 7627-7644, 1979.

Taylor, S.R. and M.N. Toksöz, Measurement of interstation phase and group velocity and Q using Wiener filtering, Bull. Seism. Soc. Am., submitted, 1980.

Taylor, S.R. and M.N. Toksöz, Crust and upper mantle velocity structure in the Appalachian orogenic belt: implications for tectonic evolution, Geol. Soc. Am. Bull., submitted, 1980.

Taylor, S.R., M.N. Toksöz and M.P. Chaplin, Crustal structure of the Northeastern United States: contrasts between the Grenville and Appalachian Provinces, Science, 208, 595-597, 1980.

Toksöz, M.N., The subduction of the lithosphere, Sci. Amer., 233, 88-98, 1975.

Toksöz, M.N., E. Arpat and F. Saroglu, East Anatolian earthquake of 24 November 1976 - field observations, Nature, 270, 423-425, 1977.

Toksöz, M.N. and P. Bird, Formation and evolution of marginal basins and continental plateaus, in Island Arcs, Deep Sea Trenches and Back Arc Basins, eds. M. Talwani and W.C. Pitman III, Maurice Ewing Series, Vol. 1, 379-393, AGU, Washington, D.C., 1977.

Toksöz, M.N. and P. Bird, Modelling of temperatures in continental convergence zones, Tectonophysics, 41, 181-193, 1977.

Toksöz, M.N., J. Nabelek and E. Arpat, Source properties of the 1976 earthquake in E. Turkey: A comparison of field data and teleseismic results, Tectonophysics, 49, 199-205, 1978.

Trehu, A.M., J.L. Nabelek and S.C. Solomon, Source characterization of two Reykjanes Ridge earthquakes: surface waves and moment tensors; P waveforms and non-orthogonal nodal planes, J. Geophys. Res., in press, 1981.

Ward, R.W. and K. Aki, Synthesis of teleseismic P waves from sources near sinking lithospheric slabs, Bull. Seism. Soc. Am., 65, 1667-1680, 1975.

UNCLASSIFIED

SECURITY CLASSIFICATION OF THIS PAGE (When Data Entered)

REPORT DOCUMENTATION PAGE	READ INSTRUCTIONS BEFORE COMPLETING FORM
1 REPORT NUMBER: AFOSR-TR-81-0465	2 GOVT ACCESSION NO. / 3 RECIPIENT'S CATALOG NUMBER
4 TITLE (and Subtitle): RESEARCH IN SEISMOLOGY (ATTENUATION AND SOURCE MECHANISMS)	5 TYPE OF REPORT & PERIOD COVERED: Final Technical 6/1/75-9/30/80
	6 PERFORMING ORG. REPORT NUMBER
7 AUTHOR(s): M. Nafi Toksöz, Keiiti Aki, Sean C. Solomon	8 CONTRACT OR GRANT NUMBER(s): F44620-75-C-0064
9 PERFORMING ORGANIZATION NAME AND ADDRESS: Dept. of Earth and Planetary Sciences, Massachusetts Institute of Technology, Cambridge, Massachusetts 02139	10 PROGRAM ELEMENT, PROJECT, TASK AREA & WORK UNIT NUMBERS: 62701E, AO 3291
11 CONTROLLING OFFICE NAME AND ADDRESS: Advanced Research Projects Agency/NMR, 1400 Wilson Blvd., Arlington, Virginia 22209	12 REPORT DATE: 3/24/81
	13 NUMBER OF PAGES: 201
14 MONITORING AGENCY NAME & ADDRESS (if different from Controlling Office): Air Force Office of Scientific Research/NP, Bolling AFB, Bldg. 410, Washington, D.C. 20332	15 SECURITY CLASS (of this report): Unclassified
	15a DECLASSIFICATION/DOWNGRADING SCHEDULE
16 DISTRIBUTION STATEMENT (of this Report): Approved for public release; distribution unlimited.	
17 DISTRIBUTION STATEMENT (of the abstract entered in Block 20, if different from Report)	
18 SUPPLEMENTARY NOTES	
19 KEY WORDS (Continue on reverse side if necessary and identify by block number): Crust-upper mantle structure, wave propagation, attenuation, source properties	

20 ABSTRACT (Continue on reverse side if necessary and identify by block number)

Research activities described in this report include detailed studies of crust-upper mantle structures and their lateral variations, surface wave propagation and attenuation over regional distances, and the determination of source properties of "anomalous" earthquakes by combined studies of body and surface waves.

At regional distances, the lateral variations of the shallow structure have strong effects on the propagation of body and surface waves. The lateral heterogeneities are present not only in "tectonic" regions but also in the old geologic provinces. The horizontally layered models are becoming less representative of the structures in continental areas. Continental growth processes that include collisions, suturing, heating and melting, leave major heterogeneities that affect wave propagation, scattering and attenuation.

Similarly, complexities of the earthquake source, even for small events, are being found with more detailed studies. Body waves from such sources are being affected by source finiteness, asperities, rupture propagation and by the geologic structure. It is difficult to separate all these effects, especially for very shallow sources, where surface reflection further complicates the problem. Detailed analysis of body and surface waves is necessary to determine the source properties. An example of how this approach was utilized to study some anomalous events is shown in this report.

DD FORM 1 JAN 73 1473

UNCLASSIFIED